Title
Investigating the Molecular Mechanisms Dictating Lens Stiffness and Growth: Functional Studies of Gap Junction and α-Crystallin Mutant Lenses

Author
Stopka, Wiktor

Publication Date
2017

Peer reviewed|Thesis/dissertation

Investigating the Molecular Mechanisms Dictating Lens Stiffness and Growth: Functional Studies of Gap Junction and α-Crystallin Mutant Lenses

by

Wiktor Gustaw Stopka

A dissertation submitted in partial satisfaction of the

requirements for the degree of

Joint Doctor of Philosophy
with University of California, San Francisco

in

Bioengineering

in the

Graduate Division

of the

University of California, Berkeley

Committee in charge:

Professor Xiaohua Gong, Chair
Professor Bo Huang
Professor Clifton M. Schor

Summer 2017

Abstract

Investigating the Molecular Mechanisms Dictating Lens Stiffness and Growth: Functional Studies of Gap Junction and α-Crystallin Mutant Lenses

by

Wiktor Gustaw Stopka

Joint Doctor of Philosophy

with University of California, San Francisco

in Bioengineering

University of California, Berkeley

Professor Xiaohua Gong, Chair

Our vision depends on several key optical properties of the eye lens including: transparency, high refractive index, and accommodation, which relies on the elastic process of lens deformation to focus light clearly onto the retina. The lens is composed of a monolayer of epithelial cells that cover the anterior hemisphere of bulk elongated fibers and is wrapped by a basement membrane called the lens capsule. Genetic studies reveal that mutation in members of key lens proteins such as gap junctions, cytoskeletal proteins, and crystallins impair lens growth, homeostasis, transparency, and / or other optical properties. However, the underlining mechanisms of how mutated genes lead to lens pathology remain not well understood. Moreover, it is unknown how mutated gap junctions, consisting of several different connexin subunits, affect lens elasticity, or how mutated αA-crystallin impairs lens growth or disrupts the cytoskeleton.

My thesis project, consisting of three parts, aims to elucidate the roles of gap junctions, the lens cytoskeleton, and crystallins in the development and maintenance of lens elasticity and lens growth. In part one, connexin mutant mouse lenses are subject to the measurement of lens stiffness by a novel muscle lever system. The results show that knockout of gap junction gene *Gja3*, also known as α3-connexin or Cx46, caused a marked increase in lens stiffness across almost all genotypes and ages. In addition, it was shown that mouse strain backgrounds, associated with variant periaxin, a cytoskeletal organization protein, had significant effects on the bulk lens stiffness, with the C57BL/6J strain background resulting in softer lenses, while the 129 strain background produced stiffer lenses. Part two investigates lenses with mutated αA-Y118D crystallin protein, which present a unique lens growth defect. Mutant lenses stop growing after 8 weeks of age and mutant lens fiber cells exhibit abnormal growth and are unable to elongate. Next, studies of αA-crystallin mutations in cultured lens epithelial cells reveal the interaction between αA-crystallin with the lens cytoskeleton. Results show that αA-crystallin is

associated with lamellar actin in wild-type cells, while αA-Y118D mutant protein tends to form aggregates with actin. Finally, part three reveals a novel regulation of lens connexin expression in cultured lens epithelium with a new cell culture medium. Treatment with SB431542 (SB), a transforming growth factor β (TGF-β) inhibitor, is important to maintain the expression of gap junction gene *Gja8*, also known as α8-connexin or Cx50, while fibroblast growth factor (FGF) treatment suppresses its expression.

My dissertation reveals the novel role of gap junctions and cytoskeletal proteins in the regulation of lens elasticity and further elucidates the unique role of αA-crystallin in the regulation of lens cytoskeletal structures in vivo and in vitro. Finally, the expression of gap junction proteins in lens epithelial cells is negatively regulated by both the TGF-β and FGF signaling pathways. This work further improves our understanding of the regulation and maintenance of lens optical properties during lens development.

Dedication

To my parents, Mr. Jan Stopka and Mrs. Grazyna Stopka.
They have always loved me and provided support in any way they could.

Table of Contents

List of Figures and Tables

Acknowledgements

With thanks to:

- Professor Xiaohua Gong. Professor Gong has always encouraged me to think critically about my research and to always look for new ideas. His guidance has helped me advance both professionally and personally, and he has my greatest appreciation.
- Dr. Chun-hong Xia. Dr. Xia has always been available to ask questions and to offer advice on experiments and technical support. Her help throughout the years has been invaluable.
- Professor Song Li. In addition to being a GSI for one of his undergraduate courses, in which I also learned a lot, Professor Li also chaired my qualifying exam. My thanks for all of his support and insights.
- My thesis committee: Professor Bo Huang and Professor Clifton Schor for all of their guidance and advice.
- Thomas Libby. Special thanks to my collaborator on the lens stiffness measurements, Tom Libby. His technical expertise and advice on data analysis was invaluable.
- Members of the Gong Lab. Thanks to all past and present members of the Gong Lab for all the help and support. Especially Stephanie Lin and Kelsey Liu for their help with data collection.
- My friends. Thank you to the new friends and colleagues I've met while in grad school, Omar, Sean, Sergey, Arunan, and Sophie, my friends from back home, especially Kamil, Jakub, and Chua, and everyone I've met and gotten to know personally over the years at the Cal Fencing Club, especially David, Samir, Daniel, Victor, Megan, Sophia, Kristina, CC, KC, Yoonji, Margaret, Shannon, Diana, and Arami, for all of your support, encouragement, and distractions.
- My family. A very special thanks to my wife Lucia, my mom and dad, and my brother Tomasz for always being there and supporting me.

Chapter 1 Introduction

1.1 Motivation and Aim of Study

Accommodation is the process by which the focusing power of the lens is adjusted to focus images clearly onto the retina. This ability to change the shape of the lens is lost as the eye becomes older in humans and monkeys. This loss in ability to accommodate is called presbyopia and is considered the most common human ocular affliction[1]. The loss of human accommodation potential is a progressive process that begins early in life and concludes with a complete inability to accommodate by age 50 to 55 years. This phenomenon has a major impact on both the developed and developing world[2], as many cases are left untreated, or undertreated. There are a number of ways to correct for presbyopia by various optical means[3], but the cost to do so, through medical devices[4,5], loss of productivity[6], or non-surgical[7] and surgical methods[8–10], is considerable. Despite these advances in ocular correction, presbyopia will affect everyone in some form or another after five decades of life, particularly those unable to access appropriate eye care. Currently there is no known method to prevent or delay the onset of presbyopia. The molecular and cellular mechanism for presbyopia remains elusive, but might be related to the modification of lens proteins that occurs during aging, affecting both lens elasticity and / or refractive index.

Through many years of research, our understanding of the development and aging of the humans lens, both biochemically and biomechanically, has improved greatly. Despite this, the exact mechanisms to allow the lens to remain elastic to allow for the shape change that occurs during accommodation, or an ability to slow the aging and growth of the lens, are unclear. Using mouse models with various mutations producing a number of interesting lens phenotypes related to lens size and stiffness[11–13], it is now possible to better understand the molecular mechanisms behind control of lens growth, cataract formation, and control of lens elasticity. By better

understanding the interaction of lens proteins with the cytoskeleton, we can gain a better appreciation for potential treatments to delay or entirely prevent the pathways that inevitably cause presbyopia in all humans.

1.2 Mammalian Lens Anatomy

The lens is an organ located just behind the iris of the eye and must remain completely transparent throughout its lifetime in order to function[14]. The job of the lens is to focus light directly onto the retina to produce a clear image. The lens is surrounded by an elastic capsule and made of only two cell types: a monolayer of lens epithelial cells just on the anterior surface, and the remaining bulk of the lens which consists of elongated lens fiber cells, going from the anterior to posterior lens poles[15–18] (Figure 1.1). During lens development, the lens consists of a simple spherical monolayer of epithelial cells. The epithelial cells on the anterior side of this sphere remain epithelial cells throughout the lifetime of the lens and continue to proliferate as such, while those epithelial cells on the posterior surface of this early lens vesicle elongate to fill the lumen in the center of the sphere, becoming the primary lens fiber cells. After this stage, the lens continues to grow in size, relying on proliferation, elongation, and differentiation of lens epithelial cells near the lens equator, becoming secondary lens fiber cells[19–22]. These secondary lens fiber cells form additional layers surrounding previous lens fiber cells, increasing the size of the lens gradually with age (Figure 1.2). Later during fiber cell differentiation, the inner fibers initiate breakdown of all cytoplasmic organelles and nuclei in order to minimize light scattering, maintaining lens transparency[23,24]. The exact process by which secondary fiber cell differentiation is controlled and organized is still unclear.

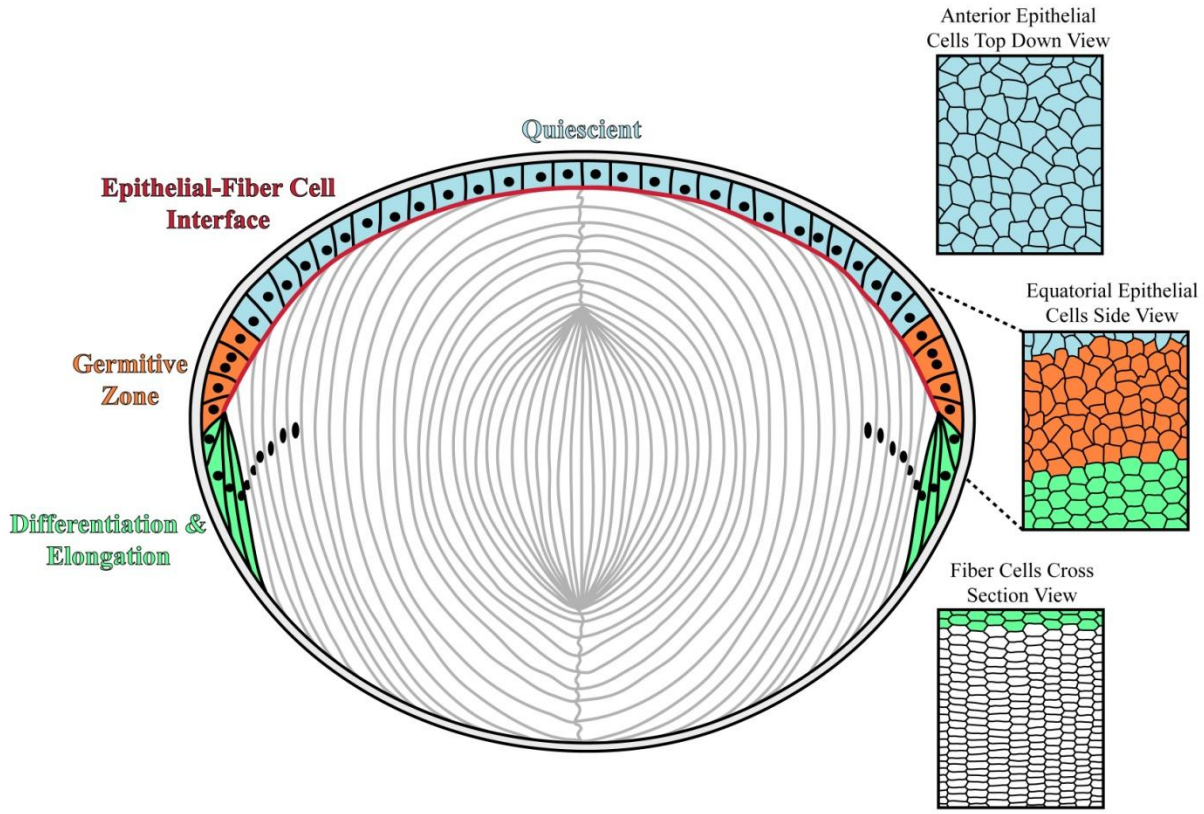

Figure 1.1. Overview of lens structure, with regions of interest highlighted. Light blue: Central Epithelium, once the lens is fully developed, epithelial cells here no longer proliferate. Orange: Germitive Zone, the region slightly above the lens equator where lens epithelial cells continue to proliferate. This zone of proliferating epithelial cells is responsible for the continued growth of the lens via additional layers of secondary lens fiber cells. Green: the region where proliferating epithelial cells from the Germitive Zone begin to elongate and differentiate into lens fiber cells. All internal organelles are eventually removed, including the nucleus. Dark red: Epithelial-Fiber Interface, the interface between the epithelial cells and the lens fiber cells. Elongating lens fiber cells crawl along the lens epithelial cells until they form a suture at both the anterior and posterior poles of the lens. Panels at right: overview of cell shape and morphology in each layer described above. Modified figure from Catherine Cheng.

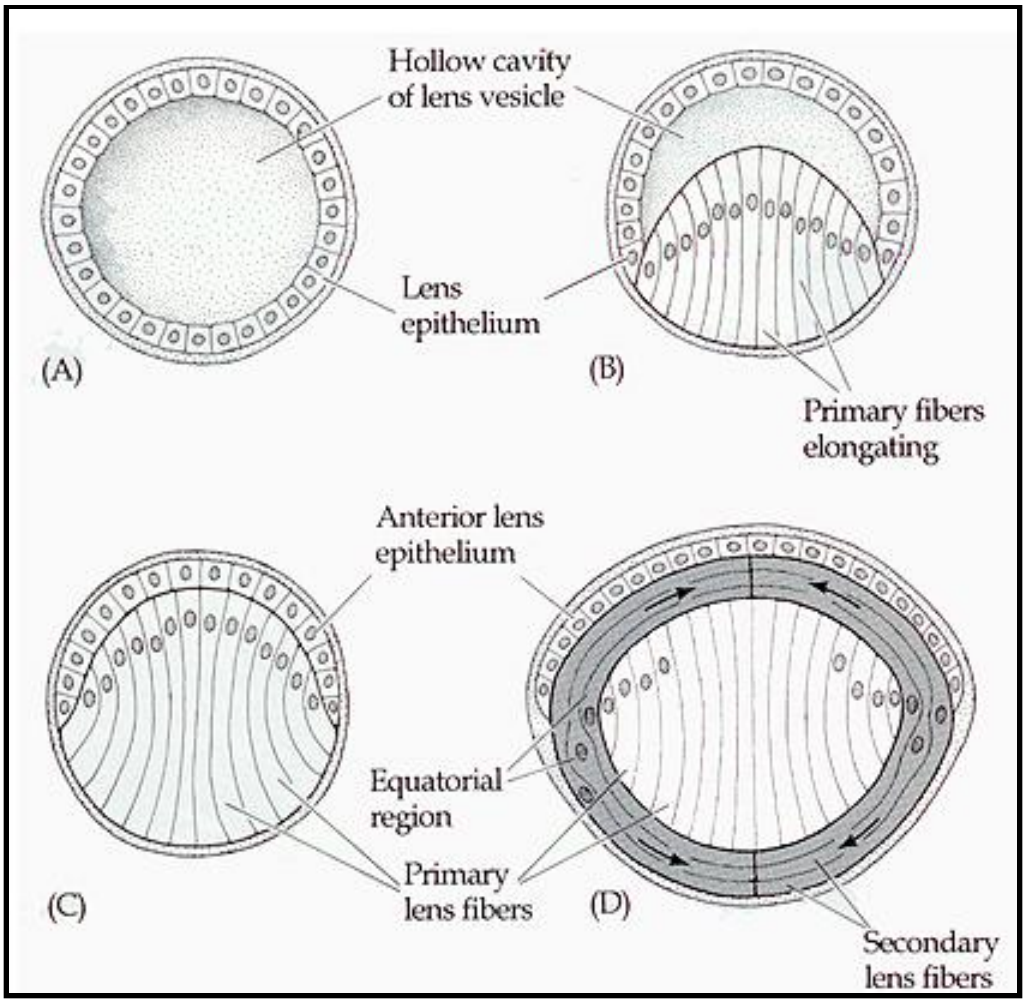

Figure 1.2. Overview of lens development. A. Lens vesicle consists of single layer sphere of lens epithelial cells. B. Epithelial cells on posterior portion of lens vesicle start to elongate to fill lumen and become primary fiber cells. C. Primary lens fibers completely fill lens vesicle while epithelial cells on anterior portion maintain epithelial function. D. Fully developed lens clearly showing primary fiber cells surrounded by layers of secondary fiber cells. Epithelial cells near the lens equator proliferate and add more layers of secondary fiber cells, increasing the size of the lens throughout our lifetime. Modified from Gilbert, 1994.

1.3 Accommodation

The process of accommodation occurs through contraction of the ciliary muscles surrounding the lens. These ciliary muscles are connected to the lens via elastic zonular fibers, which are responsible for transmitting forces to the lens. The classic theory of accommodation proposed by Helmholtz[25] states that while the eye is at rest, the ciliary muscles are relaxed and the lens is focused for distance. When the eye needs to focus on a nearby object, the ciliary muscles contract, resulting in a movement of the muscle mass forward and towards the center of the lens[26]. This results in a release of the resting tension of the zonular fibers, causing the elastic lens capsule to reshape the lens, becoming more spherical (Figure 1.3). The lens surface becomes sharper and increases in axial thickness, resulting in the necessary increase in optical power to focus on nearby objects[27]. When the ciliary muscles relax again, in the case of focusing on a far away object, this causes the zonular fibers to once again exert a resting tension on the lens, reshaping it. The fibers tug at several attachment points along the equator of the lens, effectively increasing its diameter and flattening its anterior and posterior surfaces. It is hypothesized that the major determining factor in losing this ability to change the shape of the lens is the age-related stiffening of the lens[28], but defects in any one component described above can lead to a loss in accommodation potential.

1.4 Cataracts

Cataracts are opacifications in the lens and are often categorized depending on the age, degree, and location of the cataract. Anterior and posterior cataracts occur at either the anterior or posterior poles of the lens, respectively. Nuclear cataracts occur within the nuclear center of the lens, while lamellar cataracts occur in specific layers. It is believed that presbyopia may be an early precursor of age-related nuclear cataract[29,30]. Finally, cortical cataracts refer to any opacifications that occur in the lens periphery, or cortex.

Many different factors can lead to the onset of cataracts, including genetics, inflammation, accumulation of free radicals or other forms of cell damage, and defects in metabolite or nutrition distribution[31]. Mutations in any of several key lens proteins can cause congenital cataracts, or increase the chances of cataract forming in the aging lens[32]. Repeated inflammation of ocular tissues can cause immune cells to enter the eye and release enzymes or hydrogen peroxide, leading to damage of lens cell membranes[33]. Exposure to ultraviolet light can ultimately lead to damaged lens proteins, resulting in protein aggregation or degradation, and age-related cataracts[34]. Antioxidants, particularly glutathione, are abundant throughout the lens in order to protect against such oxidative and free radical damage[35]. Unfortunately, glutathione is either unable to diffuse into the aging lens nucleus, or there is simple a lower concentration with age[36]. Deficiencies in nutrition[37,38], in the case of diseases like diabetes[39–43], can also increase the likelihood of cataract.

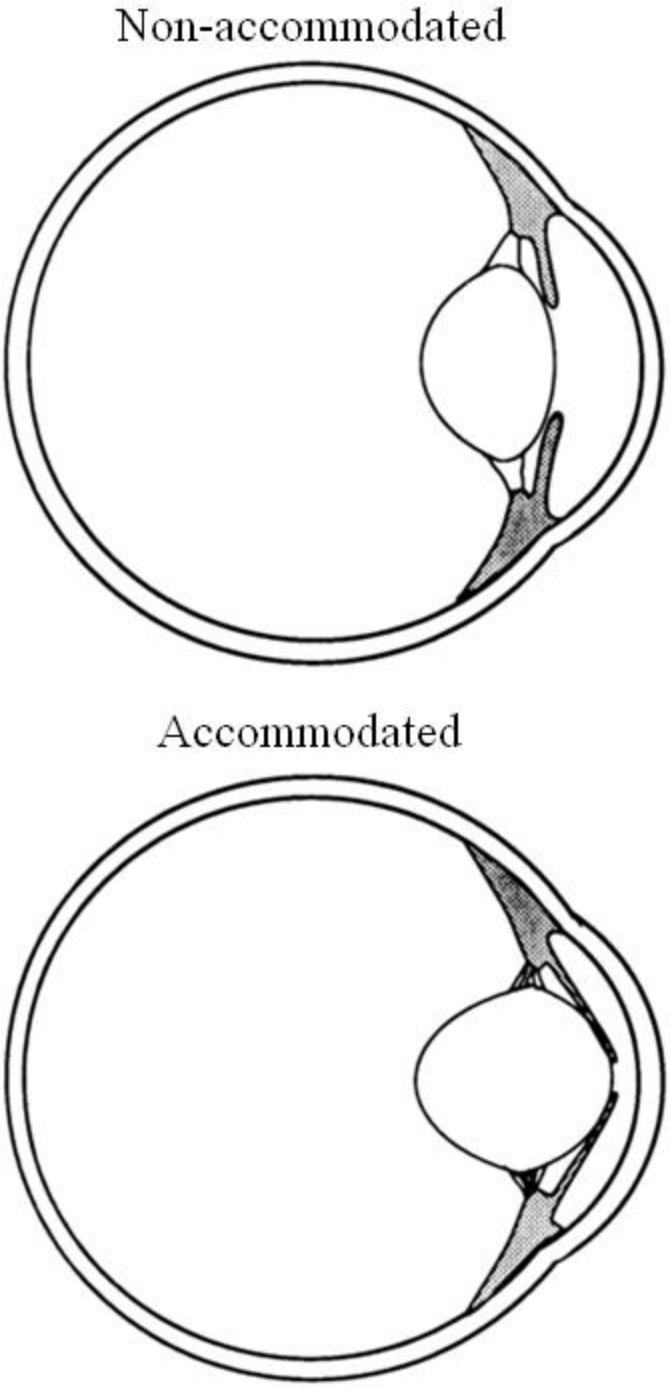

Figure 1.3. Schematic representation of lens geometry at rest and during accommodation. Modified from Crawford et al., 1990[44].

1.5 Connexins and Gap Junction Communication

The crystalline lens needs to maintain transparency in order to function, transmitting and focusing light without scattering. The lens therefore needs to maintain proper homeostasis and distribution of lens crystallins to achieve optimal solubility and avoid protein aggregation[45,46]. An extensive network of gap junction channels exists between lens cells to achieve this balance and allow for transport of many small molecules such as ions, water, and metabolites[47,48].

Connexin proteins form these gap junction channels between lens cells, creating an extensive coupling network to allow small molecules (<1200Da) to flow freely from cell to cell [49,50]. Specific networks are formed between lens epithelial-epithelial, epithelial-fiber, and fiber-fiber cells. The lens expresses three forms of connexin proteins, α8 (Cx50), α3 (Cx46), and α1 (Cx43)[51]. Connexin α8 is expressed in differentiated fibers and lens epithelial cells[52], connexin α3 is highly expressed during lens fiber cell differentiation, while connexin α1 is only expressed in low levels in epithelial cells and not at all in lens fibers.

1.6 Lens Crystallins

Crystallin proteins make up 90% of all lens proteins and consist of α, β, and γ classes, each with their own subgroups and subunits[45]. The defining characteristics of the lens that must always be maintained are that 1. it needs to be transparent to allow transmission of light through its center, and 2. it needs to keep an appropriately high refractive index to focus that light onto the retina accurately[53]. Extremely high concentrations of these lens proteins, and other small molecules, need to be maintained in an organized fashion to create the necessary high refractive index and resulting transparency[54]. This delicate balance can be disturbed during the aging process, and during formation of cataract, leading to changes in how these lens proteins interact with each other and with the fiber cell cytoskeleton[32,55,56]. High molecular weight aggregates may form, resulting in scattering of light and opacification of the lens[57–60]. Several of the mechanisms in charge of maintaining and controlling this delicate balance of high protein concentration among the crystallin and non-crystallin proteins of the lens remain unclear. Many of the events that ultimately lead to aggregation of these proteins also remains unknown, either from a breakdown in how these lens proteins interact among each other, or from external environmental factors, or a buildup of oxidative damage over time.

1.7 α-Crystallins

Alpha-crystallins consist of two subunits, αA- and αB-crystallin subunits, and make up nearly 30% of all lens proteins[61]. Alpha-crystallins exist within the lens naturally as polydispersed heteromeric aggregates, making their structure difficult to isolate and study[62]. The αA-crystallin subunit is encoded by the *CryaA* gene in mice on chromosome 17, but on human chromosome 21. The αB-crystallin subunit is encoded by the *CryaB* gene on mouse chromosome 9, but on chromosome 11 in humans. The αA-crystallin subunit is a 173 amino acid residue polypeptide while αB-crystallin is 175 amino acids long. Both subunits share about 60% amino acid sequence identity[63]. The molar ratio of αA to αB subunits also changes depending on location within the lens, ranging from 1:3 in the germinative epithelium all the way to 3:1 in differentiating

elongating fibers. The αB subunit can be found in various other non-ocular tissues such as the heart, brain, lungs, skin, and skeletal muscle, while the αA subunit is only found in small concentrations in the thymus, retina, and spleen.

1.8 Lens Cytoskeleton

The lens is a highly organized structure evidenced by its highly elongated and perfectly aligned lens fiber cells. These stacked fiber cells exhibit hexagonal packing in cross section, a property required for optical clarity[18,24,64,65]. Precise organization of several cytoskeletal elements is necessary to achieve this level of cellular arrangement, and error in this organization can affect both lens transparency and overall stiffness. Indeed previous studies with mice that have had the lens-specific intermediate filament CP49 knocked out have shown that the stiffness of the whole lens decreases as compared to wilt-type mice[66]. Other studies have shown that cytoskeletal remodeling proteins such as tropomodulin and periaxin also have an effect on fiber cell organization and whole lens stiffness[67]. For instance, Tmod1 is important for hexagonal packing of lens fiber cells[68–71], and regulating actin in the lens fiber cell maturation process[72]. The loss of CP49 alone does not cause an adverse effect on the packing geometry in the studies by Gokhin et al., but their measurements did reveal that at higher loads, the CP49 null lenses were softer. Exactly how these proteins act to orchestrate the intricate assembly of lens fiber cells remains unknown.

References for Chapter 1

1. Papadopoulos P, Papadopoulos A. Current management of presbyopia. *Middle East Afr J Ophthalmol*. 2014;21(1):10. doi:10.4103/0974-9233.124080.

2. Goertz AD, Stewart WC, Burns WR, Stewart JA, Nelson LA. Review of the impact of presbyopia on quality of life in the developing and developed world. *Acta Ophthalmol*. 2014;92(6):497-500. doi:10.1111/aos.12308.

3. Glasser A. Restoration of accommodation: Surgical options for correction of presbyopia. *Clin Exp Optom*. 2008;91(3):279-295. doi:10.1111/j.1444-0938.2008.00260.x.

4. Alió JL, Alió del Barrio JL, Vega-Estrada A. Accommodative intraocular lenses: where are we and where we are going. *Eye Vis*. 2017;4(1):16. doi:10.1186/s40662-017-0077-7.

5. Pepose JS, Burke JS, Qazi MA. Accommodating Intraocular Lenses. *Asia-Pacific J Ophthalmol*. June 2017:1-8. doi:10.22608/APO.2017198.

6. Frick KD, Joy SM, Wilson DA, Naidoo KS, Holden BA. The Global Burden of Potential Productivity Loss from Uncorrected Presbyopia. *Ophthalmology*. 2015;122(8):1706-1710. doi:10.1016/j.ophtha.2015.04.014.

7. Tsuneyoshi Y, Higuchi A, Negishi K, Tsubota K. Suppression of presbyopia progression with pirenoxine eye drops: experiments on rats and non-blinded, randomized clinical trial of efficacy. *Sci Rep*. 2017;7(1):6819. doi:10.1038/s41598-017-07208-6.

8. Monaco G, Gari M, Di Censo F, Poscia A, Ruggi G, Scialdone A. Visual performance after bilateral implantation of 2 new presbyopia-correcting intraocular lenses: Trifocal versus extended range of vision. *J Cataract Refract Surg*. 2017;43(6):737-747. doi:10.1016/j.jcrs.2017.03.037.

9. Pedrotti E, Mastropasqua R, Bonetto J, et al. Quality of vision, patient satisfaction and long-term visual function after bilateral implantation of a low addition multifocal intraocular lens. *Int Ophthalmol*. July 2017. doi:10.1007/s10792-017-0652-x.

10. Binder PS. Intracorneal Inlays for the Correction of Presbyopia. *Eye Contact Lens Sci Clin Pract*. June 2017:1. doi:10.1097/ICL.0000000000000381.

11. Gong X, Li E, Klier G, et al. Disruption of α3 connexin gene leads to proteolysis and cataractogenesis in mice. *Cell*. 1997;91(6):833-843. doi:10.1016/S0092-8674(00)80471-7.

12. Gong X, Wang X, Han J, Niesman I, Huang Q, Horwitz J. Development of cataractous macrophthalmia in mice expressing an active MEK1 in the lens. *Invest Ophthalmol Vis Sci*. 2001;42(3):539-548. http://www.ncbi.nlm.nih.gov/pubmed/11222509. Accessed April 30, 2013.

13. Xia C, Cheung D, DeRosa AM, et al. Knock-in of alpha3 connexin prevents severe cataracts caused by an alpha8 point mutation. *J Cell Sci*. 2006;119(Pt 10):2138-2144.

doi:10.1242/jcs.02940.

14. Beebe DC. Maintaining transparency: A review of the developmental physiology and pathophysiology of two avascular tissues. *Semin Cell Dev Biol*. 2008;19(2):125-133. doi:10.1016/j.semcdb.2007.08.014.

15. Wang D, Zheng W, Xie Y, et al. Tissue-specific mechanical and geometrical control of cell viability and actin cytoskeleton alignment. *Sci Rep*. 2014;4:6160. doi:10.1038/srep06160.

16. Zelenka PS. Regulation of cell adhesion and migration in lens development. *Int J Dev Biol*. 2004;48(8-9):857-865. doi:10.1387/ijdb.041871pz.

17. White TW. Unique and redundant connexin contributions to lens development. *Science*. 2002;295(5553):319-320. doi:10.1126/science.1067582.

18. Kuszak JR. The development of lens sutures. In: *Progress in Retinal and Eye Research*. Vol 14. ; 1995:567-591. doi:10.1016/1350-9462(94)00019-C.

19. Zhao H, Yang T, Madakashira BP, et al. Fibroblast growth factor receptor signaling is essential for lens fiber cell differentiation. *Dev Biol*. 2008;318(2):276-288. doi:10.1016/j.ydbio.2008.03.028.

20. Straub BK, Boda J, Kuhn C, et al. A novel cell-cell junction system: the cortex adhaerens mosaic of lens fiber cells. *J Cell Sci*. 2003;116(Pt 24):4985-4995. doi:10.1242/jcs.00815.

21. Jarrin M, Pandit T, Gunhaga L. A balance of FGF and BMP signals regulates cell cycle exit and Equarin expression in lens cells. *Mol Biol Cell*. 2012;23(16):3266-3274. doi:10.1091/mbc.E12-01-0075.

22. de Iongh RU, Chen Y, Kokkinos MI, McAvoy JW. BMP and activin receptor expression in lens development. *Mol Vis*. 2004;10(August):566-576.

23. Donaldson PJ, Grey AC, Maceo Heilman B, Lim JC, Vaghefi E. The physiological optics of the lens. *Prog Retin Eye Res*. 2016. doi:10.1016/j.preteyeres.2016.09.002.

24. Al-Ghoul KJ, Nordgren RK, Kuszak a J, Freel CD, Costello MJ, Kuszak JR. Structural evidence of human nuclear fiber compaction as a function of ageing and cataractogenesis. *Exp Eye Res*. 2001;72:199-214. doi:10.1006/exer.2000.0937.

25. Glasser A, Kaufman PL. The mechanism of accommodation in primates. *Ophthalmology*. 1999;106(5):863-872. doi:10.1016/S0161-6420(99)00502-3.

26. Strenk S a, Strenk LM, Koretz JF. The mechanism of presbyopia. *Prog Retin Eye Res*. 2005;24(3):379-393. doi:10.1016/j.preteyeres.2004.11.001.

27. Glasser A. Accommodation: mechanism and measurement. *Ophthalmol Clin North Am*. 2006;19(1):1-12, v. doi:10.1016/j.ohc.2005.09.004.

28. Lanchares E, Navarro R, Calvo B. Hyperelastic modelling of the crystalline lens: Accommodation and presbyopia. *J Optom*. 2012;5(3):110-120.

doi:10.1016/j.optom.2012.05.006.

29. Michael R, Bron AJ. The ageing lens and cataract: a model of normal and pathological ageing. *Philos Trans R Soc Lond B Biol Sci*. 2011;366(1568):1278-1292. doi:10.1098/rstb.2010.0300.

30. Heys KR, Cram SL, Truscott RJW. Massive increase in the stiffness of the human lens nucleus with age: the basis for presbyopia? *Mol Vis*. 2004;10(December):956-963. http://www.ncbi.nlm.nih.gov/pubmed/15616482.

31. Abraham AG, Condon NG, West Gower E. The new epidemiology of cataract. *Ophthalmol Clin North Am*. 2006;19(4):415-425. doi:10.1016/j.ohc.2006.07.008.

32. Graw J. Genetics of crystallins: cataract and beyond. *Exp Eye Res*. 2009;88(2):173-189. doi:10.1016/j.exer.2008.10.011.

33. Krishnaiah S, Vilas K, Shamanna BR, Rao GN, Thomas R, Balasubramanian D. Smoking and Its Association with Cataract: Results of the Andhra Pradesh Eye Disease Study from India. *Investig Opthalmology Vis Sci*. 2005;46(1):58. doi:10.1167/iovs.04-0089.

34. Balasubramanian D. PHOTODYNAMICS OF CATARACT: AN UPDATE ON ENDOGENOUS CHROMOPHORES AND ANTIOXIDANTS. *Photochem Photobiol*. 2004;81(3):498-501. doi:10.1562/2004-11-01-RA-354.

35. Rao GN, Sadasivudu B, Cotlier E. Studies on glutathione S-transferase, glutathione peroxidase and glutathione reductase in human normal and cataractous lenses. *Ophthalmic Res*. 1983;15(4):173-179. http://www.ncbi.nlm.nih.gov/pubmed/6138744. Accessed July 31, 2017.

36. Sweeney MH, Truscott RJ. An impediment to glutathione diffusion in older normal human lenses: a possible precondition for nuclear cataract. *Exp Eye Res*. 1998;67(5):587-595. doi:10.1006/exer.1998.0549.

37. Agarwal R, Iezhitsa IN, Agarwal P, Spasov AA. Mechanisms of cataractogenesis in the presence of magnesium deficiency. *Magnes Res*. 2013;26(1):2-8. doi:10.1684/mrh.2013.0336.

38. Bunce GE, Kinoshita J, Horwitz J. Nutritional Factors in Cataract. *Annu Rev Nutr*. 1990;10(1):233-254. doi:10.1146/annurev.nu.10.070190.001313.

39. Stefek M, Karasu C. Eye Lens in Aging and Diabetes: Effect of Quercetin. *Rejuvenation Res*. 2011;14(5):525-534. doi:10.1089/rej.2011.1170.

40. Wang F, Javitt JC. Eye care for elderly Americans with diabetes mellitus. Failure to meet current guidelines. *Ophthalmology*. 1996;103(11):1744-1750. http://www.ncbi.nlm.nih.gov/pubmed/8942865. Accessed August 4, 2017.

41. Chylack LT, Cheng H-M. Sugar metabolism in the crystalline lens. *Surv Ophthalmol*. 1978;23(1):26-34. doi:10.1016/0039-6257(78)90195-9.

42. Abrass CK, Spicer D, Berfield AK, St John PL, Abrahamson DR. Diabetes induces changes in glomerular development and laminin-beta 2 (s-laminin) expression. *Am J Pathol*. 1997;151(4):1131-1140. http://www.pubmedcentral.nih.gov/articlerender.fcgi?artid=1858041&tool=pmcentrez&rendertype=abstract. Accessed November 2, 2011.

43. Elanchezhian R, Palsamy P, Madson CJ, et al. Low glucose under hypoxic conditions induces unfolded protein response and produces reactive oxygen species in lens epithelial cells. *Cell Death Dis*. 2012;3:e301. doi:10.1038/cddis.2012.40.

44. Crawford KS, Kaufman PL, Bito LZ. The role of the iris in accommodation of rhesus monkeys. *Invest Ophthalmol Vis Sci*. 1990;31(10):2185-2190. http://www.ncbi.nlm.nih.gov/pubmed/2211015. Accessed August 8, 2017.

45. Bloemendal H, de Jong W, Jaenicke R, Lubsen NH, Slingsby C, Tardieu A. Ageing and vision: structure, stability and function of lens crystallins. *Prog Biophys Mol Biol*. 2004;86(3):407-485. doi:10.1016/j.pbiomolbio.2003.11.012.

46. Addison PKF, Berry V, Holden KR, et al. A novel mutation in the connexin 46 gene (GJA3) causes autosomal dominant zonular pulverulent cataract in a Hispanic family. *Mol Vis*. 2006;12:791-795. http://www.ncbi.nlm.nih.gov/pubmed/16885921. Accessed August 4, 2017.

47. Goodenough DA. The crystalline lens. A system networked by gap junctional intercellular communication. *Semin Cell Biol*. 1992;3(1):49-58. http://www.ncbi.nlm.nih.gov/pubmed/1320431. Accessed July 31, 2017.

48. Jiang JX, Goodenough D a. Phosphorylation of lens-fiber connexins in lens organ cultures. *Eur J Biochem*. 1998;255(1):37-44. http://www.ncbi.nlm.nih.gov/pubmed/9692898.

49. Donaldson P, Kistler J, Mathias RT. Molecular Solutions to Mammalian Lens Transparency. *News Physiol Sci*. 2001;15:118-123.

50. Kumar NM, Gilula NB. The gap junction communication channel. *Cell*. 1996;84(3):381-388. http://www.ncbi.nlm.nih.gov/pubmed/8608591. Accessed August 4, 2017.

51. Gong X, Cheng C, Xia C. Connexins in lens development and cataractogenesis. *J Membr Biol*. 2007;218(1-3):9-12. doi:10.1007/s00232-007-9033-0.

52. White TW, Bruzzone R, Goodenough DA, Paul DL. Mouse Cx50, a functional member of the connexin family of gap junction proteins, is the lens fiber protein MP70. *Mol Biol Cell*. 1992;3(7):711-720. http://www.ncbi.nlm.nih.gov/pubmed/1325220. Accessed July 31, 2017.

53. Andley UP. Crystallins in the eye: Function and pathology. *Prog Retin Eye Res*. 2007;26(1):78-98. doi:10.1016/j.preteyeres.2006.10.003.

54. Xia C, Liu H, Chang B, et al. Arginine 54 and Tyrosine 118 residues of {alpha}A-crystallin are crucial for lens formation and transparency. *Invest Ophthalmol Vis Sci*.

2006;47(7):3004-3010. doi:10.1167/iovs.06-0178.

55. Sharma KK, Santhoshkumar P. Lens aging: effects of crystallins. *Biochim Biophys Acta*. 2009;1790(10):1095-1108. doi:10.1016/j.bbagen.2009.05.008.

56. Andley UP. Crystallins and hereditary cataracts: molecular mechanisms and potential for therapy. *Expert Rev Mol Med*. 2006;8(25):1-19. doi:10.1017/S1462399406000111.

57. Wang K, Cheng C, Li L, et al. gammaD-Crystallin–Associated Protein Aggregation and Lens Fiber Cell Denucleation. *Invest Ophthalmol Vis Sci*. 2007;48(8):3719-3728. doi:10.1167/iovs.06-1487.

58. Li L, Chang B, Cheng C, et al. Dense nuclear cataract caused by the gammaB-crystallin S11R point mutation. *Invest Ophthalmol Vis Sci*. 2008;49(1):304-309. doi:10.1167/iovs.07-0942.

59. Huang Q, Ding L, Phan KB, et al. Mechanism of cataract formation in alphaA-crystallin Y118D mutation. *Invest Ophthalmol Vis Sci*. 2009;50(6):2919-2926. doi:10.1167/iovs.08-3070.

60. Cheng C, Xia C, Huang Q, Ding L, Horwitz J, Gong X. Altered chaperone-like activity of alpha-crystallins promotes cataractogenesis. *J Biol Chem*. 2010;285(52):41187-41193. doi:10.1074/jbc.M110.154534.

61. Groenen PJ, Merck KB, de Jong WW, Bloemendal H. Structure and modifications of the junior chaperone alpha-crystallin. From lens transparency to molecular pathology. *Eur J Biochem*. 1994;225(1):1-19. http://www.ncbi.nlm.nih.gov/pubmed/7925426.

62. Slingsby C, Norledge B, Simpson A, et al. X-ray diffraction and structure of crystallins. *Prog Retin Eye Res*. 1997;16(1):3-29. doi:10.1016/S1350-9462(96)00018-3.

63. Van Montfort R, Slingsby C, Vierling E. Structure and function of the small heat shock protein/α-crystallin family of molecular chaperones. *Adv Protein Chem*. 2001;59:105-156. doi:10.1016/S0065-3233(01)59004-X.

64. Kuszak JR, Zoltoski RK, Sivertson C. Fibre cell organization in crystalline lenses. *Exp Eye Res*. 2004;78(3):673-687. http://www.ncbi.nlm.nih.gov/pubmed/15106947. Accessed November 12, 2013.

65. Kuszak JR, Zoltoski RK, Tiedemann CE. Development of lens sutures. *Int J Dev Biol*. 2004;48(8-9):889-902. doi:10.1387/ijdb.041880jk.

66. Fudge DS, McCuaig J V, Van Stralen S, et al. Intermediate filaments regulate tissue size and stiffness in the murine lens. *Invest Ophthalmol Vis Sci*. 2011;52(6):3860-3867. doi:10.1167/iovs.10-6231.

67. Gokhin DS, Nowak RB, Kim NE, et al. Tmod1 and CP49 Synergize to Control the Fiber Cell Geometry, Transparency, and Mechanical Stiffness of the Mouse Lens. *PLoS One*. 2012;7(11):e48734. doi:10.1371/journal.pone.0048734.

68. Fischer RS, Lee A, Fowler VM. Tropomodulin and tropomyosin mediate lens cell actin cytoskeleton reorganization in vitro. *Invest Ophthalmol Vis Sci*. 2000;41(1):166-174. http://www.ncbi.nlm.nih.gov/pubmed/10634617. Accessed January 13, 2012.

69. Nowak RB, Fischer RS, Zoltoski RK, Kuszak JR, Fowler VM. Tropomodulin1 is required for membrane skeleton organization and hexagonal geometry of fiber cells in the mouse lens. *J Cell Biol*. 2009;186(6):915-928. doi:10.1083/jcb.200905065.

70. Yamashiro S, Gokhin DS, Kimura S, Nowak RB, Fowler VM. Tropomodulins: pointed-end capping proteins that regulate actin filament architecture in diverse cell types. *Cytoskeleton (Hoboken)*. 2012;69(6):337-370. doi:10.1002/cm.21031.

71. Nowak RB, Fowler VM. Tropomodulin 1 constrains fiber cell geometry during elongation and maturation in the lens cortex. *J Histochem Cytochem*. 2012;60(6):414-427. doi:10.1369/0022155412440881.

72. Cheng C, Nowak RB, Biswas SK, Lo W-K, FitzGerald PG, Fowler VM. Tropomodulin 1 Regulation of Actin Is Required for the Formation of Large Paddle Protrusions Between Mature Lens Fiber Cells. *Invest Ophthalmol Vis Sci*. 2016;57(10):4084-4099. doi:10.1167/iovs.16-19949.

Chapter 2 Lens Stiffness in Connexin Mutant Lenses

2.1 Introduction

The most significant change that leads to presbyopia is the progressive stiffening of the lens with increasing age[1–5]. An understanding of the ways in which human lenses grow stiffer could potentially provide ways to delay or prevent the onset of presbyopia and allow the lens to continue to change shape later in life[6,7].

Several changes could lead to the increase in stiffness of the aging lens[8]. For instance, the lens continues to grow in size by adding additional layers of lens fiber cells to the outside bulk of the lens[9]. A lack of protein renewal in the inner layers of the lens results in an accumulation of several post-translational modifications as well as increasing oxidative damage and cross-linking of lens proteins throughout our lifetime[10]. Therefore, the transparency of the lens decreases as the lens grows older, potentially leading to age-related cataract, a visible opacity in the lens that can cause vision loss if on the visual axis[11].

In addition, proteins required for proper organization of lens fiber cells have also been shown to affect lens stiffness. For instance, Tropomodulin1 is an actin capping protein required for the hexagonal geometry of the lens fiber cells[12–14]. Loss of Tmod1 in mice results in a

decrease in load-bearing ability[15]. Similar results were obtained upon loss of the lens-specific beaded filament CP49[16]. This study aims to investigate how interaction between lens proteins, cell cytoskeleton, and cell membrane affects bulk lens stiffness, as well as changes to the fiber cell architecture during compression, through the use of several mouse strains and lens mutants.

Although mice lack fully developed ciliary muscles and mouse lenses do not accommodate like the primate lens, mouse lenses have similar cellular architecture for lens stiffness and transparency that can be measured in vitro[15,17]. Mice are readily available, relatively inexpensive, age rapidly, and a vast variety of genetic backgrounds are available for testing. Recent studies also indicate that mouse lens stiffness is affected by age and various genetic backgrounds of mouse strains and gene mutations[7,16].

Various methods have been used to measure stiffness in human lenses, such as penetration using a conical probe[18], squeezing by an actuator[7,19], stacking several static weights on top of the lens[15], and spinning of lenses[20–22]. Here, a highly adjustable muscle lever device is used to measure stiffness of lenses from mice of several different age groups and genetic backgrounds. This device can provide an accurate measure of force and displacement exerted onto the lens, and from those measurements stiffness values can be calculated.

2.2 Methods

Mice

This study followed the ARVO Statement for the Use of Animals in Ophthalmic and Vision Research and an ACUC approved animal protocol (UC Berkeley). Animals were housed with free access to food and water, with a 12:12 h light:dark cycle, and sacrificed by CO_2 inhalation followed by cervical dislocation. All efforts were made to minimize animal suffering.

The mouse strains used in this study were: wild-type C57BL/6J (CP49(B6/B6) 294(B6/B6) Gja3+/+), wild-type 129-SvJae (CP49(129/129) 294(129/129) Gja3+/+), Gja3 connexin (Cx46 or α3) knockout (Gja3-/-) mutants in both B6 and 129 strain backgrounds (CP49(B6/B6) 294(B6/B6) Gja3-/- and CP49(129/129) 294(129/129) Gja3-/-), and periaxin variants in both B6 and 129 strain backgrounds, with both wild-type and knockout mutant Gja3 connexin (CP49(B6/B6) 294(129/129) Gja3+/+, CP49(B6/B6) 294(129/129) Gja3-/-, CP49(129/129) 294(B6/B6) Gja3+/+, and CP49(129/129) 294(B6/B6) Gja3-/-). MIT 294 is used as a genomic locus for the periaxin gene. All mice used for muscle lever compression testing were either 4 weeks or 40+ weeks old. All mice used for fiber cell width analysis were 4 weeks old.

Lens Images

Images of freshly dissected lenses were collected by using a dissection microscope (MZ16 Leica) with a digital camera. Lenses were dissected in 1X phosphate buffered saline (PBS) at 37°C. For side images, lenses were placed near a 45° right angle mirror.

Biomechanical Compression Testing Using Muscle Lever

Mouse lenses used for muscle lever experiments were extracted from sacrificed animals and imaged from the top and side immediately after dissection, as above. Lenses were then transferred to individual tubes submerged in warm, clear Dulbecco's Modified Eagle Medium (DMEM) while being transported to the muscle lever. Each lens was placed one at a time inside a clear, plastic chamber filled with warm, clear DMEM during compression testing. A hand camera was used to record lens compression during the entirety of each trial, and to visually confirm proper placement of the lens and muscle lever. Mechanical testing was performed by lowering a hardened clay top-piece attached to a needle connected to the muscle lever onto the submerged lens sample. The loading regimen used was a triangle wave with a maximum of 2mN of force, and a period of four minutes; the maximum force value of 2mN was reached after two minutes, after which the lens was unloaded back to 0mN. Force and displacement data were collected every 0.2 seconds during the testing protocol. The lever was then raised out from the chamber and the lens was continually recorded up to 3 minutes afterwards. Matlab vR2009b software was used to access and analyze the data generated by the muscle lever. The average and

standard deviation of maximum displacement measurements were plotted in Excel. Student's t-test was used to determine statistical significance.

Vibratome Sections

Lenses were compressed using a series of coverslips as described previously[23]. Briefly, freshly dissected lenses from 4 week old mice were placed in clear, plastic chambers filled with 4% paraformaldehyde (PFA) in 1X PBS and fixed for 1 hour at room temperature. For each pair of lenses extracted from each mouse, one lens was fixed uncompressed, while the other was fixed under static compression using 16 circular glass coverslips with a diameter of 12mm to mimic the compression experienced during the muscle lever experiments. Dozens of 12mm coverslips were first weighed using an analytical balance to determine an average coverslip weight. For consistency, the same set of coverslips was used for each experiment, and 16 coverslips was calculated to approximately mimic the compression experienced by the lenses during muscle lever compression. A small piece of plastic measuring approximately 1mm in height was positioned with super glue in the corner of each plastic chamber to allow the coverslips to more directly compress each lens vertically, as opposed to compressing them at an angle. After fixation, lenses were washed in 1X PBS three times for 10 minutes each.

Fixed lenses were then mounted with super glue onto an aluminum sectioning stand. Lenses were covered with warm 2.5% agar noble, then submerged in cold 1X PBS at 6-10°C and sectioned using a Leica VT 1000S microtome with a speed setting of 3 to 4, and frequency setting of 6 to 7. Lens cross sections between 100-150μm in thickness from similar depths (near the equator of each lens) in different lens samples were collected and post-fixed for 10 minutes with cold 4% PFA in 1X PBS and then washed in cold 1X PBS three times before staining.

Immunohistochemistry

Fixed and washed lens sections were incubated with Alexa Fluor 488 Phalloidin (Thermo Fisher Scientific, Inc.) and Rhodamine wheat germ agglutinin (WGA) (Vector Laboratories, Inc., Burlingame, CA) for 2 hours at room temperature in a blocking solution consisting of 3% bovine serum albumin (BSA) (Research Products International, Mt Prospect, IL), 3% normal goat serum (NGS) (Vector Laboratories, Inc., Burlingame, CA), and 0.3% Triton X-100 in 1X PBS. Slides were then washed three times in 1X PBS and mounted with DAPI VectorShield mounting medium (Vector Laboratories, Inc., Burlingame, CA). Confocal images were collected by a Zeiss LSM700 confocal microscope. Staining was repeated at least three times, and representative results are shown.

Fiber cell width analysis

63X confocal images of both uncompressed and compressed lens sections from 4 week old B6 WT mice were analyzed using ImageJ software. Rows of fiber cells were first enumerated, and each fiber cell width within a row was measured. Cells containing nuclei were omitted in the

final analysis as they artificially overinflated the average fiber cell width. The two cells neighboring each nucleus-containing cell were also omitted from the analysis as they were often pushed aside from the larger nucleus, significantly thinning their width measurement. A bounding box of 40µm in width and 100µm in height was drawn approximately 10µm from the lens surface. A second bounding box with the same dimensions was stacked next to the first, creating two distinct regions of 10-50µm from the lens surface, and 50-90µm from the lens surface. Only fiber cells fully within each bounding box were counted. The average and standard deviation of all fiber cell width measurements within each bounding box were plotted in Excel. Student's t-test was used to determine statistical significance.

2.3 Results

2.3.1 Characterization of lens genotypes

As expected, B6 wild-type (WT) lenses, CP49(B6/B6) 294(B6/B6) Gja3+/+, and 129 WT lenses, CP49(129/129) 294(129/129) Gja3+/+, at 4 weeks old were clear, as well as older lenses at 44+ weeks within the same respective strain background (Figure 2.1, first and fifth columns). Knockout of Gja3 produced a severe nuclear cataract in the pure 129 strain background, CP49(129/129) 294(129/129) Gja3-/-, but produced only a mild cataract in the B6 strain background, CP49(B6/B6) 294(B6/B6) Gja3-/-, in both age groups (Figure 2.1, third and seventh columns). Cataract severity was greatly diminished upon introduction of the B6 variant of periaxin in 129 Gja3-/- lenses, CP49(129/129) 294(B6/B6) Gja3-/- (Figure 2.1, eight column). The 129 variant of periaxin also produced a very subtle and mild cataract in B6 Gja3-/- lenses, CP49(B6/B6) 294(129/129) Gja3-/- (Figure 2.1, fourth column). Periaxin variants with wild-type Gja3 remained clear (Figure 2.1, second and sixth column).

2.3.2 Muscle lever lens compression

The muscle lever consists of a clay top-piece attached to a controllable lever arm by a thin metal pin. The position and / or force of the lever arm can be precisely controlled through Matlab software. Lens samples are submerged in warm Dulbecco's Modified Eagle Medium (DMEM) without phenol red in a clear plastic chamber with a handheld camera positioned to video record the lens during the entire compression trial, as well to confirm correct positioning of the lens and top-piece (Figure 2.2A). Videos of the entire compression process and up to three minutes after the removal of the clay top were recorded for each lens sample. Representative still images at various time points throughout the one such trial were captured from the video files and show the lens at various stages of compression (Figure 2.2B). The three minute rest period after each compression trial was found to be enough to visually observe the lens return to its original shape.

Representative displacement and force curves are presented to demonstrate typical data obtained during muscle lever compression. The force curve (green) follows a triangle wave starting at 0mN, peaking at 2mN after two minutes, and then returning to 0mN after two more minutes. The displacement curve (blue) reaches its peak value at two minutes, coinciding with the peak in force. This point of maximum displacement is what is used to compare lenses from each genotype and age group (Figure 2.2C, top). This data was also plotted as Force vs Displacement to help visualize additional mechanical properties of each compression trial (Figure 2.2C, bottom).

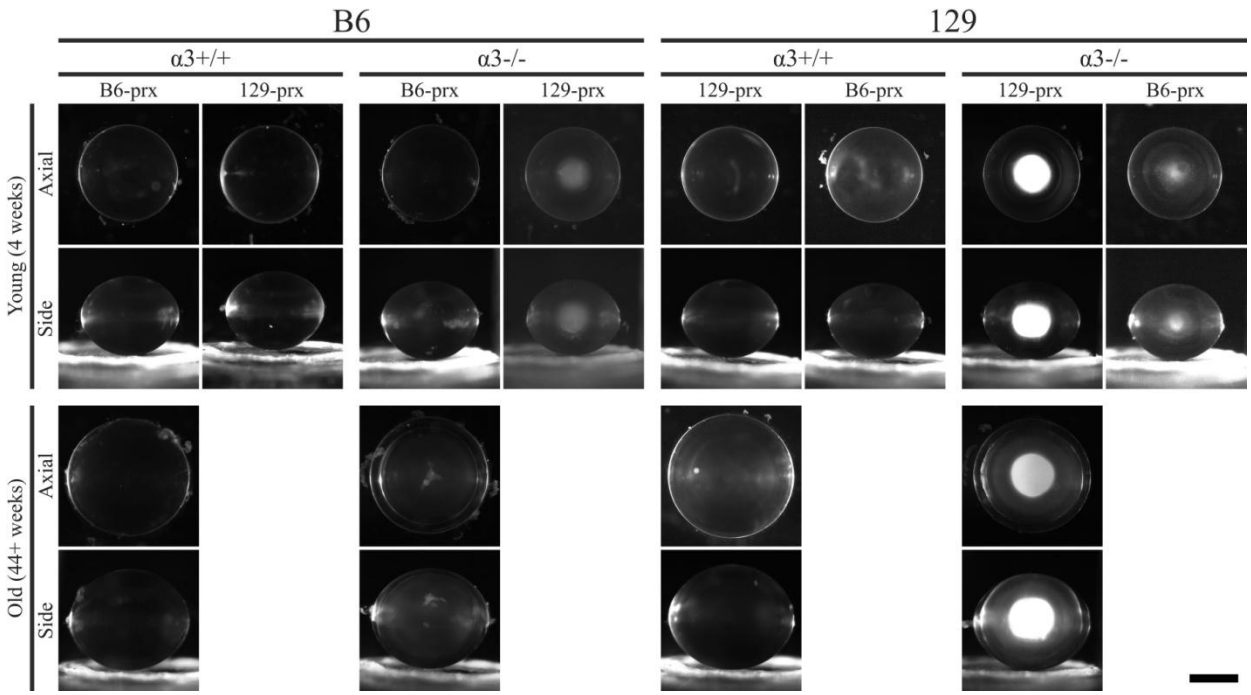

Figure 2.1. Representative lens images of all lens genotypes used for muscle lever compression. Both axial and side images of the same representative lens are shown. Young lenses (top two rows), were defined as exactly 4 weeks old, while Old lenses (bottom two rows) were 44 weeks or older. All lenses pictured in the left four columns were from the B6 strain background, CP49(B6/B6), while all lenses pictured in the right four columns were from the 129 strain background, CP49(129/129). Columns labeled as B6-prx were genotyped at MIT 294 as 294(B6/B6), while those labeled as 129-prx are 294(129/129). Scale bar, 1mm.

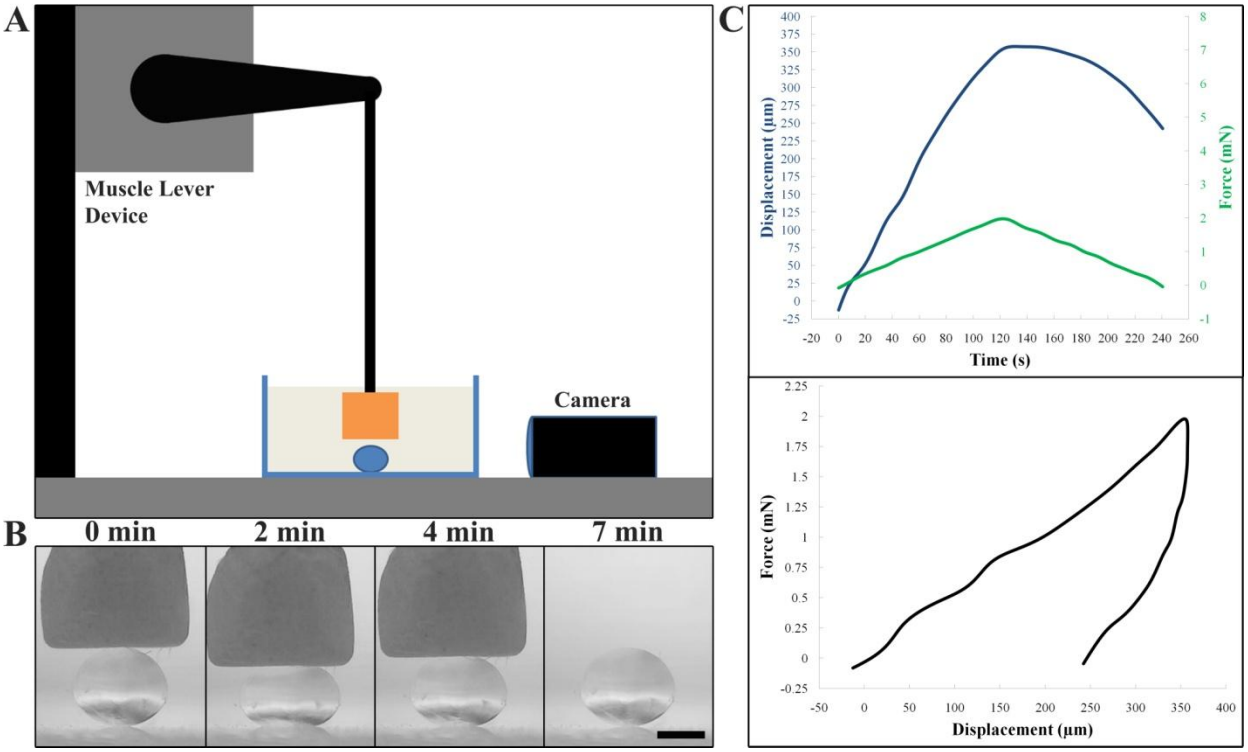

Figure 2.2. Muscle lever device setup. (A) Schematic of muscle lever system and placement of lens sample and camera. (B) Lens images at various time points throughout compression testing: first panel, 0 min, muscle lever just barely hovering over the lens; second panel, 2 min, muscle lever is exerting the maximum force, 2mN, and the lens is at its maximum displacement; third panel, 4 min, the muscle lever is exerting 0mN of force and the lens is almost fully recovered to its original shape; fourth panel, 7 min, the muscle lever was removed from the lens completely and the lens was allowed to fully recover for three additional minutes. Scale bar, 1mm. (C) Representative data generated by muscle lever system, graphed using Microsoft Excel. Top panel, displacement (µm) (blue curve) vs time (sec) on the left axis, and force (mN) (green curve) vs time (sec) on the right axis. Bottom panel, force (mN) vs displacement (µm). This particular data set was taken from a B6 WT 4 week old lens.

2.3.3 Stiffness differences between young and old lenses of different genetic backgrounds

A decrease in average maximum displacement is assumed in this study to be indicative of an increase in lens stiffness. Old lenses (40+ weeks) in both the B6 and 129 background strains appear stiffer because of their significant decrease in maximum displacement, as compared to young lenses (4 weeks) from the same genotype. Young B6 WT lenses averaged a maximum displacement of 328.5µm ± 18.9µm, n=9 lenses, while old B6 WT lenses only averaged 179.8µm ± 17.2µm, n=12. The same trend was seen in young and old lenses in the 129 strain background, with young 129 WT lenses averaging 303.7µm ± 20.7µm, n=6 and old 129 WT lenses averaging only 242.2µm ± 31.4µm, n=12 (Figure 2.3A, darker bars).

Knockout of connexin Gja3 appeared to stiffen lenses in almost all cases. Young B6 Gja3-/- lenses averaged only 251.9µm ± 39.2µm, n=16, significantly lower than their B6 WT counterparts from above ($p<0.0001$), while young 129 Gja3-/- averaged only slightly lower than 129 WT at 287.9µm ± 12.3µm, n=8 (not significant). Differences were much more drastic in older lenses, with old B6 Gja3-/- lenses averaging 128.6µm ± 24.1µm, n=12, significantly lower than from old B6 WT mice ($p<0.0001$), and old 129 Gja3-/- lenses averaging 127.0µm ± 23.2µm, n=7, also significantly lower than their old 129 WT counterparts ($p<0.0001$) (Figure 2.3A, each pair of dark and light bars).

2.3.4 Stiffness differences between different genetic backgrounds and periaxin variants

The specific variant of periaxin present appears to have an effect on the average maximum displacement. Young CP49(B6/B6) 294(129/129) Gja+/+ lenses averaging 288.9µm ± 16.5µm, n=16 did not appear significantly different than young Gja3-/- lenses of the same strain and periaxin variant, which averaged slightly lower at 273.5µm ± 31.5µm, n=15 (Figure 2.3B, first pair of bars). This indicates that the 129 variant of periaxin acts to stiffen the lens because previously these two groups of young lenses from the B6 strain background but with the B6 periaxin variant were significantly distinguishable from each other, with young CP49(B6/B6) 294(B6/B6) Gja+/+ lenses averaging a much higher average maximum displacement.

Interestingly, young CP49(129/129) 294(B6/B6) Gja+/+ lenses averaged 362.9µm ± 18.5µm, n=5, appearing significantly softer when compared with their corresponding Gja3-/- lenses of the same strain and periaxin variant, averaging 300.0µm ± 8.5µm, n=10 ($p<0.001$) (Figure 2.3B, second pair of bars). This led to the conclusion that the B6 variant of periaxin somehow acts to soften the lens because previously lenses from the 129 background with the 129 periaxin variant showed no significant difference between Gja3+/+ and Gja3-/-.

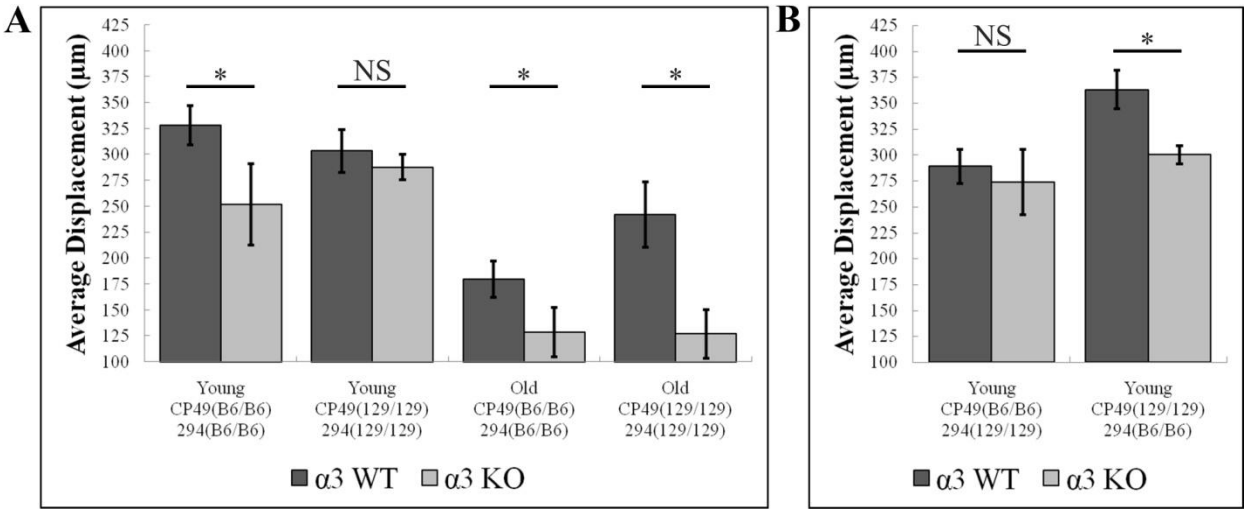

Figure 2.3. Average displacement +/- standard deviation of muscle lever at 2mN of applied force. (A) Comparison between young and old lenses of different genetic backgrounds and Gja3 knockout. (B) Comparison between different genetic backgrounds and periaxin variants. * = $p<0.001$, NS = not significant.

2.3.5 Examining lens fiber cell architecture during lens compression

Lenses from 4 week old B6 WT mice were used to further investigate the cell shape changes that might be occurring during compression of the lens. To mimic compression of the lens during muscle lever experiments, 16 glass coverslips with a diameter of 12mm were used to statically compress the lens during fixation using 4% paraformaldehyde (PFA) (Figure 2.4A). After 1 hour, coverslips were removed and compressed lenses retained their compressed shape (data not shown).

Representative 63X images from both uncompressed and compressed lenses, with bounding boxes used for ImageJ analysis outlined, are shown in Figure 2.4B. Two distinct regions were chosen to determine any potential shape changes that might be occurring during compression, approximately 10-50µm and 50-90µm from the lens surface. The width of these lens fiber cells was chosen as the representative parameter to analyze, but other parameters such as length, perimeter, aspect ratio, and total cross sectional area, were considered. Only individual fiber cell width measurements fully within each bounding box were counted and averaged for final analysis.

Two distinct shape changes appeared to occur within these two chosen regions. First, within the 10-50µm region, fiber cells in the uncompressed state averaged a width of 1.785µm ± 0.403µm, n=429 individual cell measurements across 3 lenses, while those in the compressed state averaged only 1.419µm ± 0.301µm, n=493 / 3 lenses, significantly thinner ($p<0.001$) (Figure 2.4C, first pair of bars). This indicated that near the very periphery of the lens, fiber cells appear to be stretched along their long axis during compression. Interestingly, the opposite trend was observed in the deeper 50-90µm region, with uncompressed fiber cells averaging 2.178µm ± 0.519µm, n=342 / 3 lenses and compressed fibers averaging slightly wider at 2.329µm ± 0.494µm, n=257 / 3 lenses. The average of the compressed fibers in this deeper region was found to be significantly wider than uncompressed fibers from the same region ($p<0.001$) (Figure 2.4C, second pair of bars), despite the absolute difference being quite subtle. This indicated that within this deeper region fiber cells were being stretched along their short axis during compression, taking on a more square-like cross-section

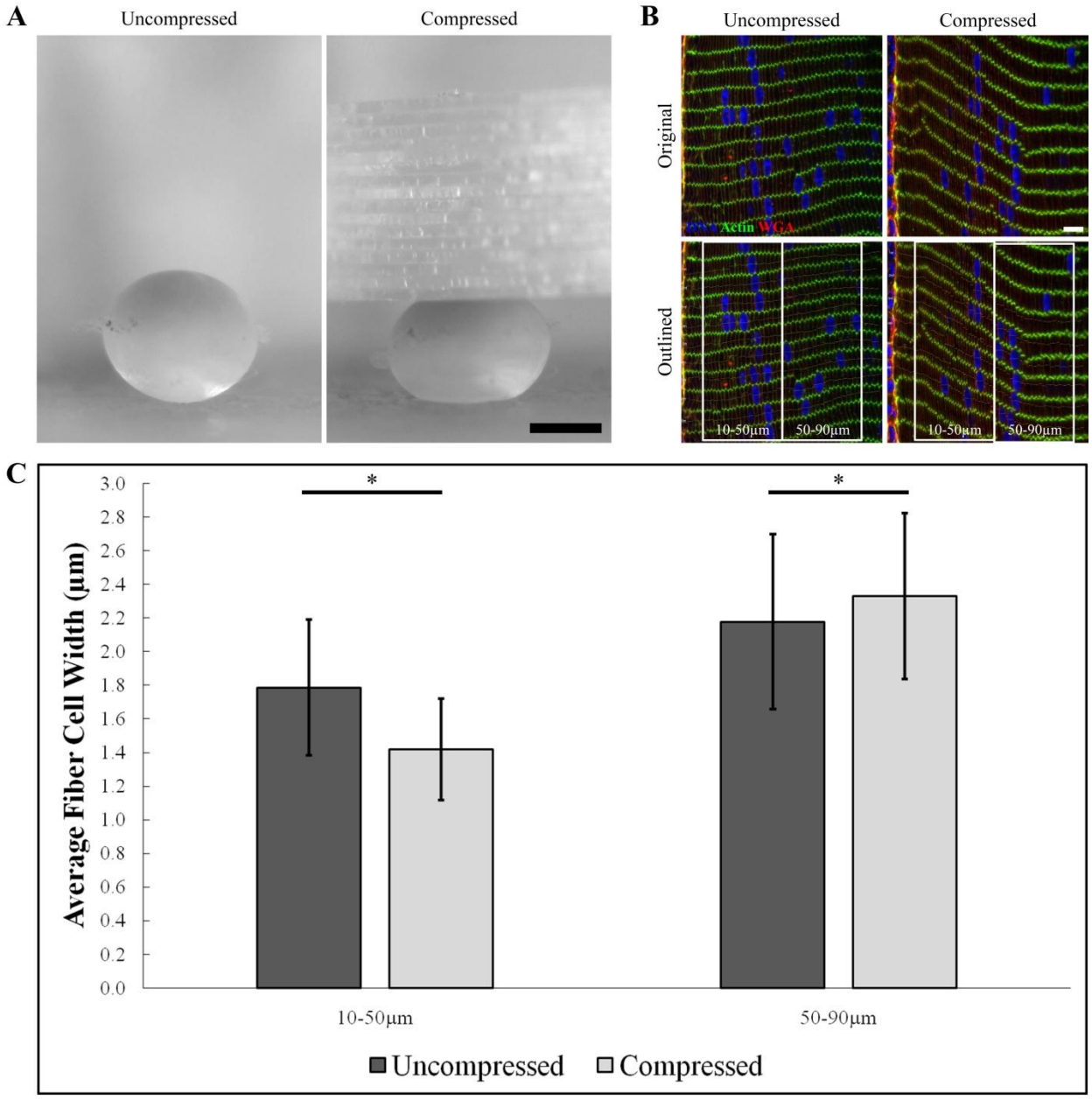

Figure 2.4. Representative images and analysis from coverslip-compressed, fixed lenses. (A) Side images of lens compression procedure using multiple coverslips. Left Panel: Uncompressed lens before application of coverslips, Right Panel: 16 coverslips are used to compress the lens while submerged in 4% PFA. Scale bar, 1mm. (B) Representative 63X images from 4 week old B6 WT lenses from Vibratome-cut lens sections in cross section. All sections were stained for DNA (DAPI, blue), Actin (phalloidin, green), and WGA (rhodamine, red). The top row displays the original 63X images, while the bottom row displays the 40µm-wide bins used to analyze the measured fiber cell widths. Scale bar, 10µm. (C) Graph summarizing the average fiber cell width measured within each 40µm-wide region between uncompressed and compressed lenses. * = $p<0.001$, Student's t-test.

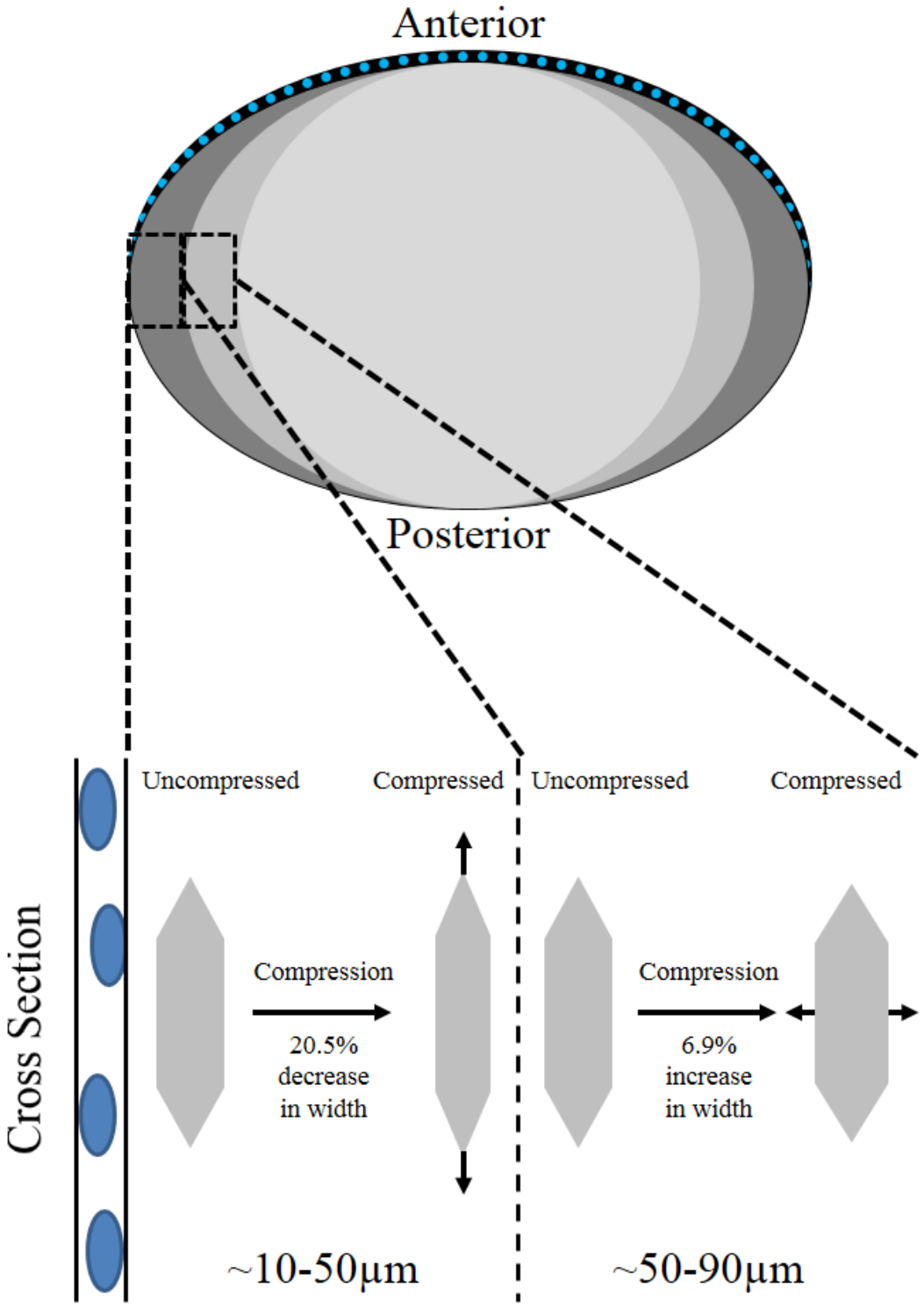

Figure 2.5. Summary of Lens Compression Model.

2.4 Discussion

This is the first time a modified muscle lever system was used to compare whole lens stiffness between lenses of different background, age, and genotype. We describe a system that is able to accurately record force and displacement data within a reasonable range for what might be experienced by a mouse lens. Several studies have linked an increase in lens stiffness with increasing age[5,7,15,21]. This increase in lens stiffness is greater in the lens nucleus; the lens nucleus is initially softer than the surrounding cortex until about the age of 40, after which the lens nucleus is stiffer[11,24]. Our measurements were on whole intact lenses, which do not permit differentiation between cortex and nucleus. Fresh whole lenses were chosen in this study to avoid any destructive structural damage that would ultimately be caused by freezing or slicing of the lens. Indeed with all samples measured we observed a return to the initial shape of the lens after removing the muscle lever clay top for three minutes, indicating that damage to the lens should be minimal.

We expected that a disruption of the lens fiber cell cytoskeleton would be reflected in the stiffness of the whole lens. Indeed previous studies with mice that have had the lens-specific intermediate filament CP49 knocked out have shown that the stiffness of the whole lens decreases as compared to wilt-type mice[16]. But the instruments used in that study were not as sensitive as the equipment used in this study, and may not have accurately measured the changes in stiffness between the two groups. In our study, the 129 background strain of mice also does not express CP49, but we found very little difference between 4 week old lenses, and actually the 129 lenses were a little stiffer. In older lenses though the difference in stiffness was much more prominent, and was actually reversed, resulting in older 129 lenses being much softer than their B6 counterparts.

Previous studies have shown that cytoskeletal remodeling proteins such as tropomodulin and periaxin do have an effect on whole lens stiffness[15]. For instance, Tmod1 is important for hexagonal packing of lens fiber cells, and it is plausible to believe that disruption of this intricate packing could have an effect on the stiffness of the whole lens[12–14]. The loss of CP49 alone does not cause an adverse effect on the packing geometry in the studies by Gokhin et al., but their measurements did reveal that at higher loads, the CP49 null lenses were softer. Our measurements use a dynamic loading regime whereas the studies by Gokhin used quasistatic procedures, with wait periods allowing for stress relaxation. This means that our measurements inherently contain a viscous component, which could account for the differences in CP49 null lens stiffness measurements.

In addition this work examined the cell structural changes that occurred during lens compression, mimicking the process of accommodation in mouse lenses, despite mouse lenses being unable to accommodate. We observed distinct shape changes near the surface of the lens corresponding to likely two regions of force distribution. The first region we defined as 10-50µm from the lens surface exhibited cells stretched along their long axis, while the second region in an area 50-90µm from the lens surface contained cells which appeared to be stretched along their short axis, resulting in a slightly wider cell (Figure 2.5). In preliminary trials, these fiber cell shape changes were found to be much more drastic in older lenses of 7 to 10 weeks of age, resulting in an almost square-like shape in deeper fibers. This indicates a system of force

distribution within the lens exists to allow for the bulk shape change of the lens that occurs during accommodation. This network, as was shown with the data presented above, can be perturbed either through disruptions in the cell to cell connections, as in the α3 connexin knockout lenses, or through differences in cytoskeletal arrangement, as in the differing variants of periaxin present in the B6 vs the 129 strain background. Further studies into exactly how these forces are distributed within the lens, and how certain lens proteins affect this distribution, will help us to reveal potential lens elasticity regulation mechanisms.

2.5 Acknowledgements

We would like to thank Tom Libby, technical director of the Center for Integrative Biomechanics in Education and Research, and Professor Robert Full for use of their facilities and the muscle lever system, and for their discussions about data analysis. We also thank Dr. Chun-hong Xia for her assistance with mice generation and management.

References for Chapter 2

1. Glasser a, Campbell MC. Biometric, optical and physical changes in the isolated human crystalline lens with age in relation to presbyopia. *Vision Res*. 1999;39(11):1991-2015. http://www.ncbi.nlm.nih.gov/pubmed/10343784.

2. Heys KR, Friedrich MG, Truscott RJW. Presbyopia and heat: changes associated with aging of the human lens suggest a functional role for the small heat shock protein, alpha-crystallin, in maintaining lens flexibility. *Aging Cell*. 2007;6(6):807-815. doi:10.1111/j.1474-9726.2007.00342.x.

3. Heys KR, Truscott RJW. The stiffness of human cataract lenses is a function of both age and the type of cataract. *Exp Eye Res*. 2008;86(4):701-703. doi:10.1016/j.exer.2007.12.009.

4. Weeber HA, van der Heijde RGL. On the relationship between lens stiffness and accommodative amplitude. *Exp Eye Res*. 2007;85(5):602-607. doi:10.1016/j.exer.2007.07.012.

5. Heys KR, Cram SL, Truscott RJW. Massive increase in the stiffness of the human lens nucleus with age: the basis for presbyopia? *Mol Vis*. 2004;10(December):956-963. http://www.ncbi.nlm.nih.gov/pubmed/15616482.

6. Manns F, Parel J-M, Denham D, et al. Optomechanical response of human and monkey lenses in a lens stretcher. *Invest Ophthalmol Vis Sci*. 2007;48(7):3260-3268. doi:10.1167/iovs.06-1376.

7. Baradia H, Nikahd N, Glasser A. Mouse lens stiffness measurements. *Exp Eye Res*. 2010;91(2):300-307. doi:10.1016/j.exer.2010.06.003.

8. Moffat BA, Landman KA, Truscott RJW, Sweeney MHJ, Pope JM. Age-related changes in the kinetics of water transport in normal human lenses. *Exp Eye Res*. 1999;69:663-669. doi:10.1006/exer.1999.0747.

9. Schachar R a. Equatorial lens growth predicts the age-related decline in accommodative amplitude that results in presbyopia and the increase in intraocular pressure that occurs with age. *Int Ophthalmol Clin*. 2008;48(1):1-8. doi:10.1097/IIO.0b013e31815eb836.

10. Sweeney MH, Truscott RJ. An impediment to glutathione diffusion in older normal human lenses: a possible precondition for nuclear cataract. *Exp Eye Res*. 1998;67(5):587-595. doi:10.1006/exer.1998.0549.

11. Michael R, Bron AJ. The ageing lens and cataract: a model of normal and pathological ageing. *Philos Trans R Soc Lond B Biol Sci*. 2011;366(1568):1278-1292. doi:10.1098/rstb.2010.0300.

12. Yamashiro S, Gokhin DS, Kimura S, Nowak RB, Fowler VM. Tropomodulins: pointed-end capping proteins that regulate actin filament architecture in diverse cell types.

Cytoskeleton (Hoboken). 2012;69(6):337-370. doi:10.1002/cm.21031.

13. Nowak RB, Fischer RS, Zoltoski RK, Kuszak JR, Fowler VM. Tropomodulin1 is required for membrane skeleton organization and hexagonal geometry of fiber cells in the mouse lens. *J Cell Biol*. 2009;186(6):915-928. doi:10.1083/jcb.200905065.

14. Fischer RS, Lee A, Fowler VM. Tropomodulin and tropomyosin mediate lens cell actin cytoskeleton reorganization in vitro. *Invest Ophthalmol Vis Sci*. 2000;41(1):166-174. http://www.ncbi.nlm.nih.gov/pubmed/10634617. Accessed January 13, 2012.

15. Gokhin DS, Nowak RB, Kim NE, et al. Tmod1 and CP49 Synergize to Control the Fiber Cell Geometry, Transparency, and Mechanical Stiffness of the Mouse Lens. *PLoS One*. 2012;7(11):e48734. doi:10.1371/journal.pone.0048734.

16. Fudge DS, McCuaig J V, Van Stralen S, et al. Intermediate filaments regulate tissue size and stiffness in the murine lens. *Invest Ophthalmol Vis Sci*. 2011;52(6):3860-3867. doi:10.1167/iovs.10-6231.

17. Nowak RB, Fowler VM. Tropomodulin 1 constrains fiber cell geometry during elongation and maturation in the lens cortex. *J Histochem Cytochem*. 2012;60(6):414-427. doi:10.1369/0022155412440881.

18. Pau H, Kranz J. The increasing sclerosis of the human lens with age and its relevance to accommodation and presbyopia. *Graefe's Arch Clin Exp Ophthalmol*. 1991;229(3):294-296. doi:10.1007/BF00167888.

19. Glasser A, Campbell MC. Presbyopia and the optical changes in the human crystalline lens with age. *Vision Res*. 1998;38(2):209-229. http://www.ncbi.nlm.nih.gov/pubmed/9536350. Accessed February 22, 2013.

20. Fisher RF. The elastic constants of the human lens. *J Physiol*. 1971;212(1):147-180. http://www.pubmedcentral.nih.gov/articlerender.fcgi?artid=1395702&tool=pmcentrez&rendertype=abstract.

21. Burd HJ, Wilde GS, Judge SJ. An improved spinning lens test to determine the stiffness of the human lens. *Exp Eye Res*. 2011;92(1):28-39. doi:10.1016/j.exer.2010.10.010.

22. Wilde GS, Burd HJ, Judge SJ. Shear modulus data for the human lens determined from a spinning lens test. *Exp Eye Res*. 2012;97(1):36-48. doi:10.1016/j.exer.2012.01.011.

23. Cheng C, Gokhin DS, Nowak RB, Fowler VM. Sequential Application of Glass Coverslips to Assess the Compressive Stiffness of the Mouse Lens: Strain and Morphometric Analyses. *J Vis Exp*. 2016;(111). doi:10.3791/53986.

24. Weeber H a, Eckert G, Pechhold W, van der Heijde RGL. Stiffness gradient in the crystalline lens. *Graefes Arch Clin Exp Ophthalmol*. 2007;245(9):1357-1366. doi:10.1007/s00417-007-0537-1.

3.1 Introduction

Several αA-crystallin point mutations were previously generated in the lab that produce a variety of interesting lens phenotypes[1]. Specifically, three point mutations examined in this work are: B6 αA(Y118D/ Y118D) (B6 L1N), B6 αA(R54C/R54C) (B6 NM3365), and B6 αA(R54H/R54H) (B6 Lop18) (Figure 3.1). The point mutation Y118D occurs within the α-crystallin domain of the α-crystallin protein, while R54C and R54H occur outside this region. L1N lenses produce a mild nuclear cataract but exhibit an interesting growth defect. They grow at a similar rate as normal wild-type lenses, but after several weeks stop growing altogether. NM3365 lenses produce a severe nuclear cataract and lenses overall suffer from extensive morphological defects. Lop18 lenses remain mostly intact but exhibit a severe nuclear cataract (Figure 3.2).

It is known that αA-crystallin can interact with several different cytoskeletal elements to maintain the structure of the lens fiber cells[2–6]. Indeed in addition to their roles as molecular chaperones and preventing aggregation of proteins to maintain transparency[7], α-crystallins are also considered structural proteins and organize in a very specific fashion within lens fiber cells[8,9]. How these interactions change when αA-crystallin is mutated is unclear, as the exact structure of α-crystallin is as of yet unknown[10–12]. Despite this, the αA-crystallin mutant lenses described above each produce a very distinct lens phenotype. This work determines to investigate the altered interaction between these αA-crystallin mutants, wild-type αB-crystallin, which usually associates with its αA subunit, and cytoskeletal proteins in cultured lens epithelial cells to elucidate part of the molecular basis for these lens phenotypes.

3.2 Methods

Mice

This study followed the ARVO Statement for the Use of Animals in Ophthalmic and Vision Research and an ACUC approved animal protocol (UC Berkeley). Animals were housed with free access to food and water, with a 12:12 h light:dark cycle, and sacrificed by CO_2 inhalation followed by cervical dislocation. All efforts were made to minimize animal suffering.

The mouse strains used in this study were: wild-type C57BL/6J (B6 WT), B6 αA(Y118D/ Y118D) (B6 L1N), B6 αA(R54C/R54C) (B6 NM3365), B6 αA(R54H/R54H) (B6 Lop18), B6 αA-/-, and B6 αB-/-. Mice used for cell harvest ranged from 3 weeks to 3 months of age.

The generation of mutant αA(Y118D/Y118D) mice was previously described, and αA(-/-) αB(-/-) double knockout mice were a generous gift from Dr. Eric Wawrousek at the National Eye Institute[1,13,14]. AlphaA(-/-) mice, used for breeding with αA(Y118D/Y118D) mice, were generated by intercrossing αA(+/-) αB(+/-) mice, which were produced by mating αA(-/-) αB(-/-) mice with WT mice in the C57BL/6J strain background. The genotyping PCR methods for αA and αB knockout mice were provided by Dr. Wawrousek.

GFP-positive (GFP+) transgenic WT mice, under the chicken β-actin promoter, were generated as previously described[15]. The PCR genotyping method can only distinguish the αA-Y118D point mutant allele from αA knockout allele but not from the wild-type αA allele. Thus, we first generated GFP+ αA(-/-) mice by breeding GFP+ WT mice with αA(-/-) mice. Next, GFP+ αA(-/-) were crossed with αA(Y118D/Y118D) mutant mice to generate GFP+ αA(Y118D/-) mice. The GFP+ αA(Y118D/-) mice were then mated with αA(Y118D/Y118D) mice to generate GFP+ αA(Y118D/Y118D) homozygous knockout mice that were screened using a UV lamp and genotyped. GFP+ WT and mutant mice with one copy of the GFP transgene were maintained for this study.

Lens Images and Weight Measurement

Images of freshly dissected lenses were collected by using a dissection microscope (MZ16 Leica) with a digital camera. To avoid cold cataracts, lenses from mice younger than postnatal day 21 (P21) were imaged in PBS at 37°C. Wet lens weight was determined by weighing at least 6 lenses from 3 different mice of each genotype at each age. The average and standard deviation were plotted in Excel.

Fiber Cell Evaluation in GFP Lenses

GFP distribution in living lenses was evaluated using a Zeiss LSM700 confocal microscopy as previously described[16,17]. Briefly, fresh intact GFP+ lenses were dissected out of the whole eye in DMEM without phenol red immediately before imaging. Live lenses were maintained in DMEM

for imaging. Z-stack images of the lens equator were collected with 1μm z-steps. ZEN 2010 software was used to analyze equatorial epithelial and fiber cells and to create three-dimensional reconstructions and two-dimensional projections.

BrdU Labeling

P7 and P21 WT and mutant mice (three mice at each age of each genotype) were injected intraperitoneally with 100μg/g body weight of 5'-bromo-2'-deoxyuridine (BrdU; Sigma-Aldrich, St. Louis, MO). Injected pups were returned to their mothers for 24 hours before euthanization. Lens cryosections for immunohistochemical staining were prepared as described above. BrdU incorporation was immunolabeled with a BrdU antibody (Roche, Palo Alto, CA) according to the manufacturer's instructions, except the methanol fixation step. Sections were labeled with an anti-mouse FITC-labeled secondary antibody (Jackson ImmunoResearch) followed by incubation in 1μg/mL DAPI (Anaspec, San Jose, CA) in PBS for 15 minutes at 37°C. Images were collected by a fluorescence microscope (Axiovert 200; Zeiss) and analyzed as previously described[18]. Briefly, BrdU-positive and unlabeled (counterstained with DAPI) nuclei were counted in three serial 10μm sections from the anterior hemisphere of each lens. The mitotic index was calculated for each section, and data was collected from six lenses at each time point for each genotype. The average and standard deviation of the mitotic index was plotted in Excel, and the Student's t-test was used for statistical analysis. P values <0.001 were considered significant.

Primary Lens Cell Culture

Lenses were immediately dissected from enucleated eyeballs of euthanized mice. After carefully removing surrounding tissue, lenses were incubated in 0.05% trypsin-EDTA (Gibco, cat#: 25300-054) at 37 °C for 10 min to further remove any non-lens cells and then transferred to a new clean dissection tray. Lens capsules were peeled off by forceps and transferred into 100 μl of dispase per pair of lenses (2 U/ml, Sigma, cat#: D4693) in Advanced DMEM-F12 medium (Gibco, cat#: 12634-010). After 5 min of dispase treatment, 100 μl of 10X TrypLE (Gibco, cat#: A12177-02) was added. After 10 min, the cell suspension was transferred to a new sterile tube and spun down at 1000 rpm for 4 min. The cell pellet was resuspended in culture medium and seeded into culture dishes. The basal culture medium, used simply for dissection of the lens as above, was Advanced DMEM/F12, supplemented with 1X Penicillin-Streptomycin (Gibco, cat#: 15140-122), 1X GlutaMax (Gibco, cat#: 35050-061), 2% Fetal Bovine Serum (FBS, Gibco, cat#: 26140-079), and 1X B-27 (Gibco, cat#: 17504-044). All cells were grown in a culture medium consisting of basal medium further supplemented with 5 μM SB431542 (SB, Stemgent, cat#: 04-0010-10). SB431542 was dissolved in DMSO to make stock solutions.

Immunostaining

Cultured mouse LECs after one week of culture were fixed in 4% paraformaldehyde (PFA) in Phosphate Buffered Saline (PBS) for 15 min and then washed with PBS 3x, blocked with 5%

normal goat serum in 0.3% Triton-X100 for one hour, and were incubated with specific primary antibodies diluted in blocking buffer overnight at 4 °C. The primary antibodies included mouse monoclonal anti-α-tubulin (Sigma-Aldrich, St. Louis, MO), rabbit polyclonal anti-αA-crystallin and anti-αB-crystallin (generously provided by Dr. Joseph Horwitz, University of California at Los Angeles). After incubation with primary antibodies, the cells were washed with PBS and incubated in appropriate secondary antibodies (Jackson ImmunoResearch Laboratories, West Grove, PA) and phalloidin-rhodamine (Life Technologies, Carlsbad, CA) diluted in blocking buffer for two hours. The cells were then placed in mounting medium containing DAPI (Vector Laboratories, cat#: H-1200) and imaged by confocal microscopy (Zeiss, LSM700). Staining was repeated at least three times, and representative results are shown.

3.3 Results

3.3.1 Characterization of αA-Y118D Mutant Lens Growth Defect

A previously described mutation in the lens structural protein αA-crystallin, αA-Y118D, causes a unique postnatal lens growth defect in mice (Figure 3.3). Growth of mutant αA-Y118D lenses slows during 3 to 5 weeks of age, and stops after 8 weeks (Figure 3.4). The mitotic index of lens epithelial cells in both wild-type and αA-Y118D lenses appeared comparable at P7, but dropped in mutant lenses at P21 (Figure 3.5). Imaging of GFP^+ whole lenses displayed perturbed fiber cell-cell alignment and aberrant or delayed fiber cell elongation in αA-Y118D mutant lenses from mice older than three weeks (Figure 3.6). Examining DAPI-stained frozen sections of wild-type and αA-Y118D mutant lenses revealed DAPI-positive nuclei present in deeper lens fibers at P7 (Figure 3.7, top panels). In older mutant lenses, inner fiber cells contained even more fragmented nuclei as compared to wild-type lenses (Figure 3.7, middle and bottom panels).

3.3.2 Aggregation of αA-Crystallin with F-Actin in Lens Epithelial Cells

Primary lens epithelial cells (LECs) were harvested from several normal and mutant mouse lenses exhibiting unique lens phenotypes: wild-type (WT), αA-Y118D (L1N), αA-R54C (NM3365), αA-R54H (Lop18), αA-/-, and αB-/-, all in the C57BL/6J (B6) mouse background strain. Cultured cells at P1 were then labeled for immunofluorescence for αA-crystallin, actin, and microtubules, and imaged by confocal microscopy. Representative images of cells from each lens mutant are displayed. Primary LECs were confirmed to express endogenous αA-crystallin. In B6 WT cells, αA-crystallin was enriched near the leading edge with lamellar F-actin (Figure 3.8, "B6 WT" row). In L1N cells containing αA-Y118D crystallin, mutant αA-crystallin formed substantial aggregates with F-actin (Figure 3.8, "L1N" row, arrows). Cells from NM3365 lenses displayed extremely enlarged cell size with an abundance of actin stress fibers. These single cells would often be several times larger than cells from any other mutant lens. Mutant αA-R54C crystallin appeared to surround actin stress fibers Figure 3.8, "NM3365" row). Finally, cells containing αA-R54H mutant crystallin protein appeared to form tube-like structures surrounding actin fibers (Figure 3.8, "Lop18" row, arrows). As expected, cells from αA-/- lenses displayed a marked decrease in αA-crystallin staining and were used a negative control (Figure 3.8, "αA-/-" row). Cells from αB-/- lenses displayed a slight reduction in αA-crystallin staining, but looked otherwise normal (Figure 3.8, "αB-/-" row).

3.3.3 Aggregation of αB-Crystallin with F-Actin in Lens Epithelial Cells

As above, cultured cells at P1 were then labeled for immunofluorescence for αB-crystallin and actin, and then imaged by confocal microscopy. Representative images of cells from each lens mutant are displayed. As expected, primary LECs were confirmed to express endogenous αB-crystallin, and in a similar staining pattern as αA-crystallin (Figure 3.9, "B6 WT" row). In L1N cells, it appears that αB-crystallin aggregates to actin in a similar fashion as mutant αA-Y118D (Figure 3.9, "L1N" row, arrows). This is likely due to αA and αB commonly associating with

each other in normal lenses. As above, similar cellular morphological changes in the remaining genotypes were observed (Figure 3.9, “NM3365” and “Lop18” rows), but it appears that αB-crystallin distribution is not particularly disturbed when mutant αA-crystallin is introduced.

3.3.4 Mutant αA-Crystallin Lacks Association with Microtubules

As above, cultured cells at P1 were then labeled for immunofluorescence for αA-crystallin and α-tubulin, and then imaged by confocal microscopy. Representative images of cells from each lens mutant are displayed. It appeared that almost none of the WT or mutant αA-crystallin proteins co-localized with microtubules in these cultured cells (Figure 3.10). The staining patter of αA-crystallin appeared similar to Figure 3.8, as expected.

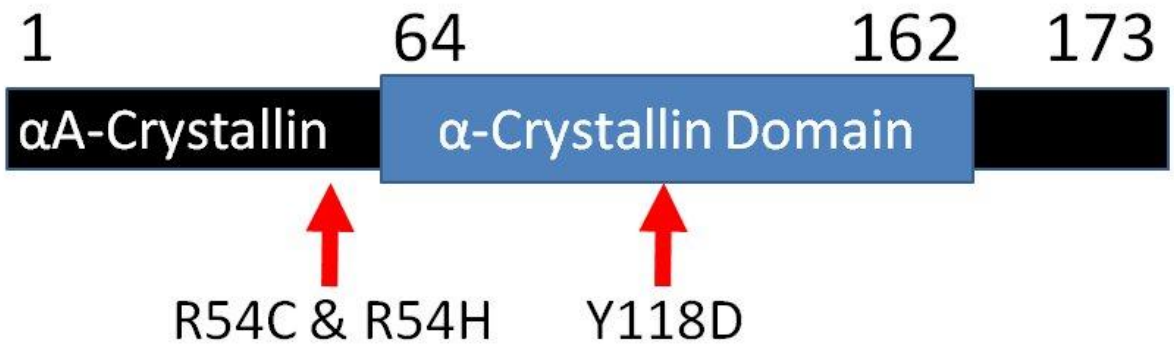

Figure 3.1. Diagram of αA-crystallin gene, with several point mutations designated.

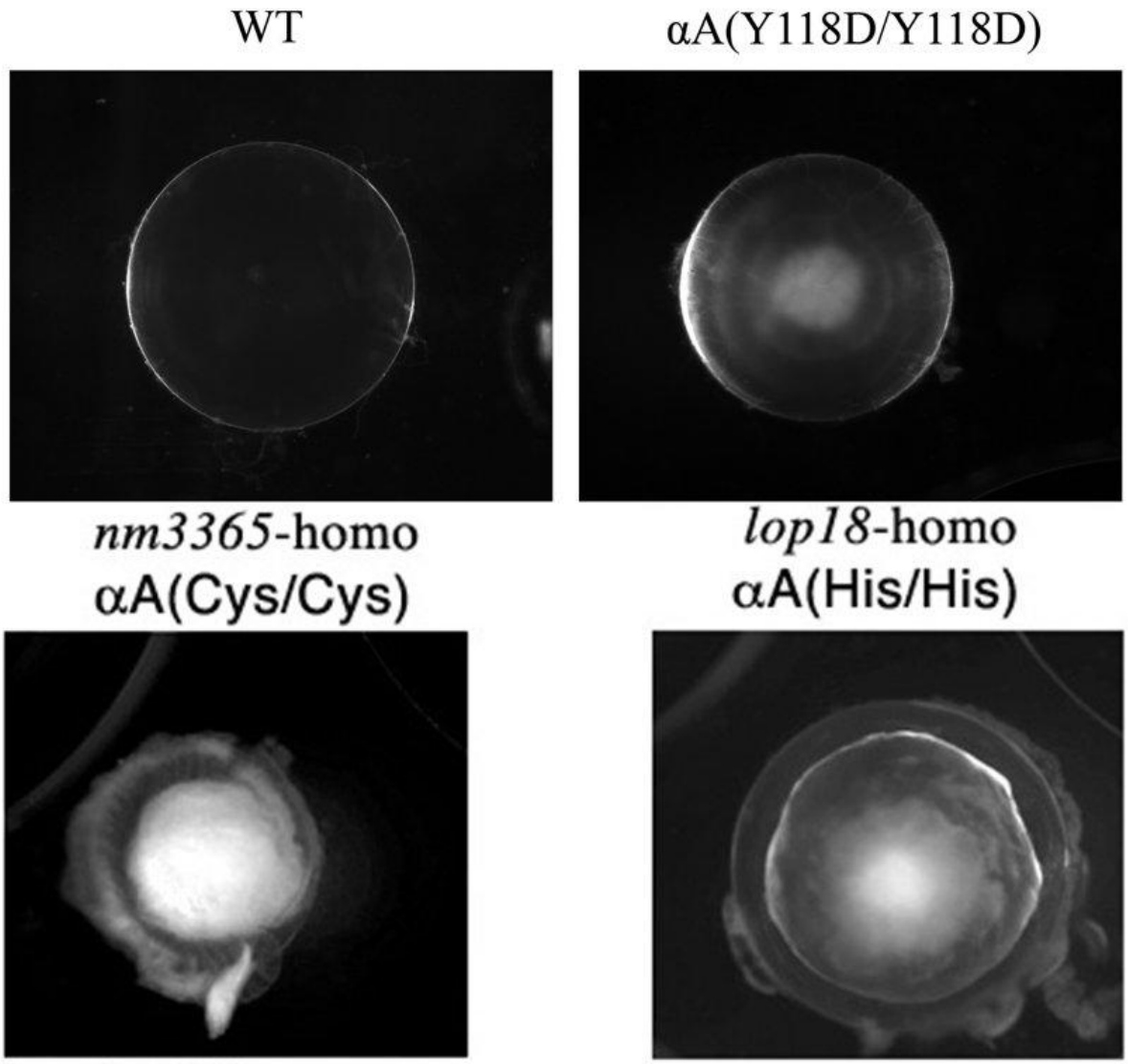

Figure 3.2. Lens phenotypes of αA-crystallin point mutations.

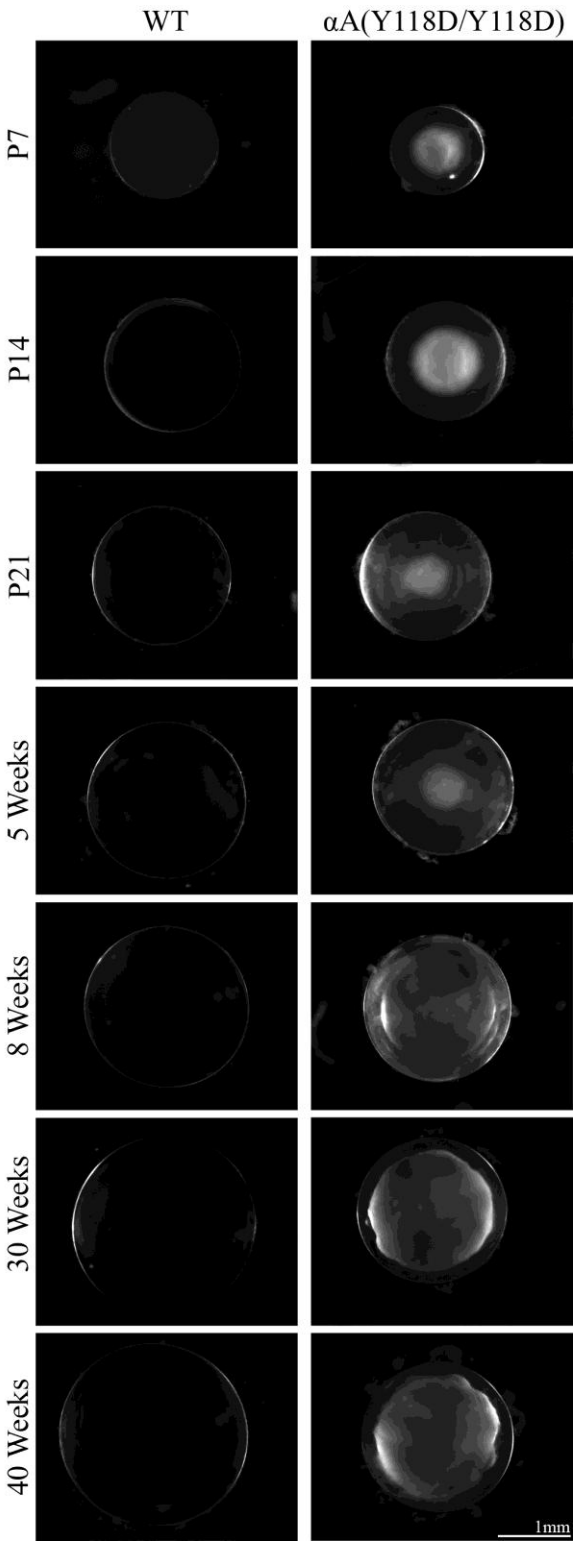

Figure 3.3. Wild-type and αA-Y118D mutant lenses at P7, P14, P21, 5 weeks, 8 weeks, 30 weeks, and 40 weeks of age. Including the formation of nuclear cataracts, the mutant lenses were smaller at later ages compared to wild-type.

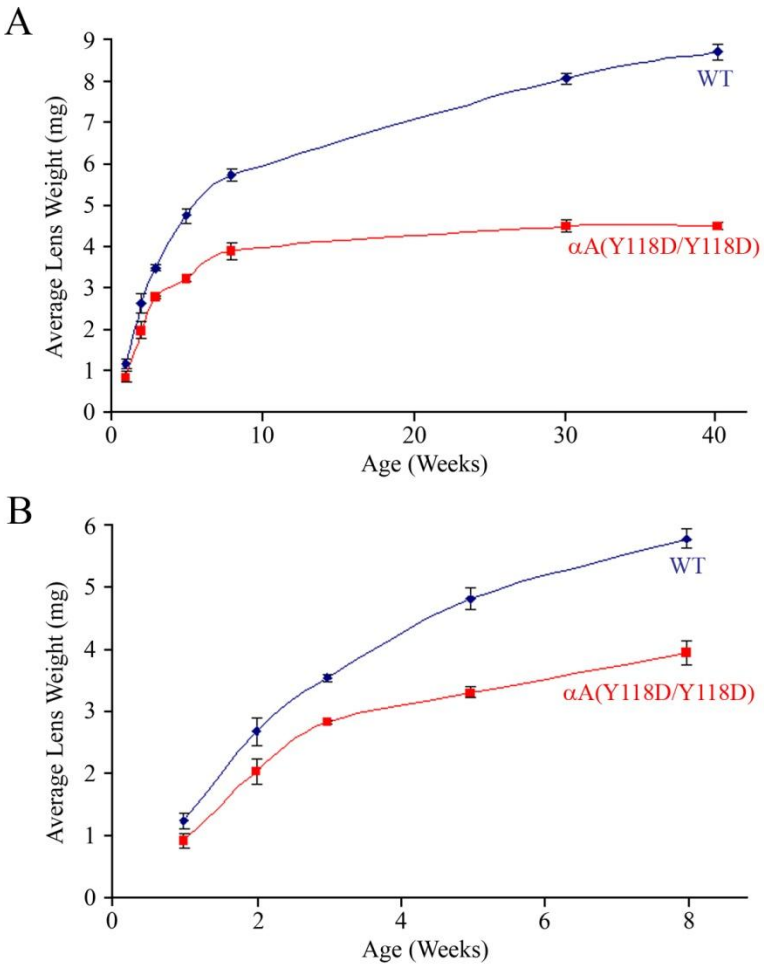

Figure 3.4. Graph of lens weight from WT and αA-Y118D mutant lenses between 1-40 weeks of age (A) and 1-8 weeks of age (B). Mutant lens growth slowed considerably after 3 weeks of age.

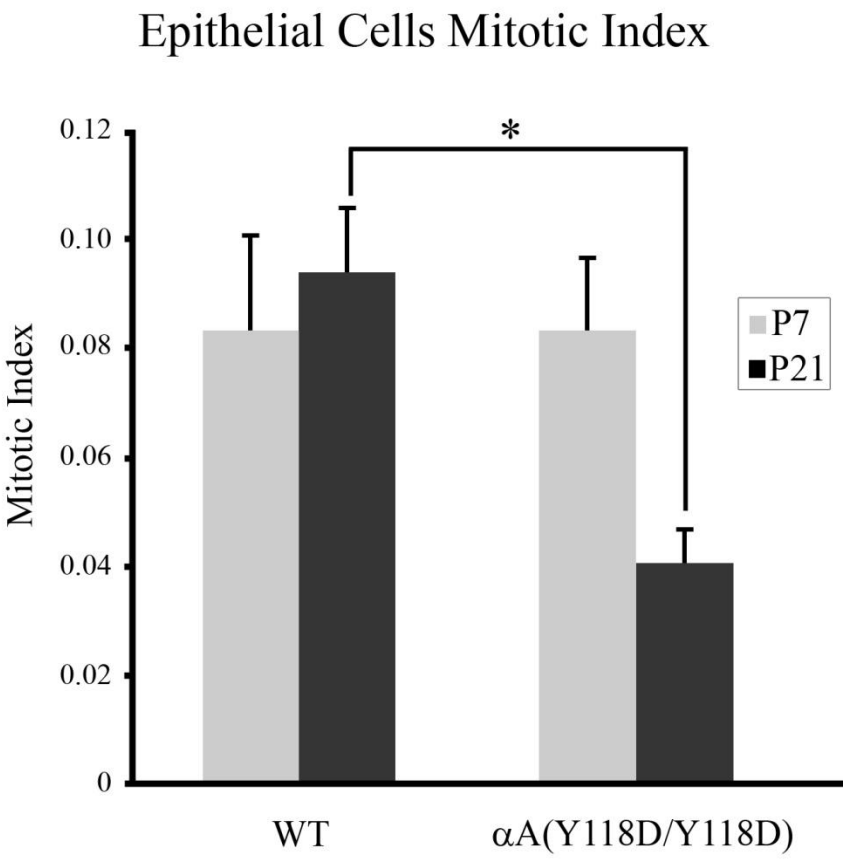

Figure 3.5. Mitotic index of P7 and P21 epithelial cells from wild-type and αA-Y118D lenses. At P21 the mitotic index of epithelial cells expressing the mutant αA-Y118D protein drops. * = $p<0.001$.

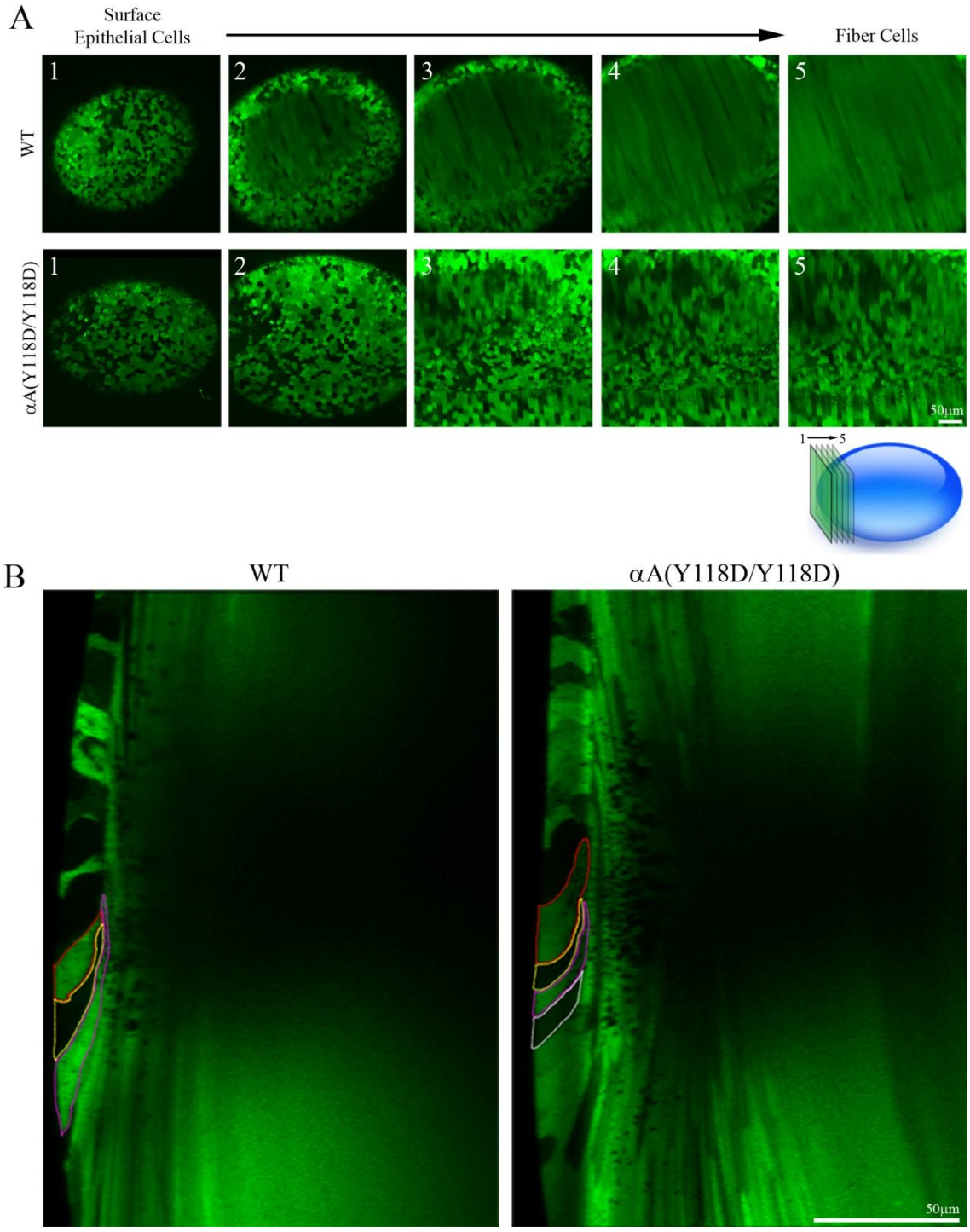

Figure 3.6. Comparing 3D reconstructions of confocal images of wild-type and αA-Y118D mutant lenses at 7 months in cross section (A), fiber cell packing appears disrupted in fiber cells expressing the mutant protein. Comparing wild-type and αA-Y118D mutant lenses at 5 weeks in anterior-posterior orientation (B), fiber cells expressing the mutant protein are unable to elongate as much as wild-type fiber cells. Scale bar, 50μm.

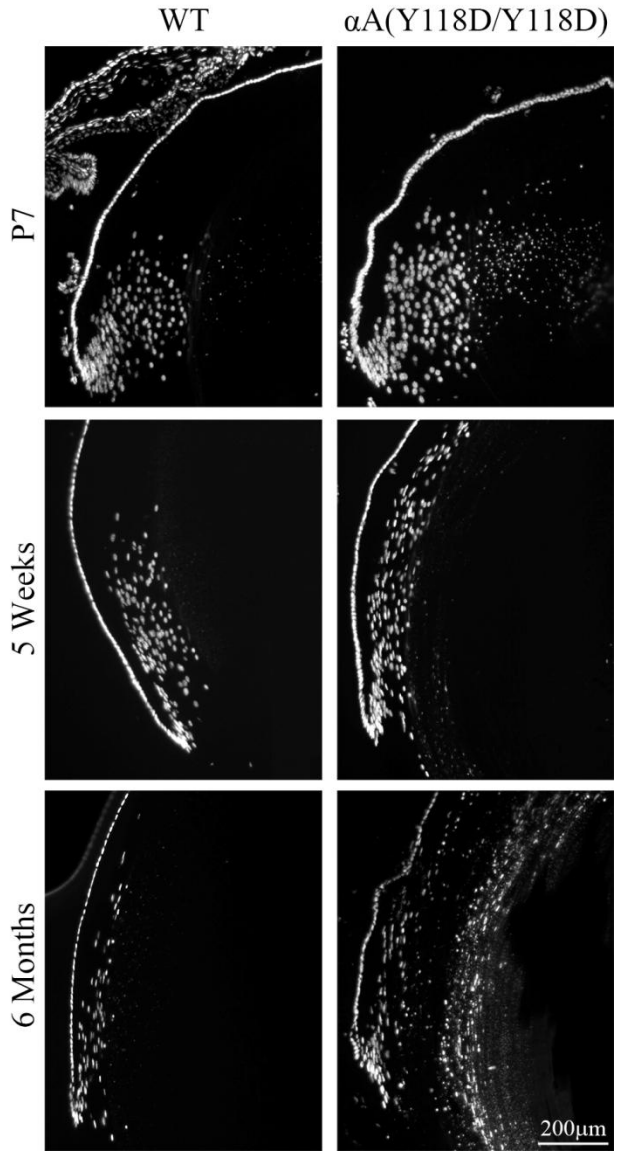

Figure 3.7. DAPI staining of frozen lens sections in anterior-posterior orientation. In αA-Y118D mutant lenses, there appears to be delayed denucleation near the lens equator region beginning at P7, becoming more evident with age. Denucleation patterns in lenses where αA-crystallin was knocked out were similar to wild-type lenses. Scale bar, 200μm.

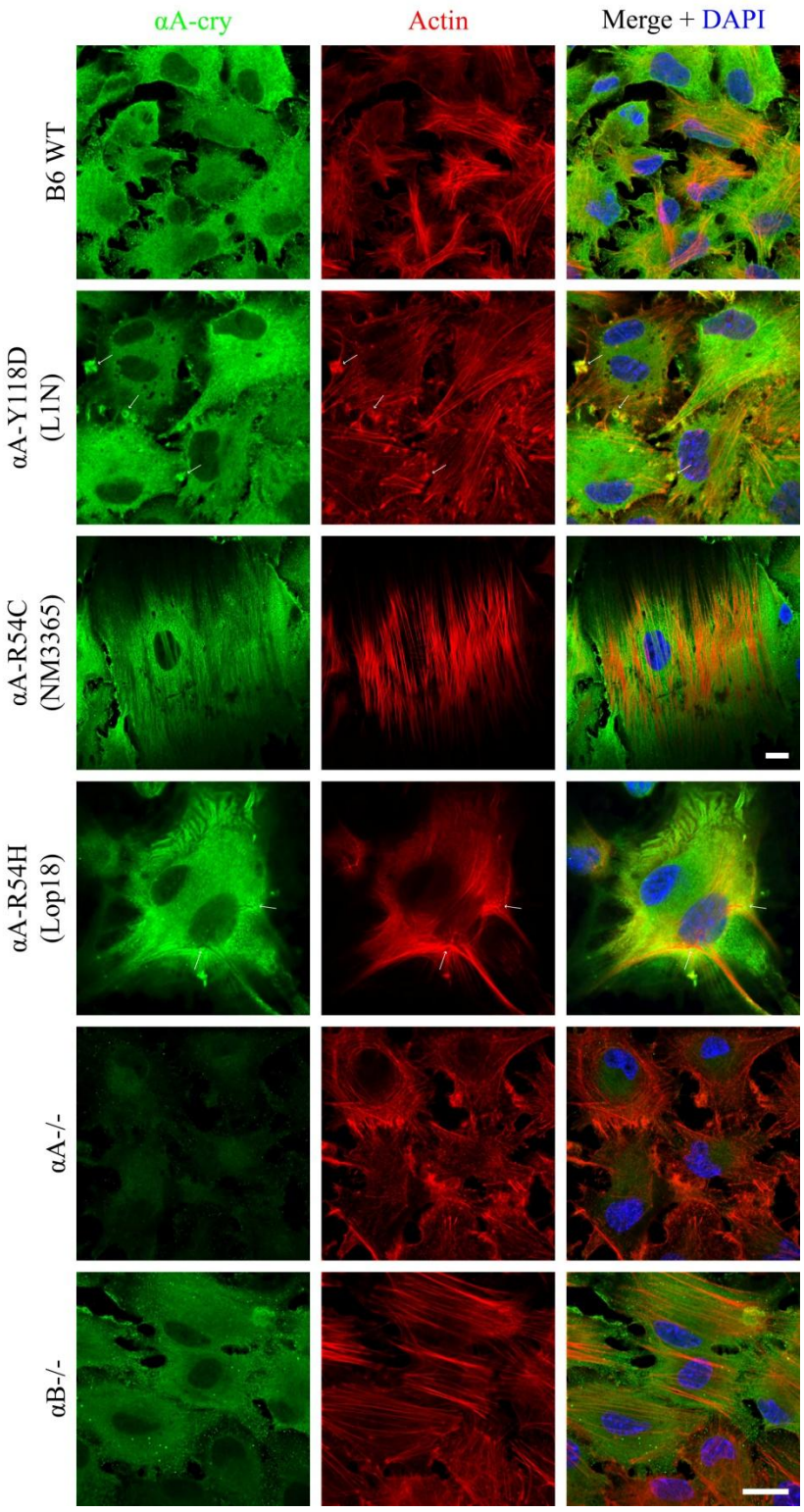

Figure 3.8. 63X confocal images of lens epithelial cells stained for αA-crystallin and actin. Scale bars, 20μm, αA-R54C (NM3365) images at 0.5X scale.

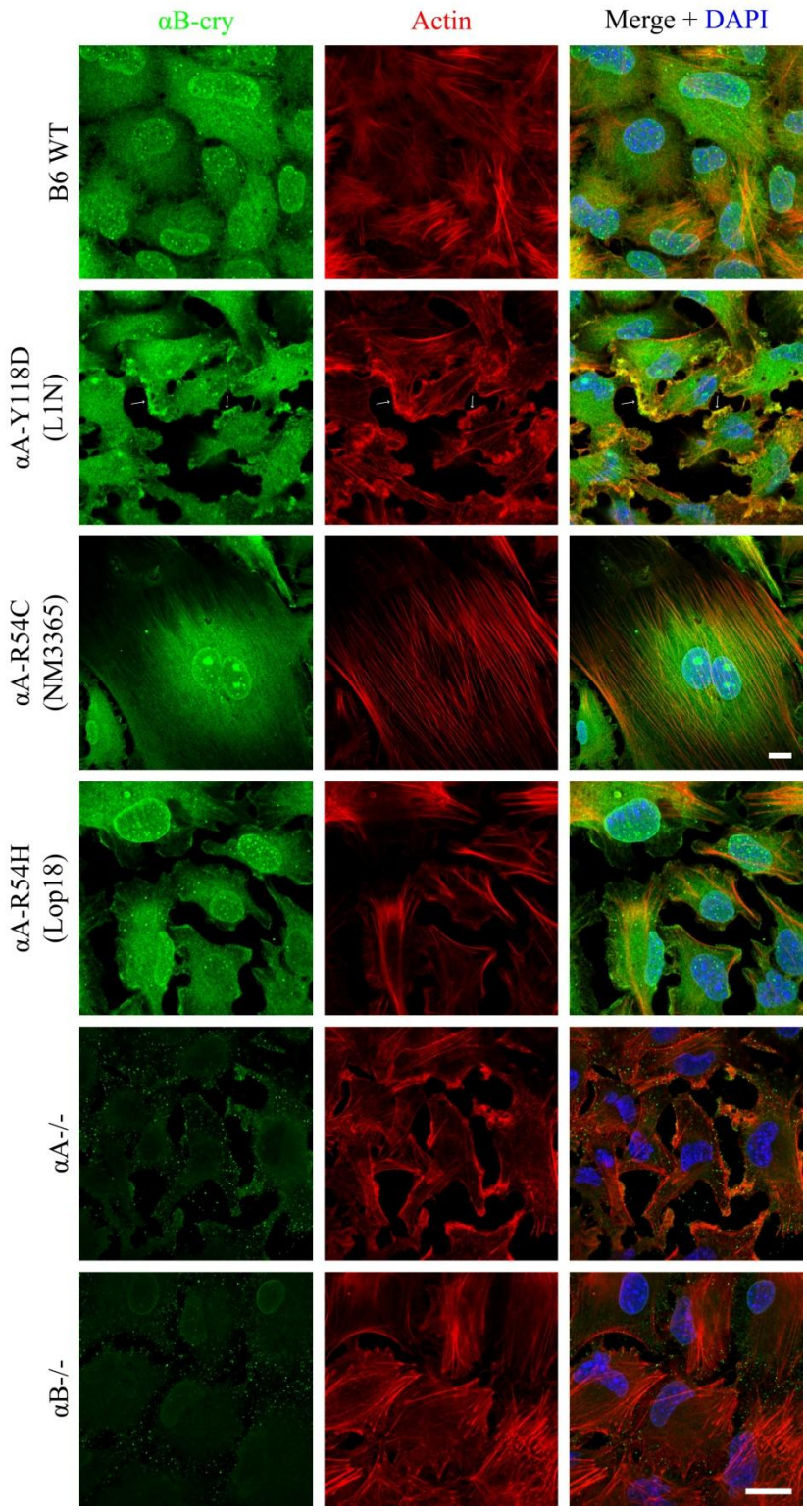

Figure 3.9. 63X confocal images of lens epithelial cells stained for αB-crystallin and actin. Scale bars, 20μm, αA-R54C (NM3365) images at 0.5X scale.

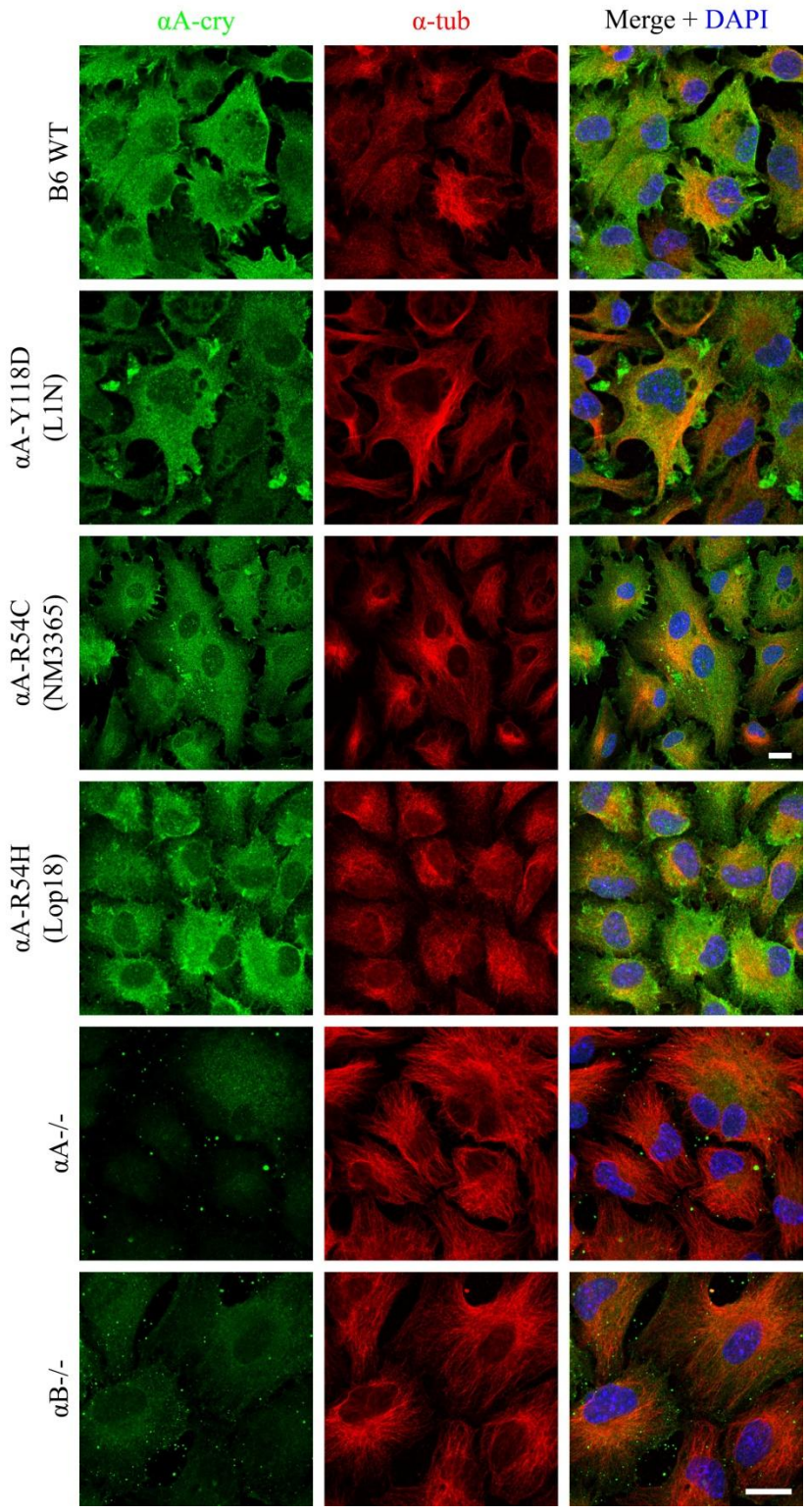

Figure 3.10. 63X confocal images of lens epithelial cells stained for αA-crystallin and α-tub. Scale bars, 20μm, αA-R54C (NM3365) images at 0.5X scale.

3.4 Discussion

The growth of the lens has previously been well documented by measuring both lens weight or lens size in mice[19–21]. Several genetically engineered mouse mutants show a number of lens growth defects, many starting early in the lens development cycle[22–26]. Uniquely, lenses containing mutant αA-Y118D crystallin exhibit only mild lens growth inhibition in initial development, and then sharply decrease in growth rate after 21 days but before 8 weeks of age, and then stop growing altogether after 8 weeks. Therefore αA-Y118D mutant lenses provide an opportunity to study not just a slower lens growth, but one that is completely halted after development of the lens. We have shown that αA-crystallin typically associates with lamellar actin near the edges of lens epithelial cells. The mutant αA-Y118D crystallin appears to form several aggregates with F-actin, while mutant αA-R54C and αA-R54H appear to promote actin stress fiber formation by potentially binding to actin fiber coating proteins. When examining αB-crystallin distribution in cells from mutant αA-Y118D lenses, the αB subunit also appeared to aggregate in a similar fashion as in the αA images. In our cultured lens epithelial cells it did not appear that α-tubulin associated strongly with αA-crystallin in any wild-type or mutant lenses.

Mutant αA-Y118D lenses might therefore provide a potential method to controlling the growth of the lens because of this unique growth defect[27,28]. Studies have revealed that a lack of protein and nutrient turnover in the core of the lens can lead to presbyopia and age related cataract. Due to the nature of the lens, with its many layers of elongated fiber cells, proper lens homeostasis depends on transport of small molecules, ions, and water from surface lens epithelial cells near the lens periphery inwards to core fiber cells. Because of the necessesity for the lens to remain completely transparent, these inner fiber cells lack any cellular organelles or nuclei, making protein turnover impossible[29–32]. Increased lens size, as additional secondary fibers are added to the periphery of the lens, increases the distance which nutrients and other metabolites need to travel to the lens core, likely disturbing maintenance of proper lens homeostasis in older lenses[33]. There are no known methods however to control or delay the growth of the lens without also affecting early development of the lens. Therefore, discovering the mechanism behind the delayed growth defect of mutant αA-Y118D lenses may yield new therapies for halting the growth of the adult lens and preventing certain age-related lens complications[20].

3.5 Acknowledgements

We thank Dr. Cathy Cheng for her previous work characterizing the lens growth defect in αA-Y118D lenses and for her guidance in data interpretation. We also thank Dr. Chun-hong Xia for mice generation and management.

References for Chapter 3

1. Xia C, Liu H, Chang B, et al. Arginine 54 and Tyrosine 118 residues of {alpha}A-crystallin are crucial for lens formation and transparency. *Invest Ophthalmol Vis Sci*. 2006;47(7):3004-3010. doi:10.1167/iovs.06-0178.

2. Bai F, Xi J, Higashikubo R, Andley UP. Cell kinetic status of mouse lens epithelial cells lacking alphaA- and alphaB-crystallin. *Mol Cell Biochem*. 2004;265(1-2):115-122. http://www.ncbi.nlm.nih.gov/pubmed/15543941.

3. Andley UP, Song Z, Wawrousek EF, Brady JP, Bassnett S, Fleming TP. Lens epithelial cells derived from alphaB-crystallin knockout mice demonstrate hyperproliferation and genomic instability. *FASEB J*. 2001;15(1):221-229. doi:10.1096/fj.00-0296com.

4. Menko AS, Andley UP. αA-Crystallin associates with α6 integrin receptor complexes and regulates cellular signaling. *Exp Eye Res*. 2010;91(5):640-651. doi:10.1016/j.exer.2010.08.006.

5. Andley UP. The lens epithelium: focus on the expression and function of the alpha-crystallin chaperones. *Int J Biochem Cell Biol*. 2008;40(3):317-323. doi:10.1016/j.biocel.2007.10.034.

6. Xi J-H, Bai F, McGaha R, Andley UP. Alpha-crystallin expression affects microtubule assembly and prevents their aggregation. *FASEB J*. 2006;20(7):846-857. doi:10.1096/fj.05-5532com.

7. Andley UP, Reilly MA. In vivo lens deficiency of the R49C alphaA-crystallin mutant. *Exp Eye Res*. 2010;90(6):699-702. doi:10.1016/j.exer.2010.02.009.

8. Makley LN, Mcmenimen KA, Devree BT, et al. Pharmacological chaperone for a-crystallin partially restores transparency in cataract models. *Science (80-).* 2015;350(6261):674-677.

9. Bai F, Xi J, Higashikubo R, Andley UP. A comparative analysis of alphaA- and alphaB-crystallin expression during the cell cycle in primary mouse lens epithelial cultures. *Exp Eye Res*. 2004;79(6):795-805. doi:10.1016/j.exer.2004.05.006.

10. Haslbeck M, Franzmann T, Weinfurtner D, Buchner J. Some like it hot: the structure and function of small heat-shock proteins. *Nat Struct Mol Biol*. 2005;12(10):842-846. doi:10.1038/nsmb993.

11. Horwitz J, Bova MP, Ding LL, Haley DA, Stewart PL. Lens alpha-crystallin: function and structure. *Eye (Lond).* 1999;13 (Pt 3b:403-408. doi:10.1038/eye.1999.114.

12. Sun Y, MacRae TH. Small heat shock proteins: Molecular structure and chaperone function. *Cell Mol Life Sci*. 2005;62(21):2460-2476. doi:10.1007/s00018-005-5190-4.

13. Brady JP, Garland D, Duglas-Tabor Y, Robison WG, Groome A, Wawrousek EF.

Targeted disruption of the mouse alpha A-crystallin gene induces cataract and cytoplasmic inclusion bodies containing the small heat shock protein alpha B-crystallin. *Proc Natl Acad Sci U S A*. 1997;94(3):884-889. http://www.ncbi.nlm.nih.gov/pubmed/9023351. Accessed August 3, 2017.

14. Brady JP, Garland DL, Green DE, Tamm ER, Giblin FJ, Wawrousek EF. AlphaB-crystallin in lens development and muscle integrity: a gene knockout approach. *Invest Ophthalmol Vis Sci*. 2001;42(12):2924-2934. http://www.ncbi.nlm.nih.gov/pubmed/11687538. Accessed August 3, 2017.

15. Okabe M, Ikawa M, Kominami K, Nakanishi T, Nishimune Y. "Green mice" as a source of ubiquitous green cells. *FEBS Lett*. 1997;407(3):313-319. http://www.ncbi.nlm.nih.gov/pubmed/9175875. Accessed August 3, 2017.

16. Cheng C, Gong X. Diverse Roles of Eph/ephrin Signaling in the Mouse Lens. Buday L, ed. *PLoS One*. 2011;6(11):e28147. doi:10.1371/journal.pone.0028147.

17. Cheng C, Xia C-H, Li L, White TW, Niimi J, Gong X. Gap junction communication influences intercellular protein distribution in the lens. *Exp Eye Res*. 2008;86(6):966-974. doi:10.1016/j.exer.2008.03.015.

18. Sellitto C, Li L, White TW. Connexin50 is essential for normal postnatal lens cell proliferation. *Invest Ophthalmol Vis Sci*. 2004;45(9):3196-3202. doi:10.1167/iovs.04-0194.

19. Augusteyn RC. On the growth and internal structure of the human lens. *Exp Eye Res*. 2010;90(6):643-654. doi:10.1016/j.exer.2010.01.013.

20. Shui Y-B, Beebe DC. Age-dependent control of lens growth by hypoxia. *Invest Ophthalmol Vis Sci*. 2008;49(3):1023-1029. doi:10.1167/iovs.07-1164.

21. Fudge DS, McCuaig J V, Van Stralen S, et al. Intermediate filaments regulate tissue size and stiffness in the murine lens. *Invest Ophthalmol Vis Sci*. 2011;52(6):3860-3867. doi:10.1167/iovs.10-6231.

22. Beby F, Commeaux C, Bozon M, Denis P, Edery P, Morlé L. New phenotype associated with an Arg116Cys mutation in the CRYAA gene: nuclear cataract, iris coloboma, and microphthalmia. *Arch Ophthalmol*. 2007;125(2):213-216. doi:10.1001/archopht.125.2.213.

23. Rong P, Wang X, Niesman I, et al. Disruption of Gja8 (alpha8 connexin) in mice leads to microphthalmia associated with retardation of lens growth and lens fiber maturation. *Development*. 2002;129(1):167-174. http://www.ncbi.nlm.nih.gov/pubmed/11782410. Accessed August 3, 2017.

24. White TW, Goodenough D a, Paul DL. Targeted ablation of connexin50 in mice results in microphthalmia and zonular pulverulent cataracts. *J Cell Biol*. 1998;143(3):815-825. http://www.pubmedcentral.nih.gov/articlerender.fcgi?artid=2148149&tool=pmcentrez&rendertype=abstract.

25. Griep AE, Kuwabara T, Lee EJ, Westphal H. Perturbed development of the mouse lens by polyomavirus large T antigen does not lead to tumor formation. *Genes Dev*. 1989;3(7):1075-1085. http://www.ncbi.nlm.nih.gov/pubmed/2550321. Accessed August 3, 2017.

26. Gong X, Wang X, Han J, Niesman I, Huang Q, Horwitz J. Development of cataractous macrophthalmia in mice expressing an active MEK1 in the lens. *Invest Ophthalmol Vis Sci*. 2001;42(3):539-548. http://www.ncbi.nlm.nih.gov/pubmed/11222509. Accessed April 30, 2013.

27. Huang Q, Ding L, Phan KB, et al. Mechanism of cataract formation in alphaA-crystallin Y118D mutation. *Invest Ophthalmol Vis Sci*. 2009;50(6):2919-2926. doi:10.1167/iovs.08-3070.

28. Cheng C, Xia C, Huang Q, Ding L, Horwitz J, Gong X. Altered chaperone-like activity of alpha-crystallins promotes cataractogenesis. *J Biol Chem*. 2010;285(52):41187-41193. doi:10.1074/jbc.M110.154534.

29. Besner S, Scarcelli G, Pineda R, Yun S-H. In Vivo Brillouin Analysis of the Aging Crystalline Lens. *Invest Ophthalmol Vis Sci*. 2016;57(13):5093-5100. doi:10.1167/iovs.16-20143.

30. Heys KR, Friedrich MG, Truscott RJW. Presbyopia and heat: changes associated with aging of the human lens suggest a functional role for the small heat shock protein, alpha-crystallin, in maintaining lens flexibility. *Aging Cell*. 2007;6(6):807-815. doi:10.1111/j.1474-9726.2007.00342.x.

31. Petrash JM. Aging and age-related diseases of the ocular lens and vitreous body. *Investig Ophthalmol Vis Sci*. 2013;54(14):54-59. doi:10.1167/iovs.13-12940.

32. Yoon K-H, Blankenship T, Shibata B, Fitzgerald PG. Resisting the effects of aging: a function for the fiber cell beaded filament. *Invest Ophthalmol Vis Sci*. 2008;49(3):1030-1036. doi:10.1167/iovs.07-1149.

33. Michael R, Bron AJ. The ageing lens and cataract: a model of normal and pathological ageing. *Philos Trans R Soc Lond B Biol Sci*. 2011;366(1568):1278-1292. doi:10.1098/rstb.2010.0300.

4.1 Introduction

Gap junctions are channels between cells that form gateways for small molecules to pass freely[1–6]. Connexin subunits make up gap junction channels[7–10], and most cells use multiple different types of connexin subunits to create a unique coupling network[11,12]. In the lens there are three main types of connexin subunits that make up gap junction channels[13]: α8 (Cx50), α3 (Cx46)[14,15], and α1 (Cx43)[16]. These are each encoded by the *Gja8*, *Gja3*, and *Gja1* genes, respectively. In the lens, α8 connexin can be found in both lens epithelial and fiber cells, connexin 46 is expressed primarily in lens fiber cells, and α1 connexin is mostly expressed in lens epithelial cells. Proper expression and formation of gap junction channels is important for maintaining lens transparency and homeostasis[17–21].

Lenses from mice containing an α8-/- knockout mutation are smaller in size and weight, only about 60% of the wet lens weight of wild-type lenses[22–27]. Knockout of α8 connexin also produces a mild nuclear cataract[28–31]. This decrease in lens size produced by α8-/- mice is somehow associated with a decrease in epithelial cell proliferation and a delay in the maturation of lens fiber cells[32]. The exact mechanism for how the loss of this particular connexin produces these smaller lenses is still unresolved. Therefore, work to discover a potential method to control

the expression of α8 connexin protein might be useful in control of lens growth and size after development. Many studies have confirmed the importance of fibroblast growth factor (FGF) in the normal development of the lens[33,34], with FGF being necessary for initiating epithelial-to-fiber differentiation, organizing fiber cell elongation and geometry, and inducing lens differentiation from ectoderm[35,36]. The potential regulation of gap junction proteins for the purposes of modulating lens growth and size through the FGF pathway is the topic of this study.

4.2 Methods

Mice

This study followed the ARVO Statement for the Use of Animals in Ophthalmic and Vision Research and an ACUC approved animal protocol (UC Berkeley). Animals were housed with free access to food and water, with a 12:12 h light:dark cycle, and sacrificed by CO_2 inhalation followed by cervical dislocation. All efforts were made to minimize animal suffering. Lenses of wild-type C57BL/6J (B6 WT) were used for LEC culture.

Primary Lens Cell Culture

Lenses were immediately dissected from enucleated eyeballs of euthanized mice. After carefully removing surrounding tissue, lenses were incubated in 0.05% trypsin-EDTA (Gibco, cat#: 25300-054) at 37 °C for 10 min to further remove any non-lens cells and then transferred to a new clean dissection tray. Lens capsules were peeled off by forceps and transferred into 100 µl of dispase per pair of lenses (2 U/ml, Sigma, cat#: D4693) in Advanced DMEM-F12 medium (Gibco, cat#: 12634-010). After 5 min of dispase treatment, 100 µl of 10X TrypLE (Gibco, cat#: A12177-02) was added. After 10 min, the cell suspension was transferred to a new sterile tube and spun down at 1000 rpm for 4 min. The cell pellet was resuspended in culture medium and seeded into culture dishes. The basal culture medium, used simply for dissection of the lens as above, was Advanced DMEM/F12, supplemented with 1X Penicillin-Streptomycin (Gibco, cat#: 15140-122), 1X GlutaMax (Gibco, cat#: 35050-061), 2% Fetal Bovine Serum (FBS, Gibco, cat#: 26140-079), and 1X B-27 (Gibco, cat#: 17504-044).

To test the effects of SB431542 (Stemgent, cat#: 04-0010-10) and bFGF (Peprotech, cat#: 100-18B), the basal medium was further supplemented with 5 µM SB431542 (SB), or 5 µM SB431542 plus 5 ng/ml bFGF (SB+FGF). SB431542 was dissolved in DMSO to make stock solutions.

To test the effects of MEK1 and MEK2 inhibition, U0126 (Invivogen, cat#: 109511-58-2) was also added to the control medium with 5 µM SB431542 plus 20 µM U0126 (SB+U0126), or 5 µM SB431542 plus 5 ng/ml bFGF plus 20 µM U0126 (SB+U0126). U0126 was dissolved in DMSO to make stock solutions.

A total of 4 different culture mediums (SB, SB+FGF, SB+U0126, SB+FGF+U0126) were tested at 37 °C with 5% CO2 and 95% humidity incubation. All cells were resuspended in either SB or SB+FGF medium immediately after harvest.

LacZ Staining

Cells were washed briefly with 1X phosphate buffered saline (PBS) at 37 °C. Culture plates were then fixed in 0.5% glutaraldehyde in 1X PBS for 5 minutes. Cells were then washed in cold 1X PBS three times before incubating in 0.02% NP-40 and 2mM $MgCl_2$ in 1X PBS for 20 minutes. Culture plates were then incubated in LacZ staining solution containing 2mM $MgCl_2$, 5mM potassium ferricyanide, 5mM potassium ferrocyanide, and 1mg/mL Xgal overnight at 37 °C in a

humidified chamber. The next day cells were washed three times with 1X PBS and then placed in mounting medium containing (Vector Laboratories, cat#: H-1200) and imaged by confocal microscopy (Zeiss, LSM700).

Immunostaining

Cultured mouse LECs after one week of culture were fixed in 4% paraformaldehyde (PFA) in Phosphate Buffered Saline (PBS) for 15 min and then washed with PBS 3x, blocked with 5% normal goat serum in 0.3% Triton-X100 for one hour, and were incubated with specific primary antibodies diluted in blocking buffer overnight at 4 °C. The primary antibodies included connexin 50 (α8-cx), connexin 46 (α3-cx), connexin 43 (α1-cx), and N-cadherin). After incubation with primary antibodies, the cells were washed with PBS and incubated in secondary antibodies (Jackson ImmunoResearch Laboratories) diluted in blocking buffer for one hour. The cells were then placed in mounting medium containing DAPI (Vector Laboratories, cat#: H-1200) and imaged by confocal microscopy (Zeiss, LSM700).

Western Blot

After one week of culture, LECs were collected in lysis buffer containing 20 mM Tris (pH 7.5),150 mM NaCl, 1 mM EDTA, 1 mM EGTA, 1% Triton X-100, and protease inhibitor cocktail (Roche, Cat#: 11 836 153 001). The cell suspension was sonicated for 10 s by a Kontes microultrasonic cell disrupter, and then centrifuged at 14,000 rpm for 10 min. The supernatant was used for experiments. Protein concentration was measured by Coomassie assay (Pierce, cat#:23200). Equal volumes of 2× sample buffer (0.1 M Tris-PO4, pH 6.8, 4% SDS, 8% Bromophenol blue, 20% Glycerol, 10% 2-mercaptoethanol) was added to the protein solution and mixed well. All procedures were performed on ice. Equal amounts of protein (10 μg) were separated by SDSPAGE and transferred to PVDF membranes. The membranes were blocked with 5% non-fat milk and incubated with antibodies against αA-, αB-, β-crystallin, or β-actin (Sigma, cat#: A5441), at 4 °C overnight. After three 5 min washes in TBST (0.15 M NaCl, 0.05 M Tris, pH 7.4, 0.1% Tween 20) buffer, the membranes were incubated in HRP-conjugated secondary antibodies for one hour. After three washes with TBST, protein bands were visualized by an Azure Biosystems c600 imager.

4.3 Results

4.3.1 Low-dose FGF does not affect connexin-50 at the expression level

We evaluated the effect of low-dose FGF on the expression of connexin-50 (α8-cx) in lens epithelial cells using LacZ staining. Lens epithelial cells were harvested from B6 α8-/- mice containing the LacZ gene tied to the α8-cx promoter and grown on several 35mm glass bottom culture plates. To determine a baseline level of LacZ staining, one set of plates was grown in regular SB media without FGF. This media is sufficient to grow lens epithelial cells in culture until confluent, as well as maintain lens epithelial cell qualities. Plates grown in SB+FGF were used to determine the effect of low-dose FGF (5ng/mL) on α8-cx expression levels, as this concentration of FGF was shown previously to be sufficient to suppress protein levels of α8-cx. First, camera images were taken of each plate to simply visually confirm the presence or absence of LacZ staining (Figure 4.1). LacZ staining in SB plates was weak to medium, but consistent across all plates, with stronger staining near the center of each plate. Cells grown in SB+FGF showed similar levels of LacZ staining compared to SB plates. Levels of LacZ staining in SB+FGF plates were well above negative control plates, which lacked any staining whatsoever. Each plate was further examined under confocal microscopy using a 20X lens to further examine the level of LacZ staining (Figure 4.2). Here, several 20X, and some 10X, images were taken from different regions around the same plate in order to make a more detailed observation about the distribution of LacZ staining. As expected, the level of staining differed between the regions near the center of the plate, and near the periphery, but in all cases but the negative control, there was some level of LacZ expression, meaning low-dose FGF was not sufficient alone to account for the complete loss of α8-cx protein previously observed in these culture cells.

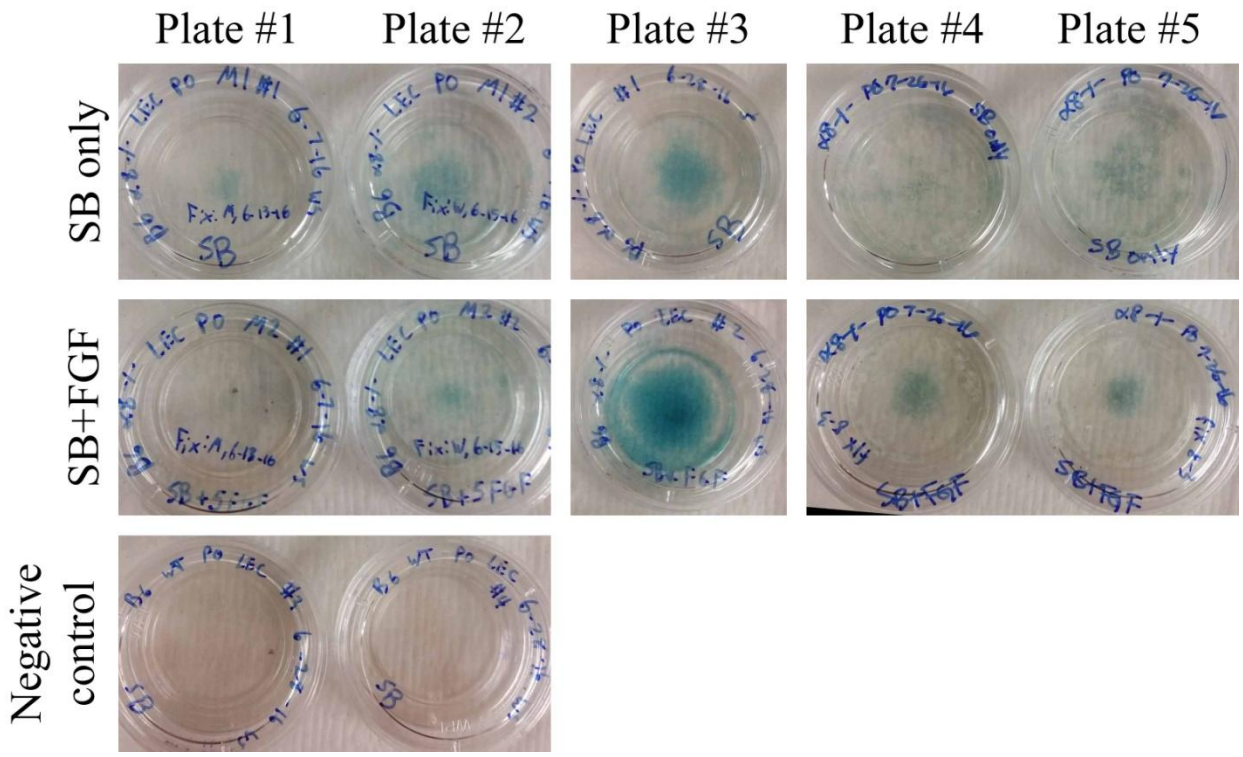

Figure 4.1. Camera images of cell culture plates with LacZ staining of lens epithelial cells. The plates in the top row were grown in SB media and were used to determine a baseline level of LacZ staining, with α8-cx presumably being expressed normally (albeit a non-functional mutant). The plates in the middle row were grown in SB+FGF media, at a concentration of 5ng/mL, which is known to suppress α8-cx at the protein level. Negative control plates were grown in SB media. Experiment plates contained cells from B6 α8-/- mice containing the LacZ reporter gene, while negative control plates contained cells from B6 WT mice without the LacZ gene.

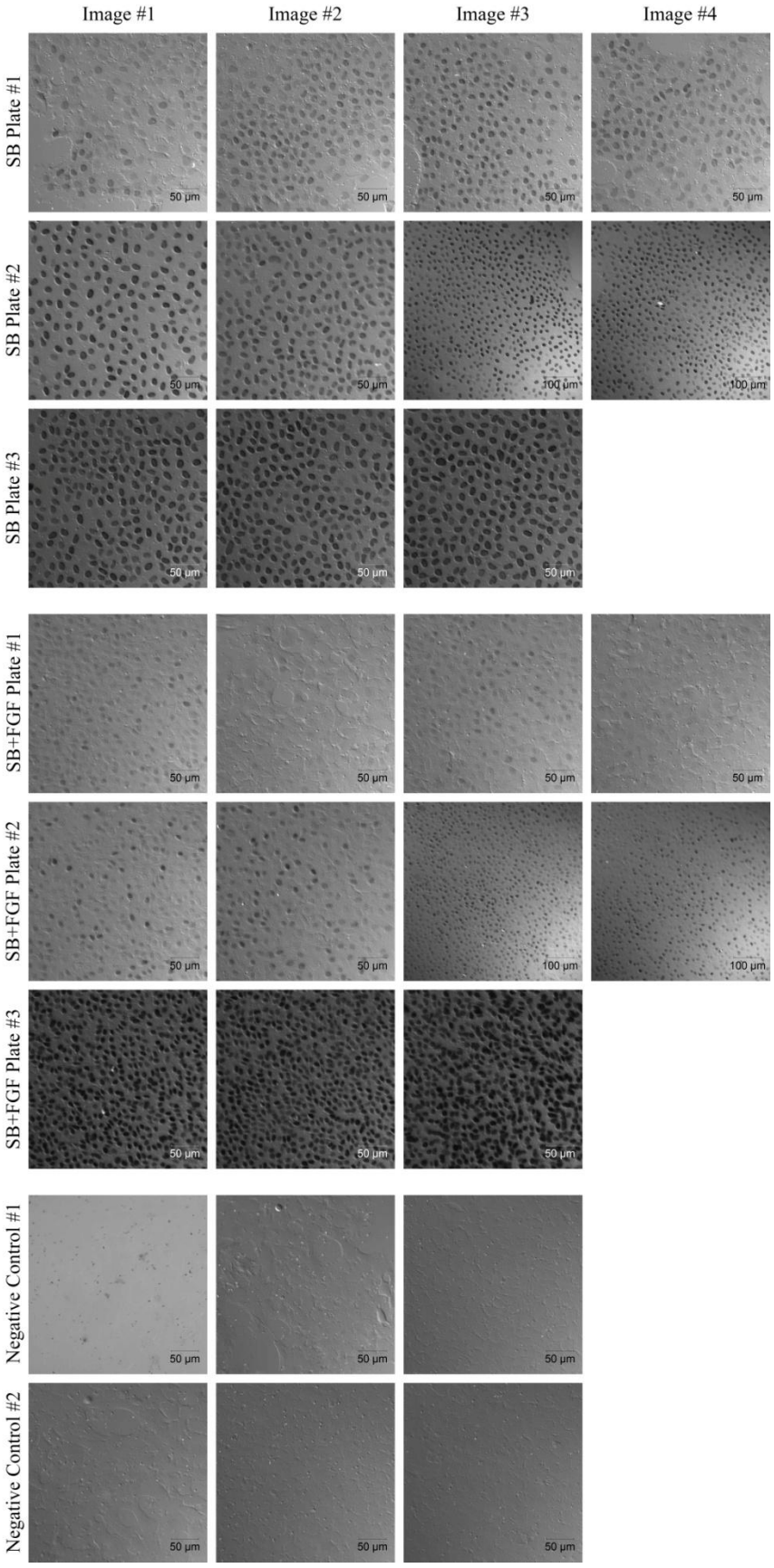
Image #1
Image #2
Image #3
Image #4
SB Plate #1
SB Plate #2
SB Plate #3
SB+FGF Plate #1
SB+FGF Plate #2
SB+FGF Plate #3
Negative Control #1
Negative Control #2
50 µm
100 µm

Figure 4.2. 20X confocal images of lens epithelial cells with LacZ staining from several plates pictured in Figure 4.1. Each column represents an image taken from separate regions of the same plate. As in Figure 4.1, cells in images in the top three rows were grown in SB media, while cells in images in the middle three rows were grown in SB+FGF media, at a concentration of 5ng/mL. Plates from columns #4 or #5 from Figure 4.1 were not imaged at 20X and were just used for visual confirmation of LacZ staining. Scale bars, 50µm or 100µm.

4.3.2 Effect of Low-Dose FGF on Connexin-50, -46, & -43 Protein Levels in Lens Epithelial Cell Culture

To test the effects of culture medium on expression of the three major connexins in the lens, connexin 50 (α8-cx), connexin 46 (α3-cx), and connexin 43 (α1-cx), primary lens epithelial cells were grown in culture, immunostained for each of these proteins, and images examined for differences in localization or intensity. The effects of both low dose FGF as well as the MEK1 and MEK2 inhibitor U0126, and their potential interaction, were tested by growing cells a total of six different culture conditions. For each condition, cells were grown in an initial culture medium for one to two weeks to allow for expansion, and then switched to a different culture medium for 48 hours before fixation. The six culture mediums tested were: 1. SB only, 2. SB initially, then SB+FGF for 48 hours, 3. SB initially, then SB+U0126 for 48 hours, 4. SB initially, then SB+FGF+U0126 for 48 hours, 5. SB+FGF initially, then SB+FGF+U0126 for 48 hours, and 6. SB+FGF only.

When examining connexin 50 immunostaining in our cultured lens epithelial cells, we confirmed that supplementation with SB but without FGF maintains expression of connexin 50. We observed decent to strong expression of connexin 50 in most lens epithelial cells imaged cultured in condition 1 (SB only) (Figure 4.3). For condition 2, when initially grown in SB but later incubated for 48 hours in SB+FGF, we observed somewhat weaker connexin 50 staining in one of four total repeats, but otherwise expression was similar to condition 1 (Figure 4.4). This means that a 48 hour treatment of FGF after lens epithelial cells are already established has little to no effect on connexin 50 expression. Next, as expected, for condition 3 we found that the drug alone had little to effect on connexin 50 expression, with staining patterns similar to control condition 1 (Figure 4.5). For condition 4, where cells were grown initially in SB but then incubated with SB+FGF+U0126, the expression pattern of connexin 50 looked mostly similar to control condition 1, indicating that the drug could be countering the effects of FGF, or that 48 hours isn't enough to have an appreciable effect (Figure 4.6). For both conditions 5 and 6, where cells were grown initially in SB+FGF medium, our previous findings were confirmed and almost no connexin 50 staining was visible in either case (Figures 4.7, 4.8). As for condition 5, this might also indicate once again that 48 hours might not be a long enough incubation time for the drug U0126 to reverse the effects of FGF treatment.

We next completed an immunostaining panel by examining the effects of each culture condition on the other two major connexins found in the lens, connexins 46 and 43. Condition 1 produced decent to strong staining of connexin 46 (Figure 4.9), while condition 2 actually greatly reduced connexin 46 expression compared to condition 1 (Figure 4.10). This might indicate that connexin 46 might be more sensitive to FGF treatment compared to connexin 50 because 48 hours appeared to be enough to visually lower its level of staining. Condition 3 produced somewhat similar connexin 46 staining as control condition 1 (Figure 4.11), but condition 4 was inconsistent across several repeats (Figure 4.12). This might further confirm that connexin 46 levels are indeed more sensitive to culture medium supplementation. Finally, condition 5 displayed decreased levels of connexin 46 (Figure 4.13), indicating that FGF treatment might decrease but not completely abolish connexin 46 expression. Immunostaining of connexin 43 produced weak to inconsistent staining in lens epithelial cells across almost all above culture conditions (Figures 4.14-18). Further experimentation or a more sensitive antibody might be necessary to further examine the effects of FGF or U0126 treatment on connexin 43.

4.3.3 Examination of the Effect of Low-Dose FGF on Protein Levels of Connexin-50

In order to examine more precisely the effect of FGF on whole protein levels of connexin-50, we performed a series of western blot experiments using the various culture conditions described above. We confirmed that supplementation of SB media with low dose (5ng/mL) FGF was enough to almost completely suppress connexin-50 protein levels (Figure 4.19, 4.20). We then collected whole protein samples from primary lens epithelial cells grown in the remaining culture conditions described above. We initially saw similar results as in Figure 4.6a, with strong bands of connexin 50 in SB control lanes and reduced levels in SB+FGF lanes, but almost no other culture condition that we expected produced strong bands (Figure 4.21). Culture conditions that exhibited similar staining levels as the control SB condition did not show a corresponding strong band, such as condition 3 (SB+U026). This is despite almost every band producing a consistent β-actin loading control band. After a second attempt, each lane produced a consistent β-actin loading control band but once again it was difficult to discern any connexin 50 band in most culture condition lanes (Figure 4.22). Due to repeat testing and troubleshooting, some repeat lanes had to be omitted in this second round of western gels.

One possible explanation for the observed inconsistency is that culture plates for protein sample collection were usually kept in culture long enough to allow for cells to grow more fully confluent to obtain the maximal amount of whole protein upon protein harvest. We suspect that because some culture plates were kept in culture longer than two weeks this might have started to affect their connexin 50 protein levels. Future experiments might need to be further standardized in order to obtain reliable and meaningful connexin 50 protein readings.

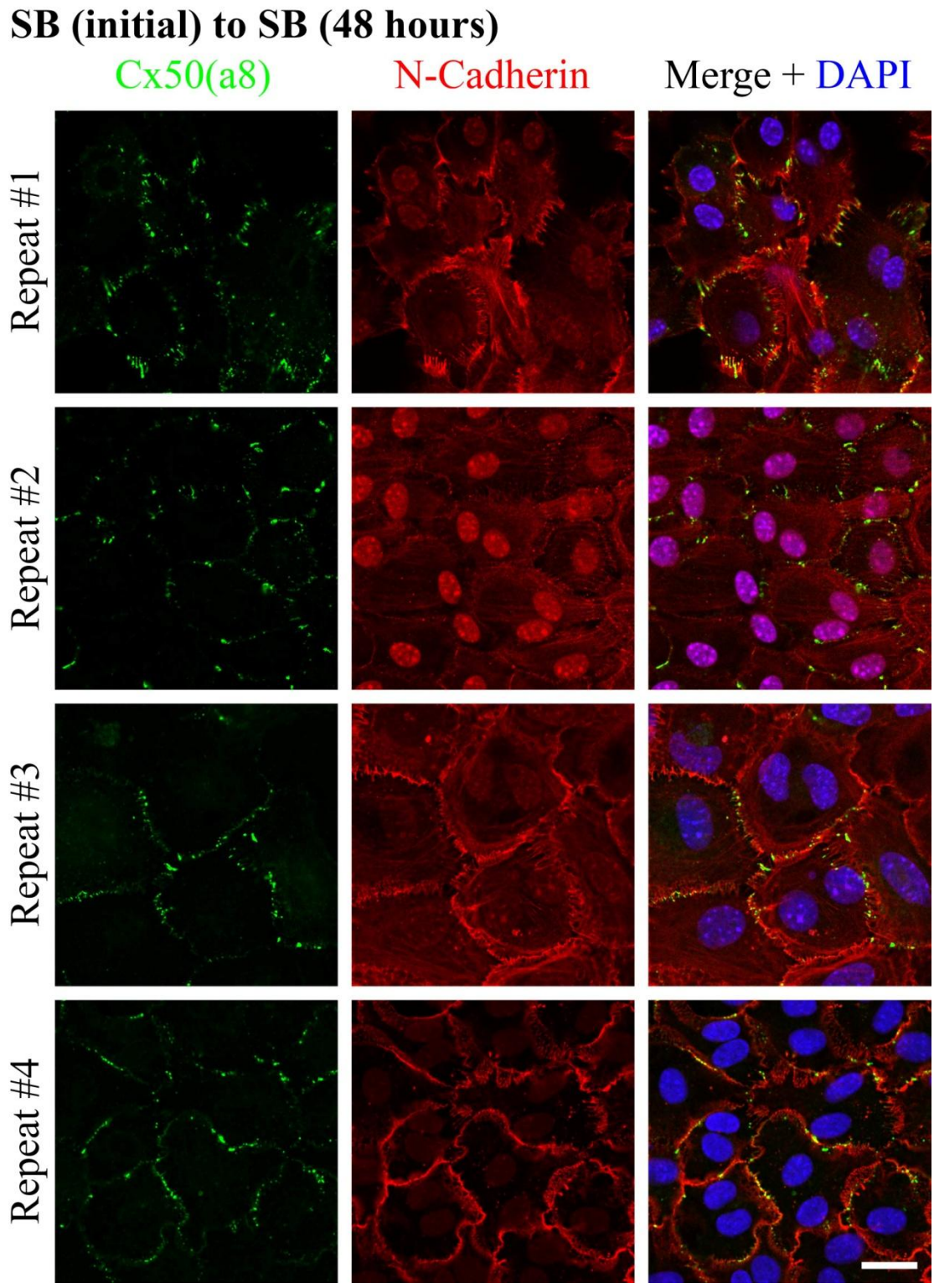

Figure 4.3. Connexin-50 (green) and N-cadherin (red) staining in lens epithelial cells initially grown in SB media until confluent, and then continually grown in SB media for 48 hours until fixation. Scale bar, 20µm.

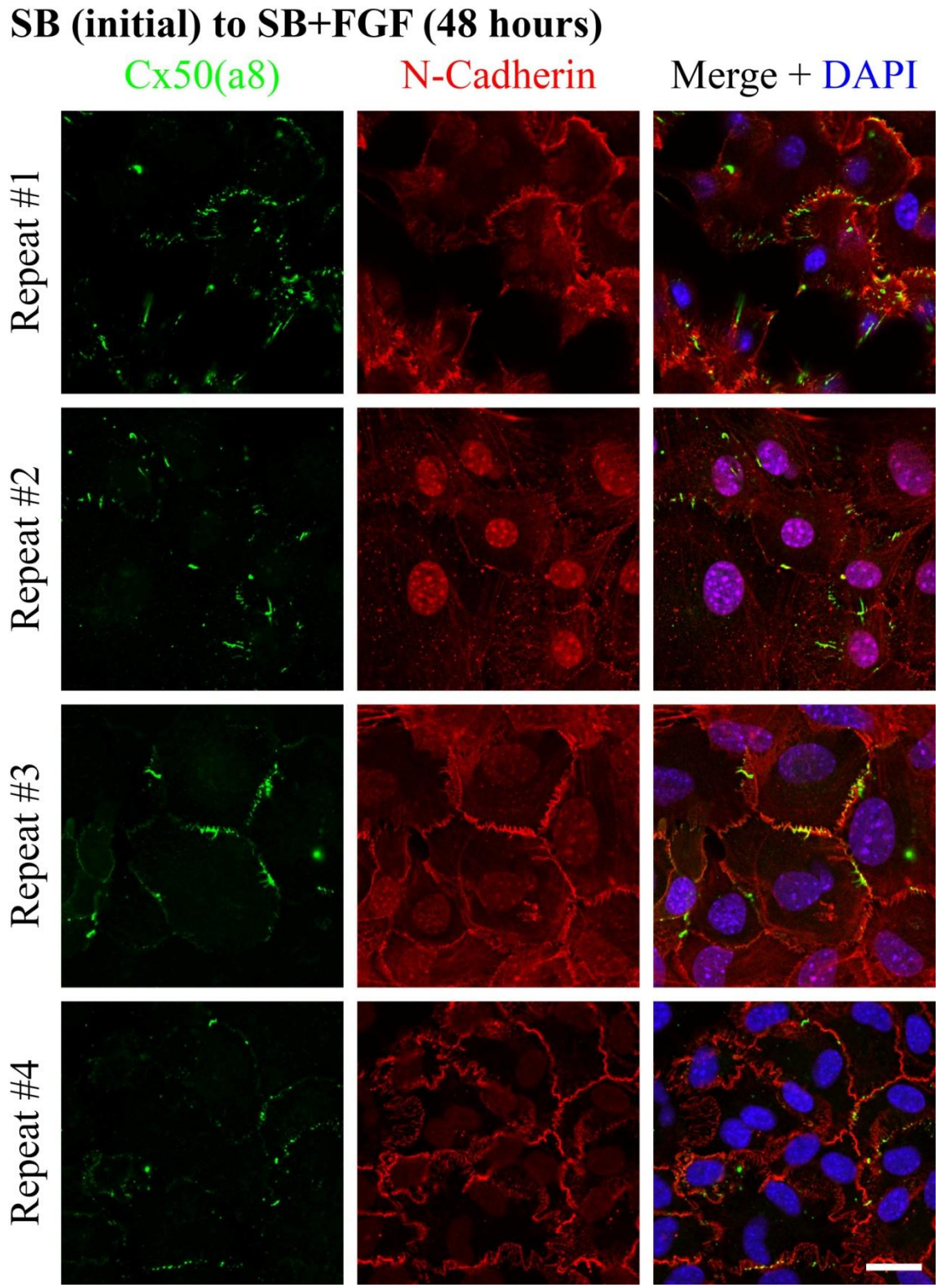

Figure 4.4. Connexin-50 (green) and N-cadherin (red) staining in lens epithelial cells initially grown in SB media until confluent, and then continually grown in SB+FGF media for 48 hours until fixation. Scale bar, 20µm.

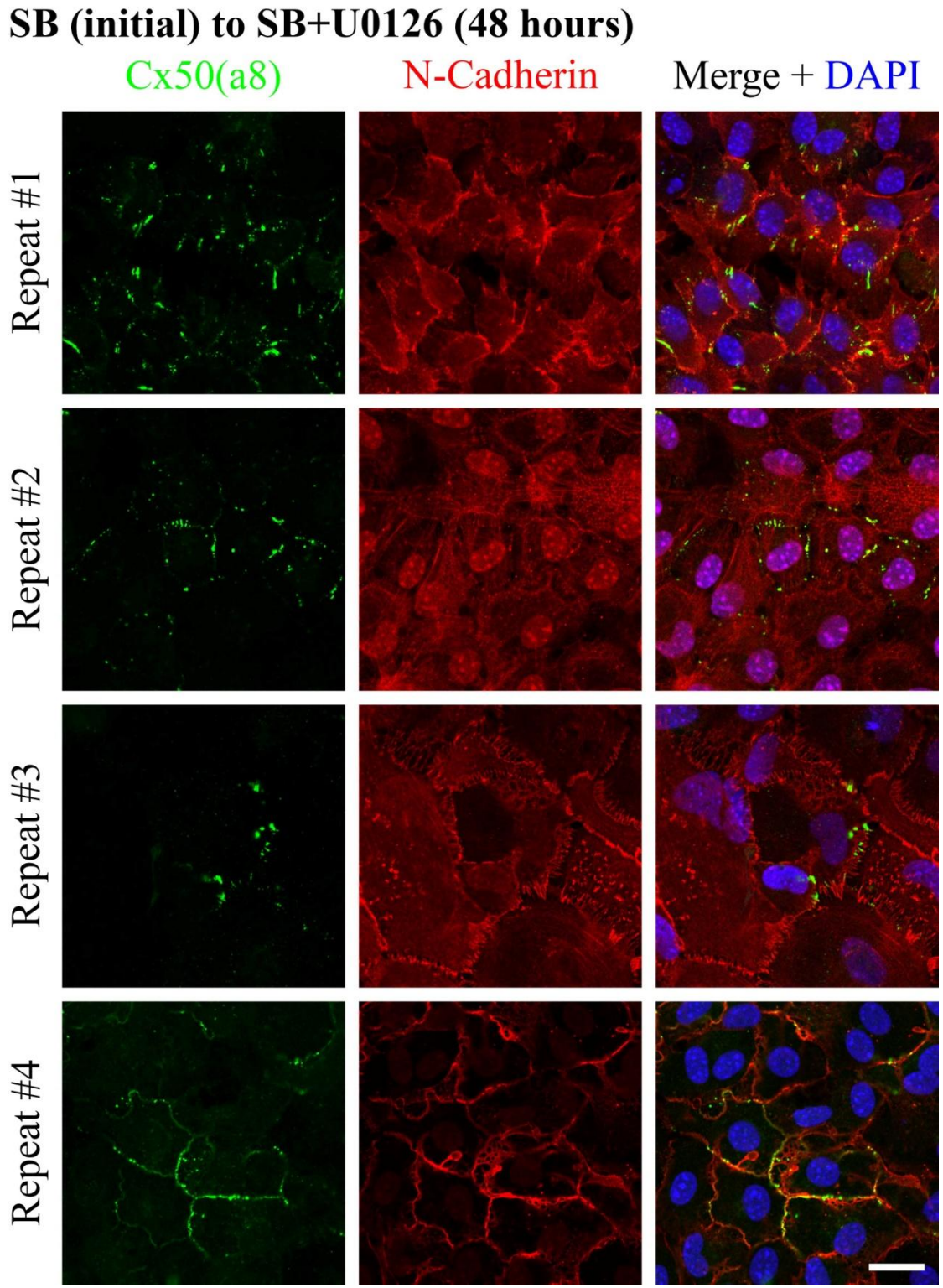

Figure 4.5. Connexin-50 (green) and N-cadherin (red) staining in lens epithelial cells initially grown in SB media until confluent, and then continually grown in SB+U0126 media for 48 hours until fixation. Scale bar, 20µm.

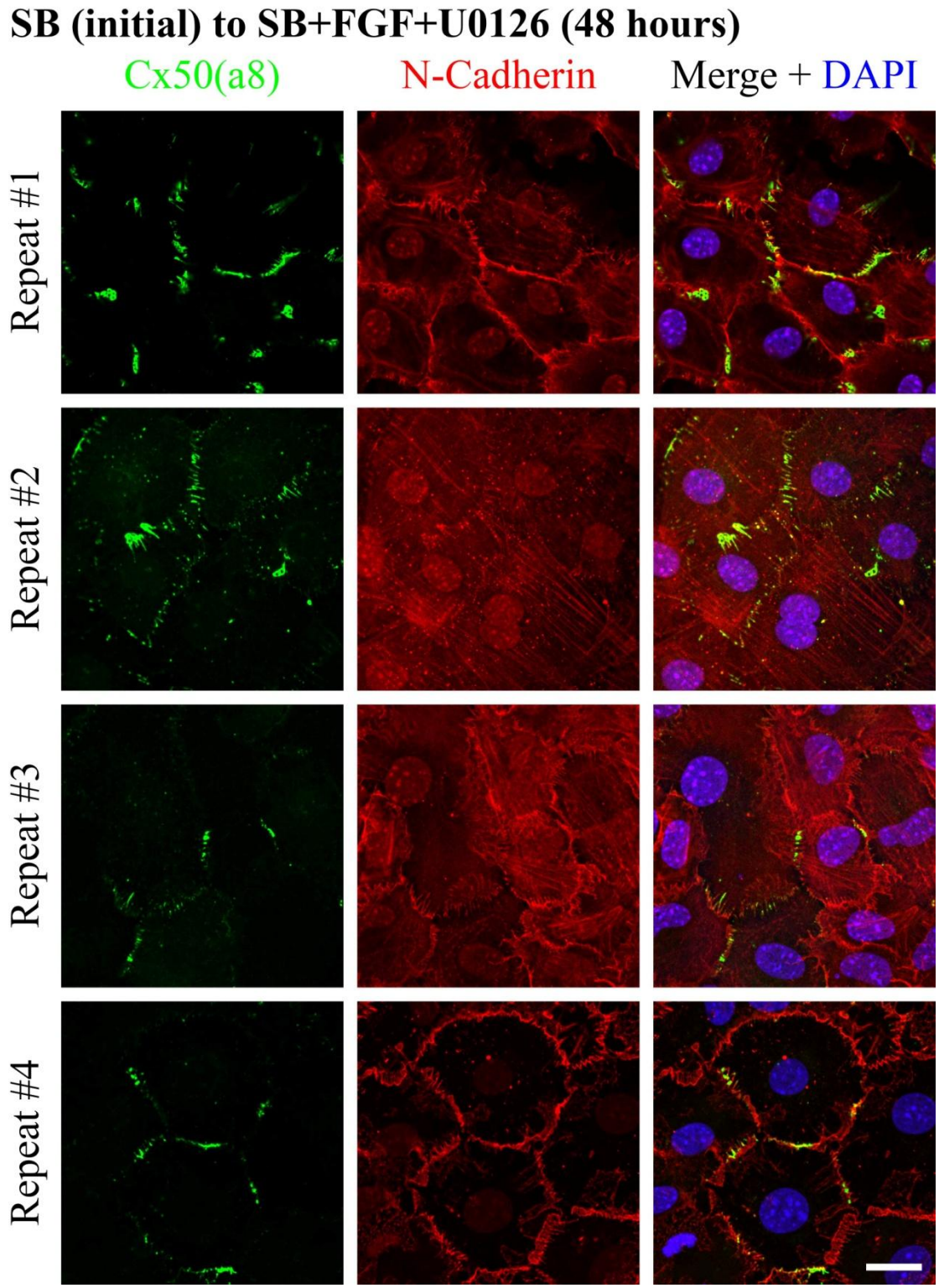

Figure 4.6. Connexin-50 (green) and N-cadherin (red) staining in lens epithelial cells initially grown in SB media until confluent, and then continually grown in SB+FGF+U0126 media for 48 hours until fixation. Scale bar, 20µm.

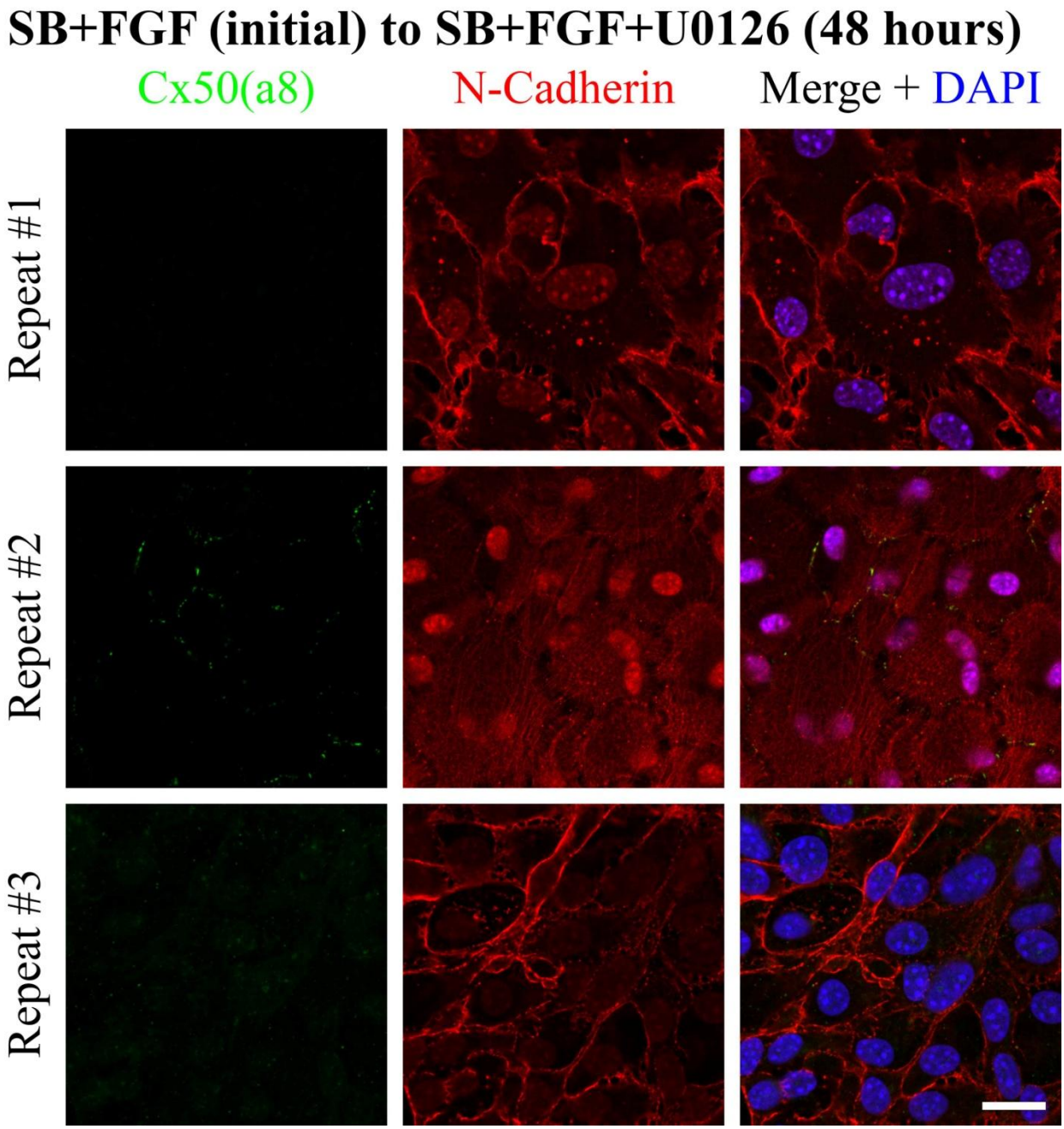

Figure 4.7. Connexin-50 (green) and N-cadherin (red) staining in lens epithelial cells initially grown in SB+FGF media until confluent, and then continually grown in SB+FGF+U0126 media for 48 hours until fixation. Scale bar, 20µm.

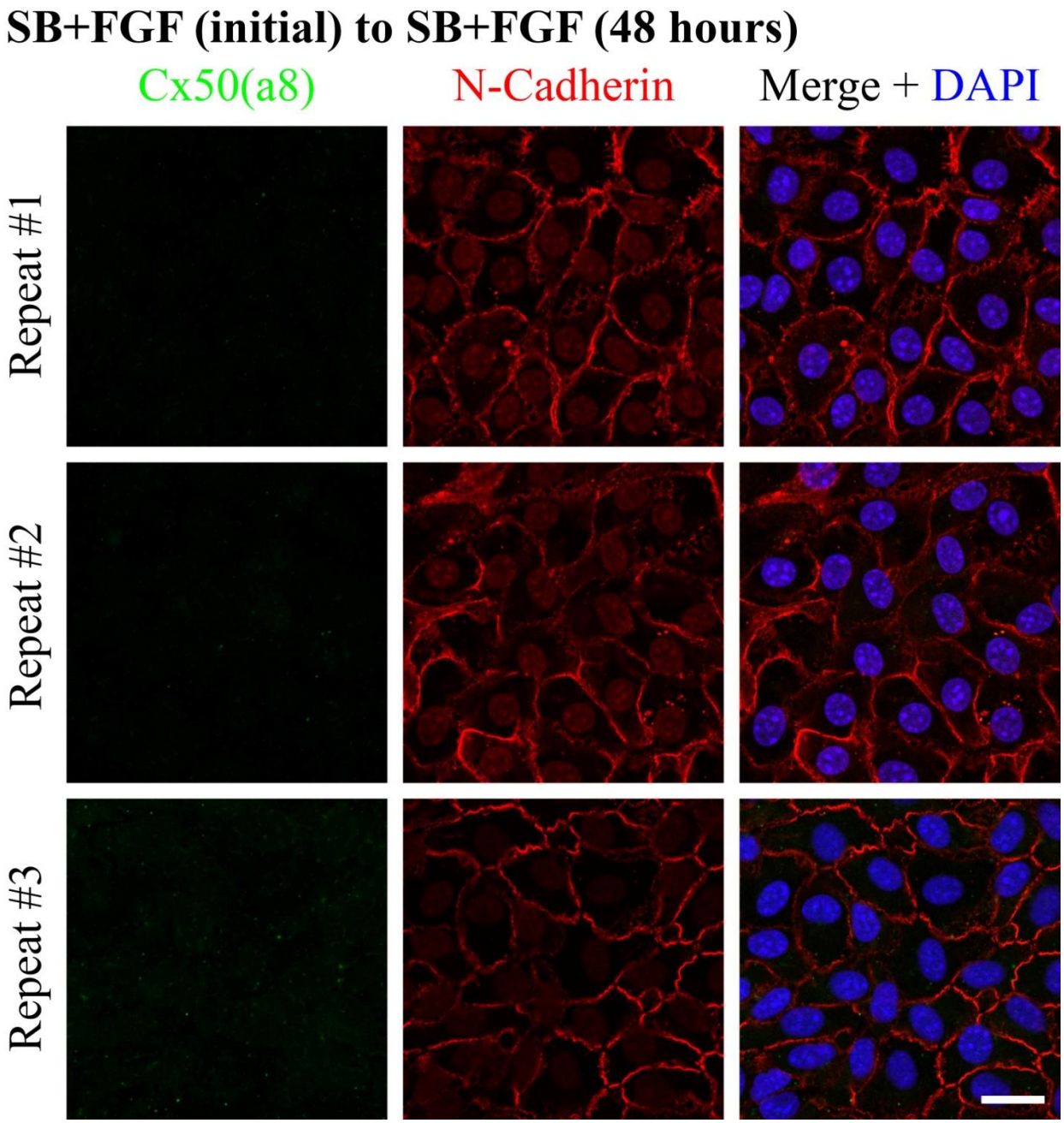

Figure 4.8. Connexin-50 (green) and N-cadherin (red) staining in lens epithelial cells initially grown in SB+FGF media until confluent, and then continually grown in SB+FGF media for 48 hours until fixation. Scale bar, 20µm.

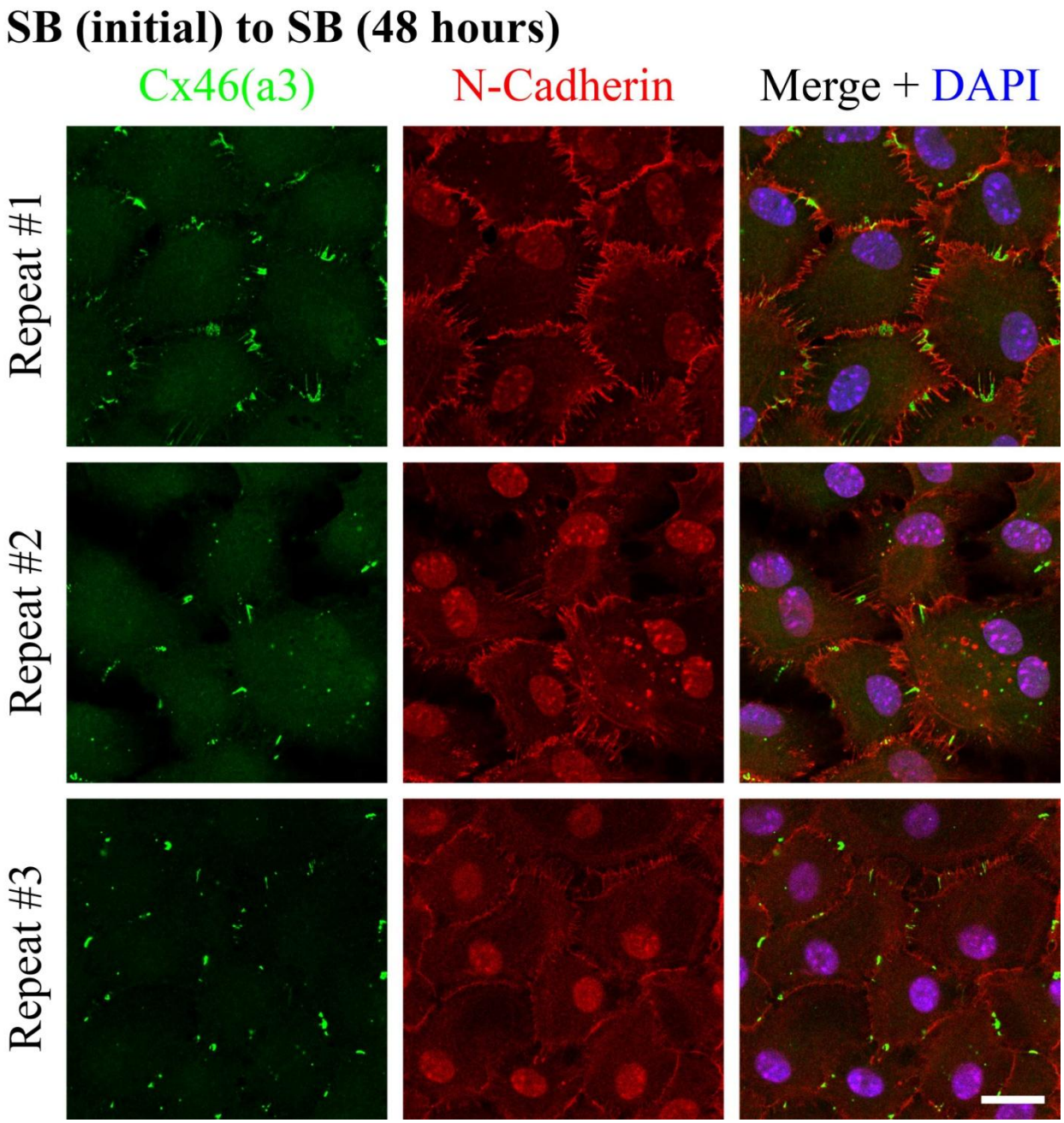

Figure 4.9. Connexin-46 (green) and N-cadherin (red) staining in lens epithelial cells initially grown in SB media until confluent, and then continually grown in SB media for 48 hours until fixation. Scale bar, 20µm.

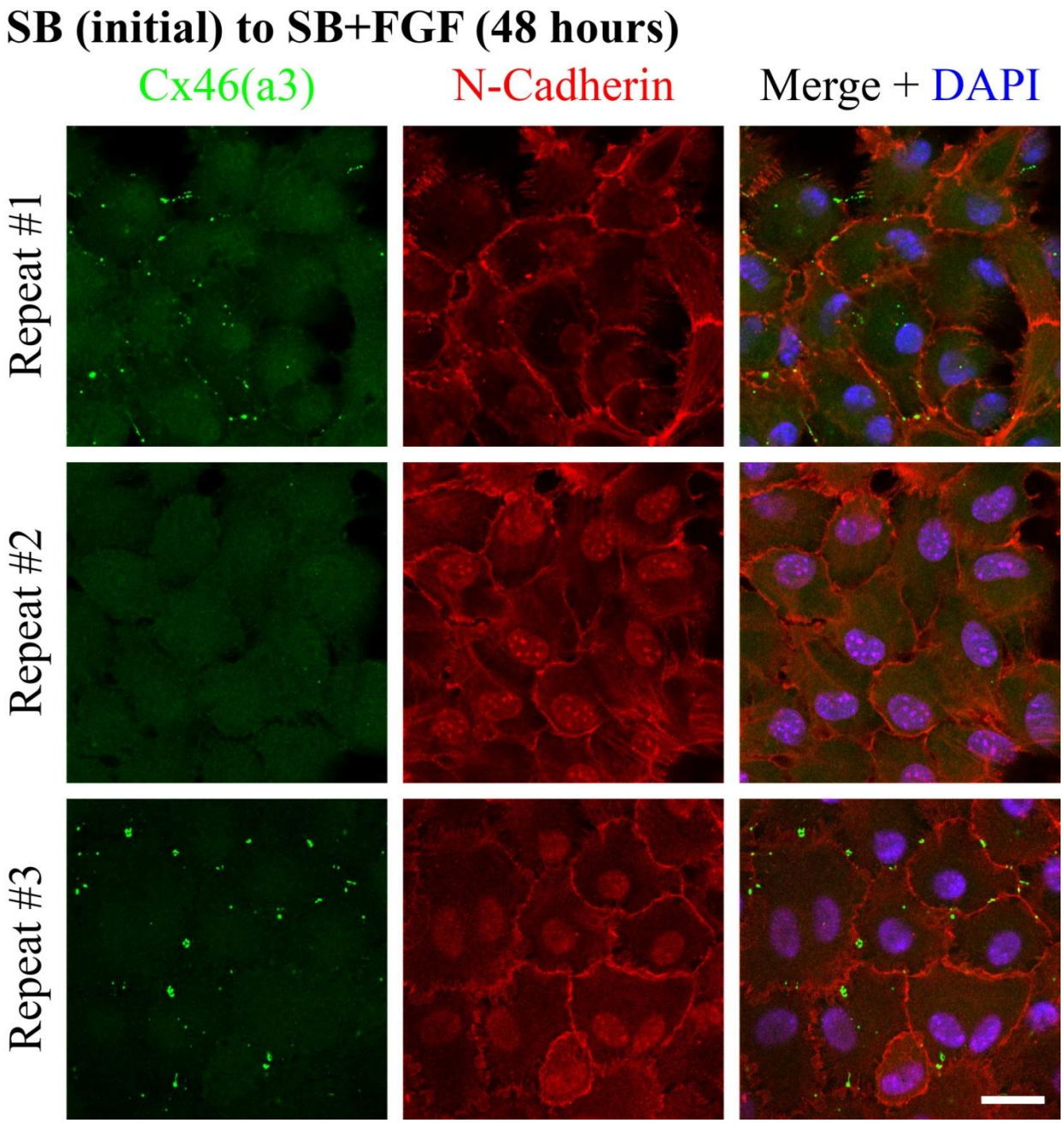

Figure 4.10. Connexin-46 (green) and N-cadherin (red) staining in lens epithelial cells initially grown in SB media until confluent, and then continually grown in SB+FGF media for 48 hours until fixation. Scale bar, 20μm.

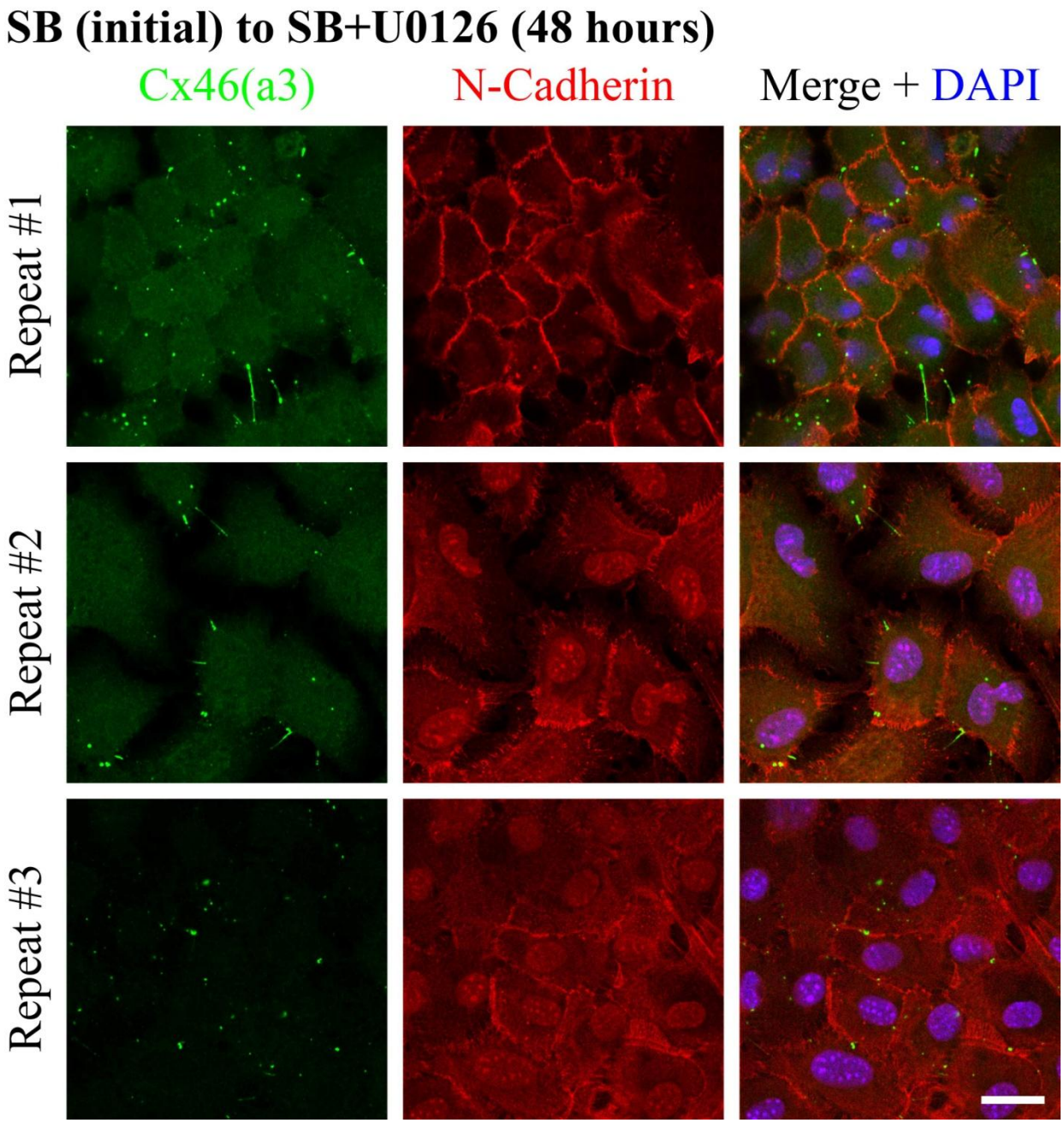

Figure 4.11. Connexin-46 (green) and N-cadherin (red) staining in lens epithelial cells initially grown in SB media until confluent, and then continually grown in SB+U0126 media for 48 hours until fixation. Scale bar, 20μm.

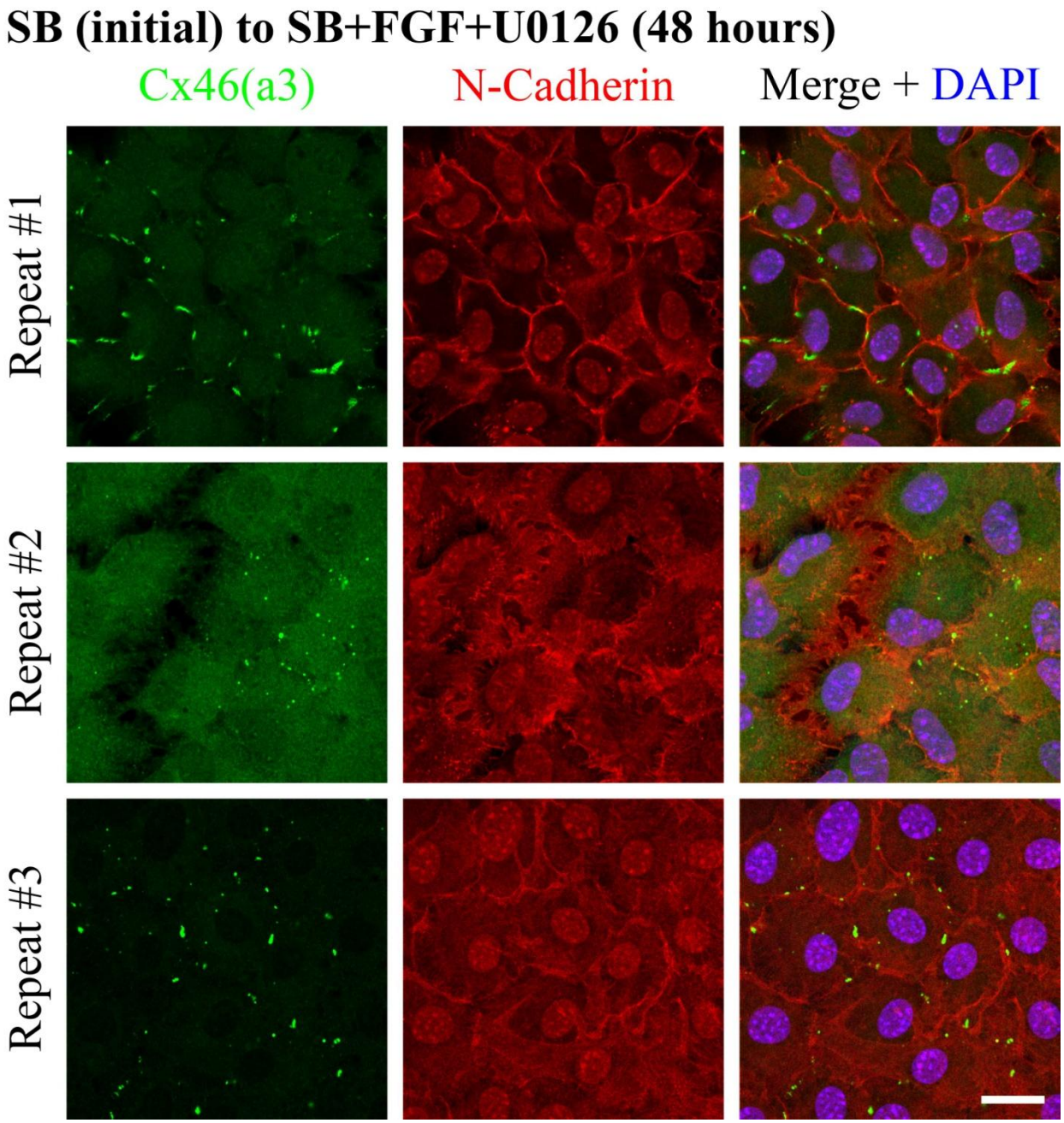

Figure 4.12. Connexin-46 (green) and N-cadherin (red) staining in lens epithelial cells initially grown in SB media until confluent, and then continually grown in SB+FGF+U0126 media for 48 hours until fixation. Scale bar, 20µm.

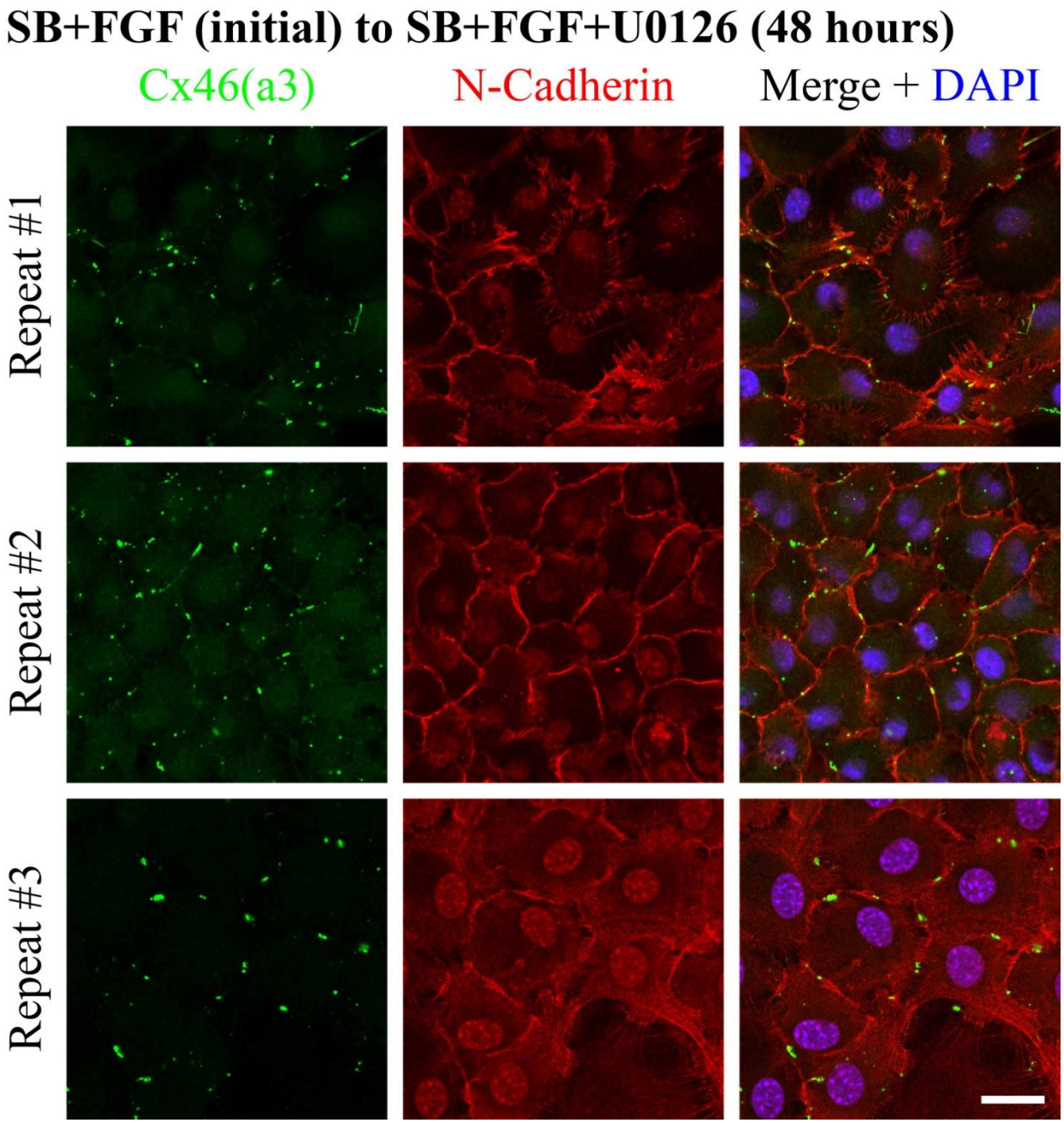

Figure 4.13. Connexin-46 (green) and N-cadherin (red) staining in lens epithelial cells initially grown in SB+FGF media until confluent, and then continually grown in SB+FGF+U0126 media for 48 hours until fixation. Scale bar, 20µm.

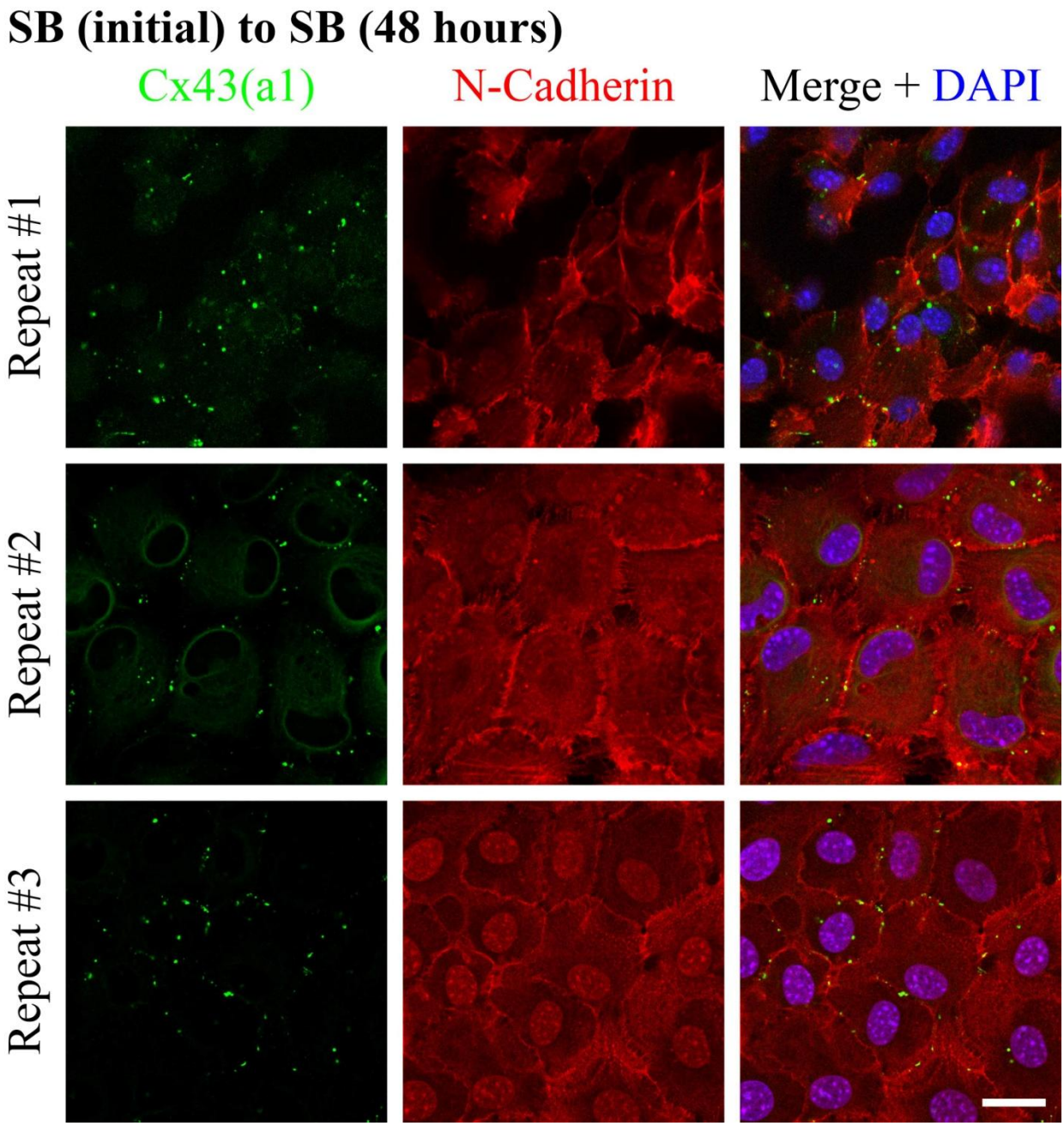

Figure 4.14. Connexin-43 (green) and N-cadherin (red) staining in lens epithelial cells initially grown in SB media until confluent, and then continually grown in SB media for 48 hours until fixation. Scale bar, 20µm.

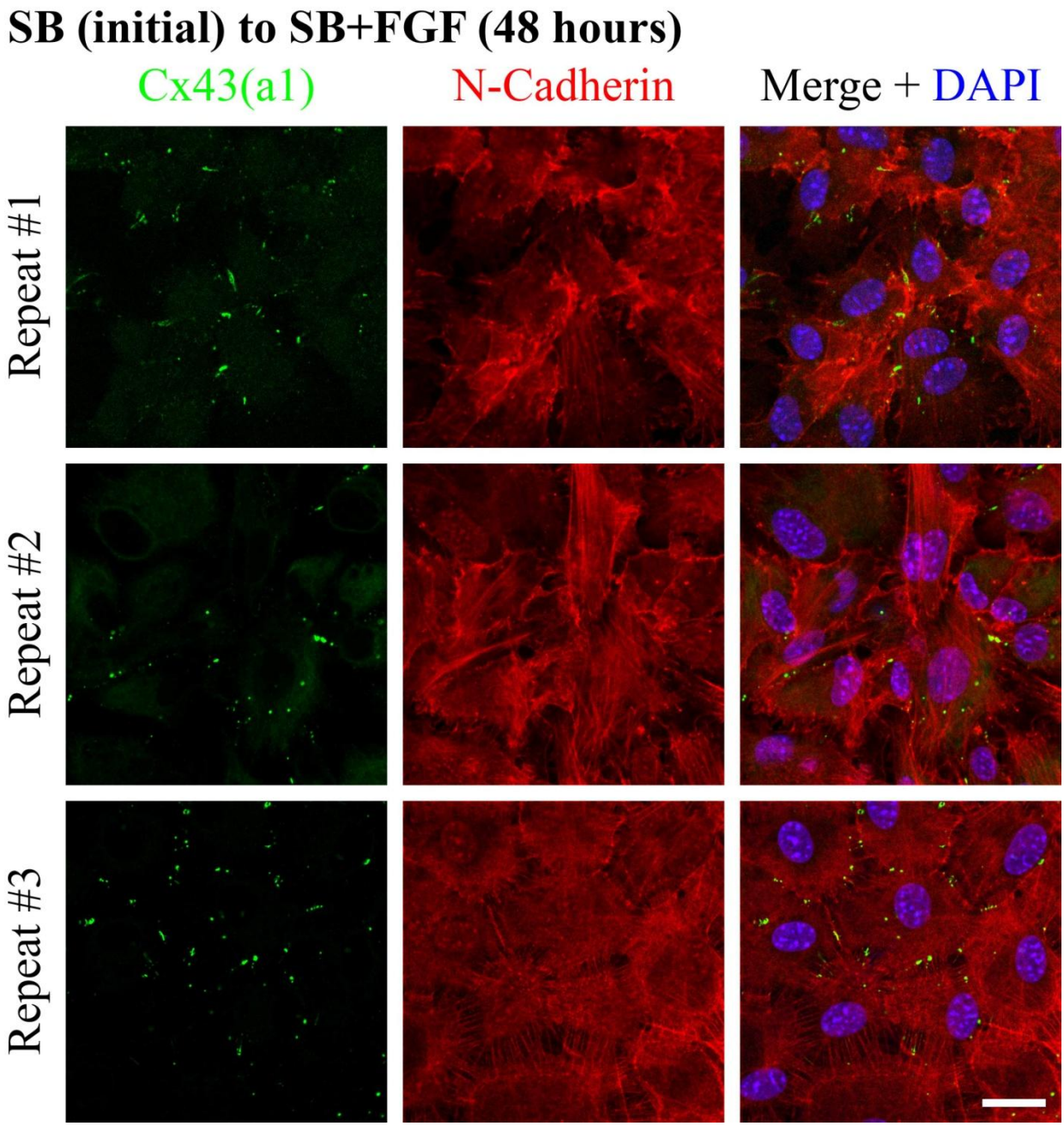

Figure 4.15. Connexin-43 (green) and N-cadherin (red) staining in lens epithelial cells initially grown in SB media until confluent, and then continually grown in SB+FGF media for 48 hours until fixation. Scale bar, 20μm.

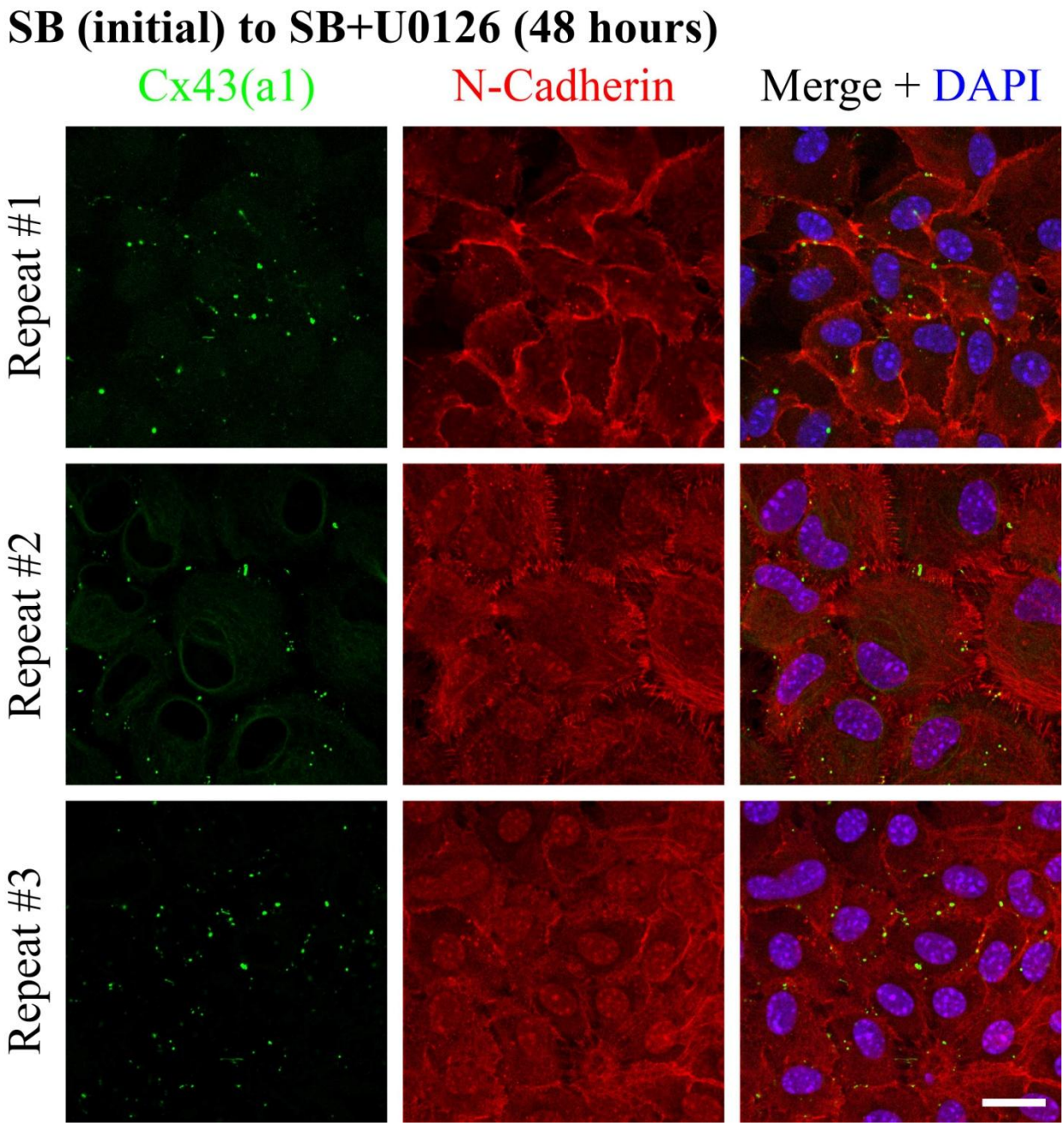

Figure 4.16. Connexin-43 (green) and N-cadherin (red) staining in lens epithelial cells initially grown in SB media until confluent, and then continually grown in SB+U0126 media for 48 hours until fixation. Scale bar, 20µm.

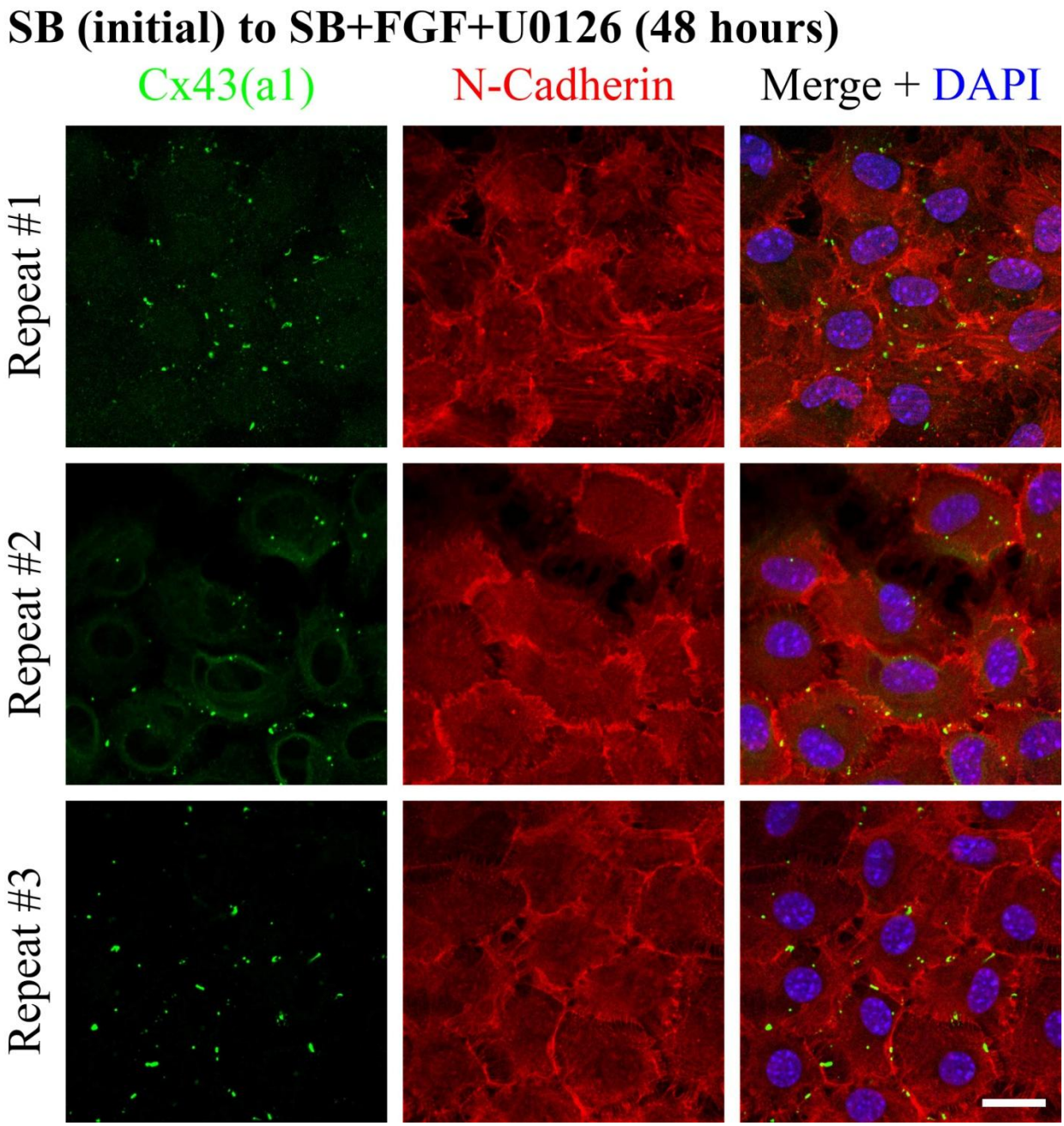

Figure 4.17. Connexin-43 (green) and N-cadherin (red) staining in lens epithelial cells initially grown in SB media until confluent, and then continually grown in SB+FGF+U0126 media for 48 hours until fixation. Scale bar, 20µm.

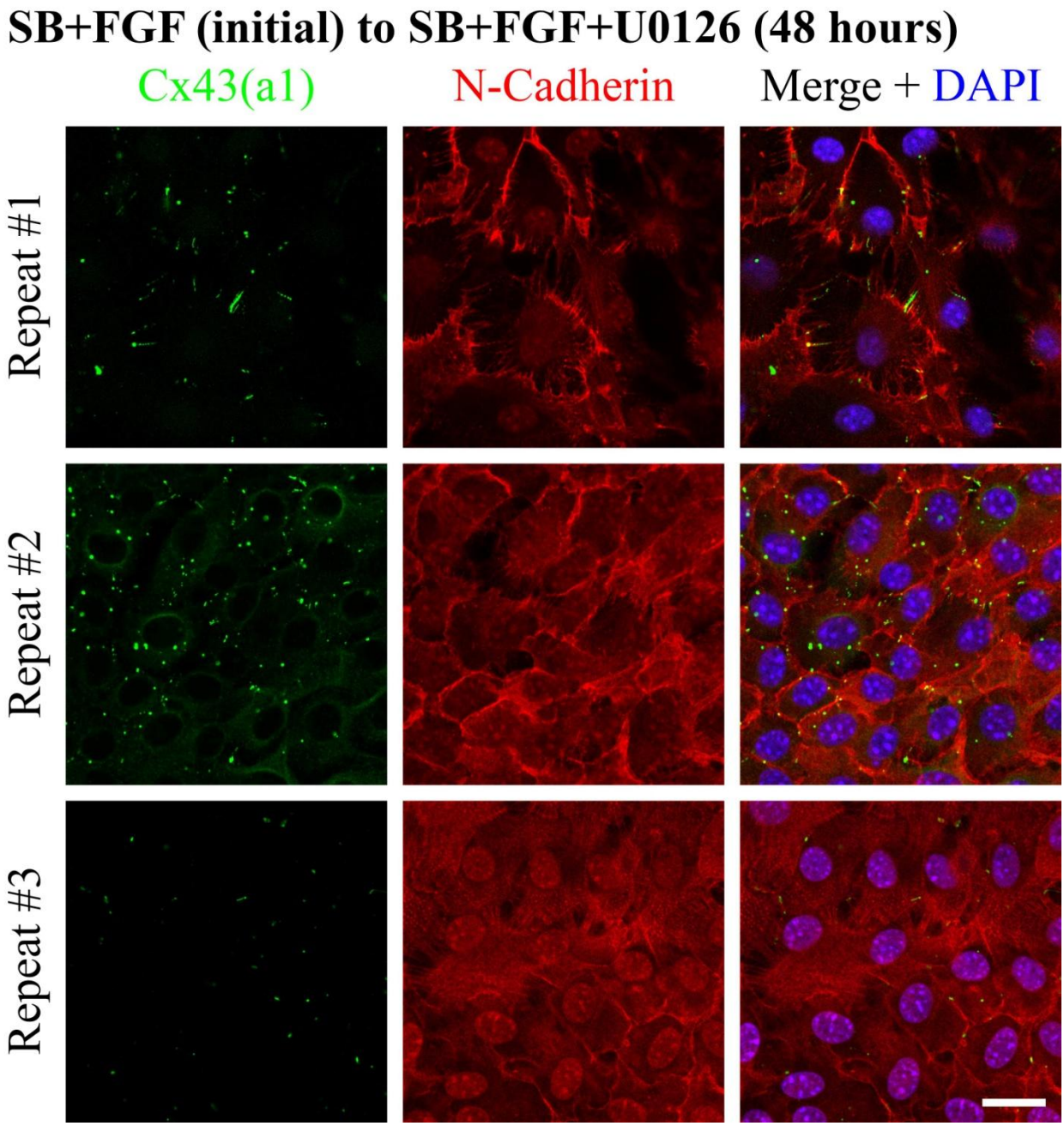

Figure 4.18. Connexin-43 (green) and N-cadherin (red) staining in lens epithelial cells initially grown in SB+FGF media until confluent, and then continually grown in SB+FGF+U0126 media for 48 hours until fixation. Scale bar, 20µm.

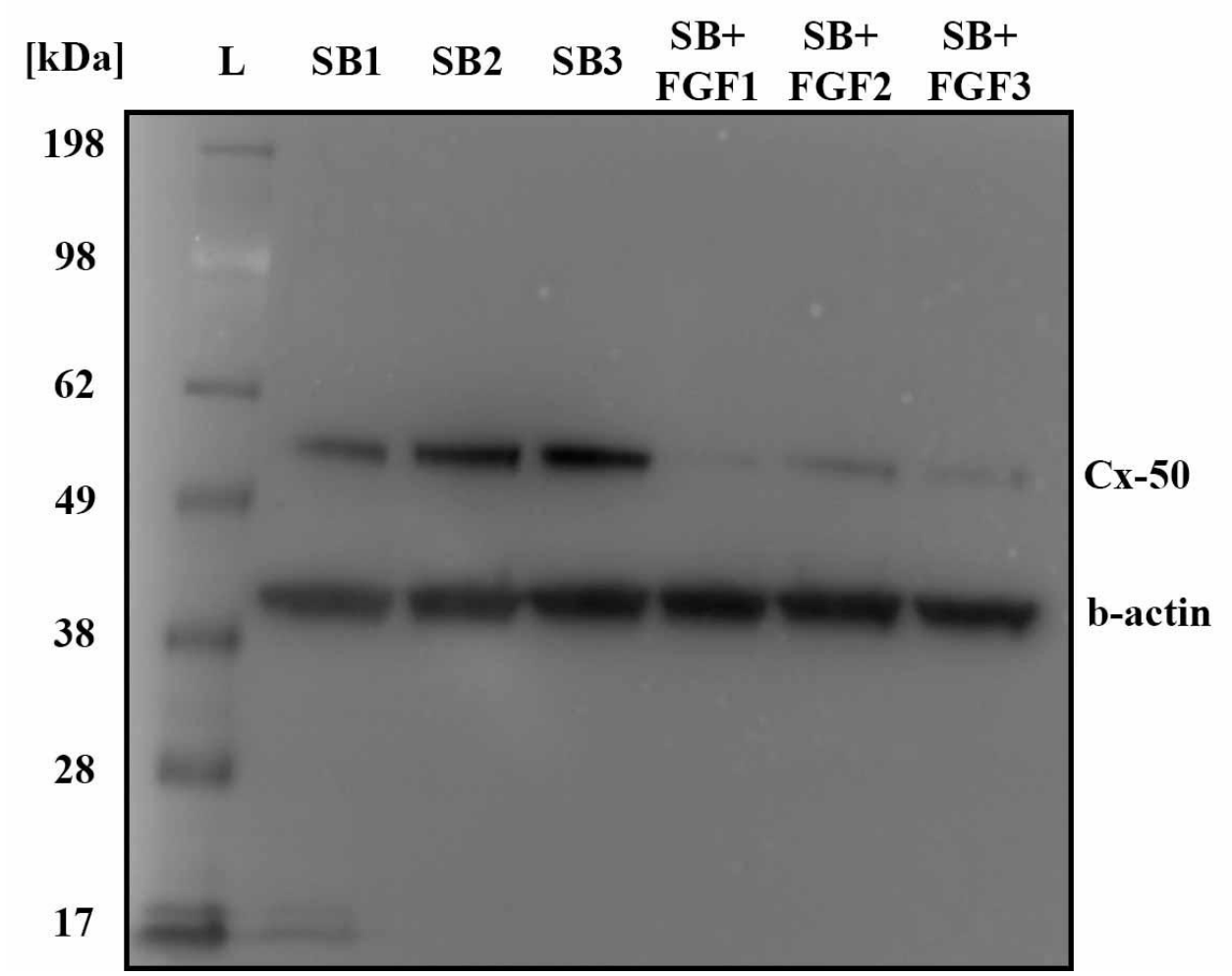

Figure 4.19. Western blot showing connexin-50 protein levels between SB and SB+FGF culture conditions. Beta-actin is shown as a loading control.

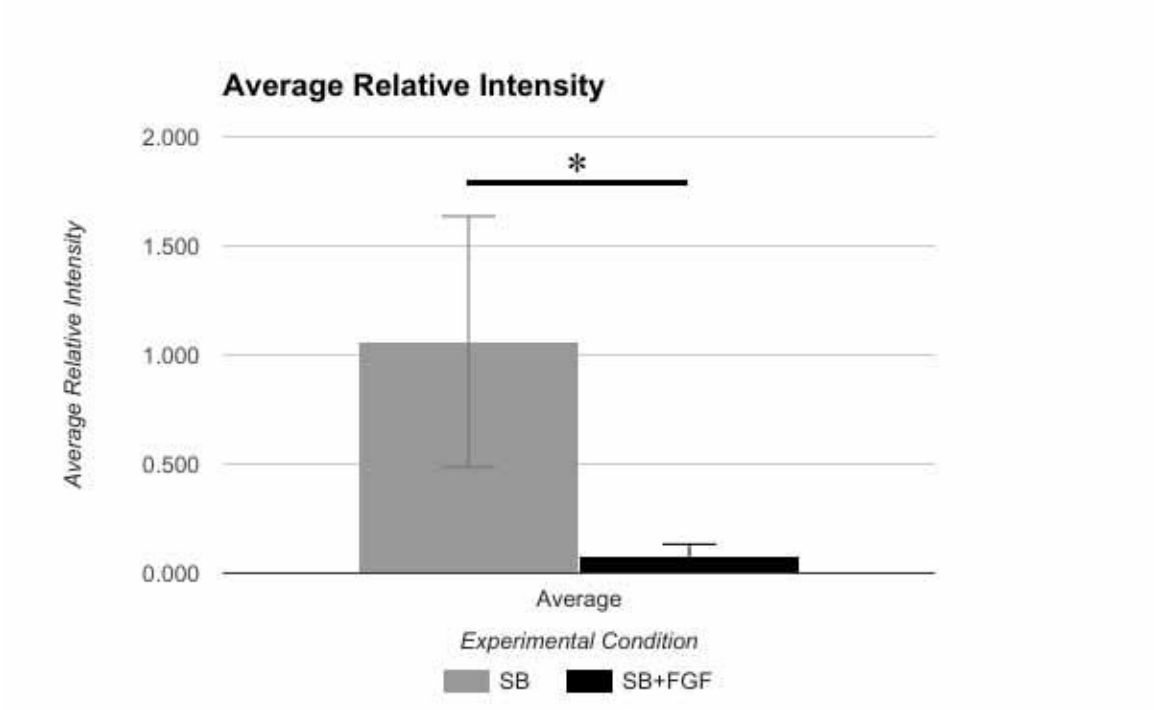

Figure 4.20. Relative intensity measurement of bands from Figure 4.6a. Data demonstrates that treatment with a low dosage of FGF severely reduces connexin-50 protein levels. * = $p<0.001$.

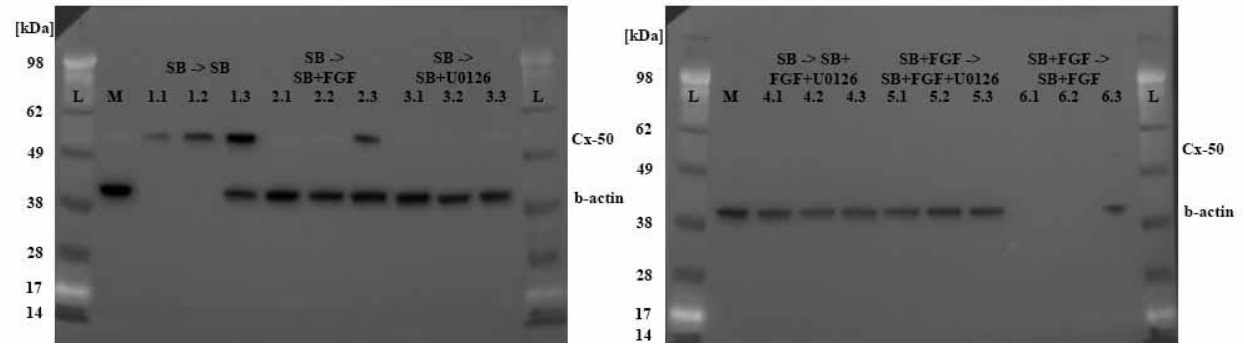

Figure 4.21. First repeat of western blot including three samples from all culture conditions. Lanes labeled "M" was the master lane containing a mix of all three samples from SB+U0126 culture condition and was used to normalize between gels.

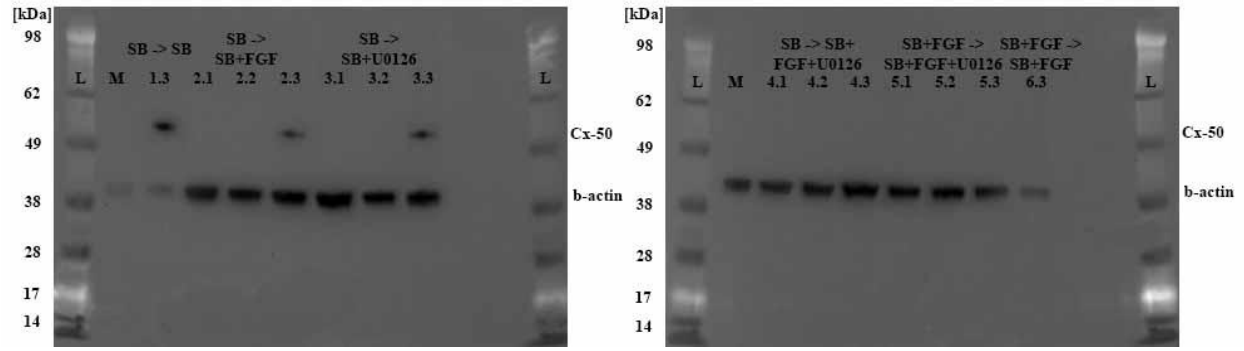

Figure 4.22. Second repeat of western blot including three samples from all culture conditions. Some conditions only contain one sample as protein ran out. Lanes labeled "M" was the master lane containing a mix of all three samples from SB+U0126 culture condition and was used to normalize between gels.

4.4 Discussion

Using a novel system previously developed in the lab, we confirmed that SB431542 treatment is enough to maintain and grow mouse lens epithelial cells in culture. This culture system was used extensively to allow for rapid expansion of culture cells to test multiple different conditions for immunostaining and western blot.

A combination of SB and FGF was confirmed to have decreased levels of connexin-50, both after immunostaining, and examining approximate whole protein levels using western blot. The staining results for connexin-46 showed that FGF might have a similar effect as with connexin-50, but more testing is required. It appears that FGF might lower but not completely abolish connexin-46 protein levels, which might provide an interesting avenue of study if simply lowering connexin levels is desired. The expression of connexin-43 is already low in lens epithelial cells so it was challenging to determine through immunostaining whether FGF had an effect.

We found that in almost all cases the supplementation of any culture medium with the MEK1 and MEK2 inhibitor U0126 produced little to no effect on the expression patterns of any of the connexin proteins, or the approximate protein level of connexin-50 via western blot. We hypothesized initially that a low dosage of FGF might be activating an ERK/MEK pathway that ultimately leads to the targeted degradation of connexin-50 protein[37]. Use of the U0126 molecule would have blocked activation of MEK1 and MEK2, potentially reversing the effects of low dose FGF. Because we saw no evidence of this occurring, we now suspect that either another pathway exists to link FGF with protein degradation, or somehow this system bypasses MEK1 and MEK2 specifically. Further research is needed to discover the exact mechanisms behind control of connexin 50 expression. A better understanding of this system might allow for control of lens growth, allowing for a slower or completely halted growth rate after the lens is fully developed.

4.5 Acknowledgements

We thank Dr. Dong Wang for development of the cell culture system used in this study and help with design of experiments. We also thank Dr. Chun-hong Xia for mice generation and management.

References for Chapter 4

1. Yeager M, Nicholson BJ. Structure of gap junction intercellular channels. *Curr Opin Struct Biol*. 1996;6(2):183-192. http://www.ncbi.nlm.nih.gov/pubmed/8728651. Accessed August 4, 2017.

2. Fleishman SJ, Unger VM, Yeager M, Ben-Tal N. A Calpha model for the transmembrane alpha helices of gap junction intercellular channels. *Mol Cell*. 2004;15(6):879-888. doi:10.1016/j.molcel.2004.08.016.

3. Unger VM, Kumar NM, Gilula NB, Yeager M. Three-dimensional structure of a recombinant gap junction membrane channel. *Science*. 1999;283(5405):1176-1180. http://www.ncbi.nlm.nih.gov/pubmed/10024245. Accessed August 4, 2017.

4. Cheng C, Xia C-H, Li L, White TW, Niimi J, Gong X. Gap junction communication influences intercellular protein distribution in the lens. *Exp Eye Res*. 2008;86(6):966-974. doi:10.1016/j.exer.2008.03.015.

5. Goodenough DA. The crystalline lens. A system networked by gap junctional intercellular communication. *Semin Cell Biol*. 1992;3(1):49-58. http://www.ncbi.nlm.nih.gov/pubmed/1320431. Accessed July 31, 2017.

6. Simpson I, Rose B, Loewenstein WR. Size limit of molecules permeating the junctional membrane channels. *Science*. 1977;195(4275):294-296. http://www.ncbi.nlm.nih.gov/pubmed/831276. Accessed August 4, 2017.

7. Martinez-Wittinghan FJ, Sellitto C, White TW, Mathias RT, Paul D, Goodenough DA. Lens gap junctional coupling is modulated by connexin identity and the locus of gene expression. *Invest Ophthalmol Vis Sci*. 2004;45(10):3629-3637. doi:10.1167/iovs.04-0445.

8. Gao J, Sun X, Martinez-Wittinghan FJ, Gong X, White TW, Mathias RT. Connections between connexins, calcium, and cataracts in the lens. *J Gen Physiol*. 2004;124(4):289-300. doi:10.1085/jgp.200409121.

9. White TW, Bruzzone R, Wolfram S, Paul DL, Goodenough DA. Selective interactions among the multiple connexin proteins expressed in the vertebrate lens: the second extracellular domain is a determinant of compatibility between connexins. *J Cell Biol*. 1994;125(4):879-892. http://www.ncbi.nlm.nih.gov/pubmed/8188753. Accessed August 4, 2017.

10. White TW. Unique and redundant connexin contributions to lens development. *Science*. 2002;295(5553):319-320. doi:10.1126/science.1067582.

11. Grosely R, Sorgen PL. A History of Gap Junction Structure: Hexagonal Arrays to Atomic Resolution. *Cell Commun Adhes*. 2013;20(1-2):11-20. doi:10.3109/15419061.2013.775256.

12. Kumar NM, Gilula NB. The gap junction communication channel. *Cell*. 1996;84(3):381-

388. http://www.ncbi.nlm.nih.gov/pubmed/8608591. Accessed August 4, 2017.

13. Evans WH, Martin PEM. Gap junctions: structure and function (Review). *Mol Membr Biol*. 2002;19(2):121-136. doi:10.1080/09687680210139839.

14. Beyer EC, Kistler J, Paul DL, Goodenough DA. Antisera directed against connexin43 peptides react with a 43-kD protein localized to gap junctions in myocardium and other tissues. *J Cell Biol*. 1989;108(2):595-605. http://www.ncbi.nlm.nih.gov/pubmed/2537319. Accessed August 4, 2017.

15. Paul DL, Ebihara L, Takemoto LJ, Swenson KI, Goodenough DA. Connexin46, a novel lens gap junction protein, induces voltage-gated currents in nonjunctional plasma membrane of Xenopus oocytes. *J Cell Biol*. 1991;115(4):1077-1089. http://www.ncbi.nlm.nih.gov/pubmed/1659572. Accessed August 4, 2017.

16. Mathias RT, White TW, Gong X. Lens Gap Junctions in Growth, Differentiation, and Homeostasis. *Physiol Rev*. 2010;90(1):179-206. doi:10.1152/physrev.00034.2009.

17. Clark JMI, Matsushima H, David LL, Clark JMI. Lens cytoskeleton and transparency: a model. *Eye (Lond)*. 1999;13 (Pt 3b(3b):417-424. doi:10.1038/eye.1999.116.

18. Mittag T. Role of oxygen radicals in ocular inflammation and cellular damage. *Exp Eye Res*. 1984;39(6):759-769. http://www.ncbi.nlm.nih.gov/pubmed/6097470. Accessed August 4, 2017.

19. Moffat BA, Landman KA, Truscott RJW, Sweeney MHJ, Pope JM. Age-related changes in the kinetics of water transport in normal human lenses. *Exp Eye Res*. 1999;69:663-669. doi:10.1006/exer.1999.0747.

20. Truscott RJ. Age-related nuclear cataract: a lens transport problem. *Ophthalmic Res*. 32(5):185-194. doi:55612.

21. Pau H, Graf P, Sies H. Glutathione levels in human lens: regional distribution in different forms of cataract. *Exp Eye Res*. 1990;50(1):17-20. http://www.ncbi.nlm.nih.gov/pubmed/2307192. Accessed August 4, 2017.

22. Baldo GJ, Gong X, Martinez-Wittinghan FJ, Kumar NM, Gilula NB, Mathias RT. Gap junctional coupling in lenses from alpha(8) connexin knockout mice. *J Gen Physiol*. 2001;118(5):447-456. http://www.ncbi.nlm.nih.gov/pubmed/11696604. Accessed August 4, 2017.

23. Gong X, Li E, Klier G, et al. Disruption of α3 connexin gene leads to proteolysis and cataractogenesis in mice. *Cell*. 1997;91(6):833-843. doi:10.1016/S0092-8674(00)80471-7.

24. Xia C, Cheng C, Huang Q, et al. Absence of alpha3 (Cx46) and alpha8 (Cx50) connexins leads to cataracts by affecting lens inner fiber cells. *Exp Eye Res*. 2006;83(3):688-696. doi:10.1016/j.exer.2006.03.013.

25. DeRosa AM, Xia C-H, Gong X, White TW. The cataract-inducing S50P mutation in Cx50 dominantly alters the channel gating of wild-type lens connexins. *J Cell Sci*. 2007;120(Pt

23):4107-4116. doi:10.1242/jcs.012237.

26. Xia C, Liu H, Chang B, et al. Arginine 54 and Tyrosine 118 residues of {alpha}A-crystallin are crucial for lens formation and transparency. *Invest Ophthalmol Vis Sci*. 2006;47(7):3004-3010. doi:10.1167/iovs.06-0178.

27. Rong P, Wang X, Niesman I, et al. Disruption of Gja8 (alpha8 connexin) in mice leads to microphthalmia associated with retardation of lens growth and lens fiber maturation. *Development*. 2002;129(1):167-174. http://www.ncbi.nlm.nih.gov/pubmed/11782410. Accessed August 3, 2017.

28. Chang B, Wang X, Hawes NL, et al. A Gja8 (Cx50) point mutation causes an alteration of alpha 3 connexin (Cx46) in semi-dominant cataracts of Lop10 mice. *Hum Mol Genet*. 2002;11(5):507-513. http://www.ncbi.nlm.nih.gov/pubmed/11875045. Accessed August 4, 2017.

29. Dahm R, van Marle J, Prescott AR, Quinlan RA. Gap junctions containing alpha8-connexin (MP70) in the adult mammalian lens epithelium suggests a re-evaluation of its role in the lens. *Exp Eye Res*. 1999;69(1):45-56. doi:10.1006/exer.1999.0670.

30. Li L, Cheng C, Xia C, White TW, Fletcher DA, Gong X. Connexin mediated cataract prevention in mice. Lewin A, ed. *PLoS One*. 2010;5(9):e12624. doi:10.1371/journal.pone.0012624.

31. Vanita V, Hennies HC, Singh D, Nürnberg P, Sperling K, Singh JR. A novel mutation in GJA8 associated with autosomal dominant congenital cataract in a family of Indian origin. *Mol Vis*. 2006;12:1217-1222. http://www.ncbi.nlm.nih.gov/pubmed/17110920. Accessed August 4, 2017.

32. Sellitto C, Li L, White TW. Connexin50 is essential for normal postnatal lens cell proliferation. *Invest Ophthalmol Vis Sci*. 2004;45(9):3196-3202. doi:10.1167/iovs.04-0194.

33. Boswell BA, Overbeek PA, Musil LS. Essential Role of BMPs in FGF-Induced Secondary Lens Fiber Differentiation. *Dev Biol*. 2008;324(2):202-212. doi:10.1016/j.ydbio.2008.09.003.Essential.

34. Schulz MW, Chamberlain CG, de Iongh RU, McAvoy JW. Acidic and basic FGF in ocular media and lens: implications for lens polarity and growth patterns. *Development*. 1993;118(1):117-126. http://www.ncbi.nlm.nih.gov/pubmed/7690700. Accessed August 8, 2017.

35. Lovicu FJJ, McAvoy JWW. Growth factor regulation of lens development. *Dev Biol*. 2005;280(1):1-14. doi:10.1016/j.ydbio.2005.01.020.

36. Robinson ML. An essential role for FGF receptor signaling in lens development. *Semin Cell Dev Biol*. 2006;17(6):726-740. doi:10.1016/j.semcdb.2006.10.002.

37. Gong X, Wang X, Han J, Niesman I, Huang Q, Horwitz J. Development of cataractous macrophthalmia in mice expressing an active MEK1 in the lens. *Invest Ophthalmol Vis*

Sci. 2001;42(3):539-548. http://www.ncbi.nlm.nih.gov/pubmed/11222509. Accessed April 30, 2013.

Chapter 5 Summary

Our studies indicate that both gap junctions and α-crystallins act on multiple pathways to control the lens size, growth, and stiffness of the lens. Elucidating the mechanical mechanisms behind each of these pathways was the focus of this thesis.

Lens Stiffness is Regulated by Gap Junctions and Cytoskeleton Organization

We have shown that several factors can contribute to the softening or stiffening of the mouse lens using a novel muscle lever system. We compared the bulk stiffness of several mouse lenses across several age groups and strain backgrounds, discovering along the way that drastic changes can exist even within two normal mouse strains. The loss of Connexin-46 triggered both the onset of nuclear cataract, as well as an increase in stiffness across all mouse lenses. In addition, periaxin was one potential protein that could explain the differences in stiffness we observed between mouse strains, with the 129 variant stiffening the lens, while the B6 variant softening the lens. Further studies are needed to determine exactly how Connexin-46 and periaxin interact with the lens fiber cell architecture to produce these changes in bulk stiffness.

αA-Crystallin Point Mutations Affect Different Types of F-Actin Networks

Using cultured mouse lens epithelial cells from several α-crystallin mutant lenses, we demonstrated that mutant crystallin protein can have differing effects on the cytoskeleton, potentially accounting for the lens phenotypes observed. Epithelial cells containing αA-Y118D mutant protein tended to have aggregates forming on actin fibers, while those containing αA-R54C and αA-R54H created morphological distortions, and potentially aggregated with actin binding proteins.

Connexin Expression in Lens Epithelial Cells is Regulated by TGF-beta and FGF Signaling

Utilizing a novel culture medium developed previously in the lab, we were able to culture and grow primary lens epithelial cells. Low doses of FGF were shown previously to reduce levels of Connexin-50 in these cells. Work was performed to investigate whether this reduction acted through an ERK/MEK pathway by the use of a MEK1 and MEK2 inhibitor molecule, U0126. This specific drug was unable to alter the effects of low dose FGF, confirming that another pathway might be responsible for the large reduction in Connexin-50 protein levels.

In summary, the work presented above provides key insights into the mechanisms behind controlling lens size and growth. Many of the details governing these mechanisms remain unknown, but we now know that gap junctions and α-crystallins, along with their interactions with the cell cytoskeleton, act to precisely maintain control over several physical properties of the lens. Ongoing research into exactly how these key molecules interact with lens fiber cells to soften the lens, or reduce its size, could help to delay or prevent the onset of presbyopia.